Exploring the Role of ADAM17 in Vascular Smooth Muscle Cells and Macrophages Within the Atherosclerotic Plaque

by

Tolga Kilic

A thesis submitted in partial fulfillment of the requirements for the degree of

Master of Science

Department of Physiology

University of Alberta

ABSTRACT

Atherosclerosis, characterized by arterial fat deposits, is the root cause of many cardiovascular diseases. Plaque deposition results from a series of events initiated by elevated plasma cholesterol, inflammation of the arterial wall, cholesterol uptake, macrophage-derived foam cell formation, and transformation of vascular smooth muscle cells (VSMC) into lipid-laden foam cells. ADAM17 is a membrane-bound protease that can proteolytically process several substrates involved in inflammation, proliferation, lipid metabolism, and cell-cell interactions, thereby regulating cellular events that could lead to plaque deposition. Recent literature suggests that the role of ADAM17 is cell specific. This thesis examines the role of ADAM17 in vascular smooth muscle cells and macrophages, two cell types central to plaque deposition by their ability to form lipid-laden foam cells. We generated mice lacking ADAM17 in vascular smooth muscle cells (VSMC) using the $Adam17^{flox/flox}/Myh11^{cre/ERT2}$ model. These mice were bred onto an $Ldlr^{-/-}$ (low-density lipoprotein receptor) background, a widely utilized model in atherosclerosis research. This background induces elevated plasma cholesterol and mirrors a genetic predisposition to atherosclerosis, akin to individuals with familial hypercholesterolemia. Mice were fed a high cholesterol diet (48% fat, 1.3%cholesterol) for 5 months to raise plasma lipids and induce atherosclerosis. Plaques were analyzed by oil red O lipid staining of the whole aorta (*en face,* facing forward) from male animals. Primary cell cultures of aortic VSMC and bone marrow-derived macrophages (BMDM) were employed to analyze cell responses to oxidized LDL (oxLDL) after treatment with a control or *Adam17*-specific siRNA. Female VSMC were additionally isolated and employed to reinforce the male data. This approach was necessary since *Myh11* promoter is located on the Y chromosome, and hence not expressed in females. Mice deficient in ADAM17 within vascular smooth muscle cells

(*Adam17*^{KD}) exhibit a marked increase in plaque area compared to control counterparts. In cell culture investigations, *Adam17*^{KD} VSMCs and macrophages demonstrated heightened lipid accumulation when exposed to oxLDL as an atherogenic stimulant. *Adam17*^{KD} VSMCs displayed an elevated propensity to transform into macrophage-like cells. Moreover, these cells exhibited diminished cholesterol efflux *in vitro*, coupled with attenuated mRNA expression of the cholesterol efflux transporter *Abca1* in response to oxLDL. Mice lacking ADAM17 in VSMCs (*Adam17*^{KD}) have significantly increased plaque area as compared to controls. Cell culture studies revealed that *Adam17*^{KD} VSMC and BMDM have augmented lipid content when oxidized LDL (oxLDL) is used as an atherogenic stimulant. *Adam17*^{KD} VSMC leads to elevated transformation into macrophage-like cells. Furthermore, these cells showed reduced cholesterol efflux *in vitro,* along with blunted *Abca1* mRNA expression in response to oxLDL. Efferocytosis, the clearance of dying cells, is another important factor in atherosclerosis to prevent accumulation and further inflammation in the plaque cores. BMDM display elevated efferocytotic capacity (by their ability to bind apoptotic cells) when ADAM17 is deleted, a phenomenon that does not occur in VSMC. This thesis highlights the important cell-specific roles of ADAM17, along with its protective effect in VSMC in atherosclerosis.

PREFACE

This MSc thesis represents the original work of Tolga Kilic. All research presented in this thesis was carried out at the laboratory of Dr. Zamaneh Kassiri in the Heritage Medical Research Center, 474, Department of Physiology, University of Alberta, Edmonton, AB, Canada. The study protocols received approval from the Human Research Ethics Review Process (HERO) at the University of Alberta. Animal procedures adhered to the ARRIVE (Animal Research: Reporting of in vivo Experiments) guidelines and followed the standards outlined by the Animal Care and Use Committee (ACUC) and the Canadian Council of Animal Care (CCAC), with the protocol numbers for this study being AUP1362. The majority of data collection and analysis were undertaken by me, with additional support from Dr. Mei Hu, Dr. Ilamaran Meganathan, and Nikki Antanasova. Dr. Mei Hu helped with performing the efflux assay on VSMC. Dr. Ilamaran Meganathan helped with ORO and Dil-oxLDL staining in female VSMC. Nikki Antanasova helped with TaqMan experiments. Dr. Z Kassiri served as my project supervisor, contributing to experimental design, the generation of transgenic mice, assistance with presentations and papers, as well as offering guidance on manuscript preparation and editing.

DEDICATIONS

Dedicated to Anne and Baba.

ACKNOWLEDGMENTS

I would like to express my heartfelt gratitude to my dedicated and motivating supervisor, Dr. Zamaneh Kassiri. Her consistent support not only guided me through every facet of this research project but also imparted valuable lessons in hard work, focus, and professionalism that extend beyond the realm of academia.

Equally appreciative are my esteemed committee members, Dr. Carlos Fernandez-Patron and Dr. Dawei Zhang. Their ongoing support, genuine concern, and intellectual contributions have significantly enriched my project. Their invaluable advice on presentations played a pivotal role in enhancing the effectiveness of my talks and refining proposals and other written documents. Additionally, I owe thanks to Carlos for making me a better human on the Jiu-Jitsu mats.

Special thanks go to Dr. Alan Murray and Dr. Spencer Proctor for their crucial roles in organizing and evaluating my candidacy examination. Their constructive feedback on proposals and presentations has been immensely valuable. I would also like to express my deep appreciation to Dr. Jesse Jackson for his encouraging words.

I am profoundly thankful for the support provided by the Alberta Graduate Excellence Scholarship (AGES) and the David Lawson Award, both of which have significantly contributed to the success of our research endeavors.

TABLE OF CONTENTS

LIST OF TABLES

LIST OF FIGURES

LIST OF ABBREVIATIONS

ABCA1	ATP-binding-cassette protein A1
ABCG1	ATP-binding-cassette protein G1
ACUC	Alberta Animal Care and Use Committee
ADAM	A disintegrin and metalloproteinase
ADAMTS	A disintegrin and metalloproteinase with thrombospondin motif
ANOVA	Analysis of variance
ApoB-100	Apolipoprotein B-100
ApoE	Apolipoprotein E
ARRIVE	Animal Research: Reporting of in vivo Experiment
BMDM	Bone marrow-derived macrophage
BSA	Bovine serum albumin
CCAC	Canadian Council of Animal Care
CD	Cluster of Differentiation
cDNA	Complementary deoxyribonucleic acid
CSF	Colony-stimulating factor
DAPI	4′,6-diamidino-2-phenylindole dihydrochloride
DMEM	Dulbecco's modified eagle medium
ECM	Extracellular matrix
EGF	Epidermal growth factor

EGFR	Epidermal growth factor receptor
FBS	Fetal Bovine Serum
FPLC	Fast-protein liquid chromatography
CSF	Colony-stimulating factor
HBSS	Hanks' balanced salt solution
HCD	High cholesterol diet
HDL	High-density lipoprotein
H&E	Hemotoxylin and eosin
IF	Immunofluorescence
IL	Interleukin
JAM	Junction-associated molecule
KCL	Potassium chloride
KDa	Kilodalton
LDL	Low-density lipoprotein
LDLR	Low-density lipoprotein receptor
LOX1	Lectin-like oxidized LDL receptor 1
LRP1	LDL receptor-associated protein 1
MCP-1	Monocyte chemotactic protein 1
MHY11	Myosin heavy chain-11
MI	Myocardial infarction

MMP	Metalloproteinase
NO	Nitric oxide
OCT	Optimal cutting temperature
OLR1	Oxidized low-density lipoprotein receptor 1
ORO	Oil Red-O
oxLDL	Oxidized LDL
PBS	Phosphate-buffered saline
PDGF	Platelet-derived growth factor
PFA	Paraformaldehyde
PMA	Phorbol ester
RCT	Reverse cholesterol transport
RFU	Relative fluorescent unit
RPM	Revolutions per minute
RT	Room temperature
α-SMA	Smooth muscle alpha-actin
SM22	Smooth muscle 22
SMC	Smooth muscle cell
SM-MHC	Smooth muscle myosin heavy chain
SPF	Specific pathogen-free
SR-A1	Scavenger receptor class A1

SR-B1	Scavenger receptor B1
TACE	Tumor necrosis factor-α converting enzyme
TGFβ	Transforming growth factor beta
TIMP	Tissue inhibitors of matrix metalloprotein
TNFα	Tumor necrosis factor alpha
TNFR	Tumor necrosis factor receptor
VAF	Viral antibody-free
VCAM-1	Vascular cell adhesion protein 1
VE-cadherin	Vascular endothelial cadherin
VLDL	Very low-density lipoprotein
VSMC	Vascular smooth muscle cell
VVG	Verhoeff-Van Gieson

CHAPTER 1

INTRODUCTION

1.1 Prologue

Atherosclerosis is a chronic and multifactorial inflammatory pathology and the underlying cause of cardiovascular disease, the leading cause of death worldwide.[1] Briefly, atherosclerosis is the accumulation of lipid-laden foam cells in arterial wall, comprised mainly of transformed vascular smooth muscle cells and macrophages (Figure 1.1). Reducing serum cholesterol is an important tool for treatment of atherosclerosis to prevent the formation of macrophage and smooth muscle cell-derived foam cells, as exemplified by statins.[2] Hence, vascular smooth muscle cells and macrophages play a crucial role in plaque formation as they are the primary cells that undergo transformation into foam cells. Therefore, these cells will be the focal point of this study. Atherosclerosis begins at an early age with fatty streaks in the inner lining of blood vessels, the endothelium. As an individua consumes a high-cholesterol diet (HCD), dysregulation of the endothelium may result in the retention and chemical modification of apoB-containing lipoproteins within the sub-endothelium. ApoB-100 measurements reflect total low-density lipoprotein (LDL), intermediate-density lipoprotein (IDL), and very low-density lipoprotein (VLDL), and Lp(a) cholesterol levels, making it a useful tool in atherogenic lipoprotein assessment.[3] LDL can undergo multiple forms of modification including oxidation, glycosylation, aggregation, glycation, and carbamylation, increasing their atherogenic propensity and subsequent uptake through various scavenger receptors.[43,5-7] This initiates an inflammatory cascade, as endothelial cells express cell surface adhesion molecules that bind circulating leukocytes that take up the accumulated cholesterol and become foam cells.[8] Production of inflammatory cues modulate vascular smooth muscle cells (VSMC) and can initiate their migration from the tunica media to the intima where they secrete extracellular matrix (ECM) proteins, proliferate, become macrophage-like and take up cholesterol, and assemble the fibrous

cap.[9] Vulnerable plaques prone to rupture and subsequent thrombosis contain many cells with CD68 markers assumed to be macrophages, and a large necrotic core comprised of lipid-filled foam cells.[10] A disintegrin and metalloproteinases 17 (ADAM17) is a membrane-bound protease which 'sheds' (cleaves from their transmembrane form into their soluble form) various substrates from the cell membrane involved in regulating inflammation, cell-cell permeability and communication, leukocyte recruitment, proliferation and neovascularisation, thereby making it an attractive target in vascular pathologies.[11] This protein is a member of the metalloproteinase family of proteases and plays a major role in shedding numerous growth factors and cytokines, notably the inflammatory mediator tumor necrosis factor-α(TNF-α), as well as remodeling and cell to cell adhesion.[12]

ADAM17 is a ubiquitously expressed 134 kDa membrane-bound metalloproteinase which is cleaved to its proteolytically active form of 98 kDa where it cleaves a wide range of extracellular substrates.[13,14] Originally coined tumor necrosis factor-alpha converting enzyme (TACE), this protease is responsible for shedding growth factors and cytokines inactively bound to the cell membrane into their soluble, active forms that can subsequently induce a cellular response.[15] The role ADAM17 plays in atherosclerosis varies depending on the cell type it is analyzed in. In rabbit VSMCs, gene silencing of ADAM17 enhanced plaque stability (increased VSMC and collagen content) and decreased macrophage and lipid content.[16] However, contradicting data which utilized ADAM17 hypomorphic mice show increased TNFR2 signaling, stimulating cell survival, macrophage proliferation, and stronger adhesion to endothelial cells, exacerbating the pathology.[17,18] Colony-stimulating factor-1 (CSF-1) is another ADAM17 substrate, and in leukocytes lacking ADAM17, macrophage proliferation seems to be defective.[19] ADAM17 deficient macrophages show increased efferocytosis and enhanced anti-

inflammatory phenotype via a CD36-dependent pathway, a scavenger receptor which plays a role in lipid uptake as well as recognition of apoptotic cells for efferocytosis.[20] By promoting MerTK cleavage on macrophages, another receptor which binds apoptotic cells, ADAM17 has been shown to promote the detrimental effects of angiotensin II on atherosclerosis and impair efferocytosis.[21] Interestingly, myeloid deficiency of ADAM17 was shown to increase plaque development and stability with increased VSMC and collagen content, though no mechanism was reported.[22] Furthermore, ADAM17 was found to be critical in ABCA1 expression by promoting cholesterol efflux in macrophages through HDL, an anti-atherogenic lipoprotein which is responsible for cholesterol efflux from peripheral cells.[23] It seems in macrophages, ADAM17 has the potential to manipulate efferocytosis and lipid loading, which can thereby influence plaque regression and foam cell formation, respectively. Not much is known of the role of ADAM17 in smooth muscle cells with respect to atherosclerosis, therefore this will be a novel study into the role of ADAM17 in this disease.

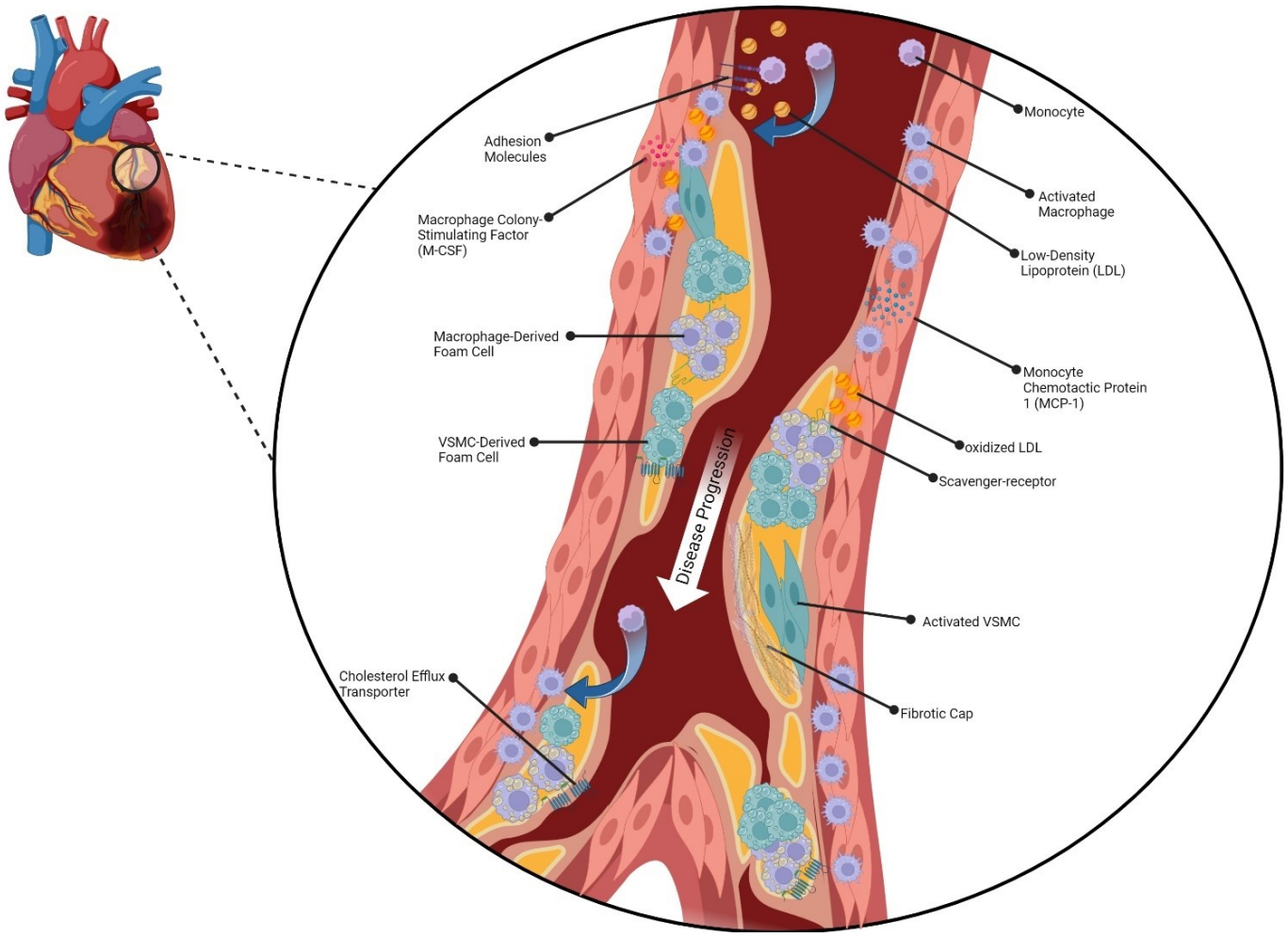

Figure 1.1 Atherosclerotic Plaque Formation in the Arterial Wall

Atherosclerotic plaque formation in the arterial wall is an inflammation-driven pathology manifesting in foam cell formation derived from two key cell types: VSMC and macrophages.

1.2 Anatomy and Physiology of the Aorta

The largest artery in the body, the aorta, is responsible for carrying oxygenated blood and nutrients out of the left cardiac ventricle, into the mesenteries and smaller arteries, and finally into the capillary beds where oxygen is supplied to peripheral tissues. In mice, this artery is heavily studied and used for various models due to its large size relative to other murine arteries. The aorta starts at the base of the heart and descends along the spine, coming to an end at the bifurcations of the iliac arteries. Though the structure is mechanical in nature, the strict regulation of cellular processes in the aorta makes it a highly dynamic structure.

1.2.1 Structure and function of the aorta

The aorta is comprised of three layers; the innermost tunica intima comprised of endothelial cells, the tunic media which is the thickest layer and consists of vascular smooth muscle cells (VSMC), and the outermost tunica adventitia which contains fibroblasts and progenitor cells.[24] The mechanical properties of the aorta are determined by the elastin and collagen content, which provide compliance and tensile strength, respectively.

The aorta senses and responds to stimuli and adjust accordingly to maintain cardiovascular homeostasis. Endothelial cells sense and respond to changes in blood flow, namely wall shear stress (WSS), which results in changes in gene expression to the endothelial cells, providing an anti-clotting, anti-inflammatory, and low-resistance barrier to the vessel.[25] Notably, endothelial cells synthesize nitric oxide via endothelial nitric oxide synthase (eNOS), which allows for vessel relaxation and prevents endothelial apoptosis induced by inflammatory or atherosclerotic factors.[26,27] Fibroblasts (along with differentiated VSMC) regulate the balance

between synthesis and degradation of ECM.[24] In response to mechanical stress, fibroblasts can regulate matrix deposition by controlling their expression of collagen.[28,29]

1.2.2 Tunica Intima and Adventitia

The inner most layer of the aortic wall, facing the arteries lumen, consists of a monolayer of squamous endothelial cells called the tunica intima. In the healthy aorta, this layer provides a barrier between the blood stream and the vessel wall. Maintenance of the permeability between endothelial cells is a tightly regulated process mediated by adherens and tight junctions. The primary adherens junctions include VE-cadherin and catenins, while tight junctions consist of claudin, junction-associated molecule (JAM) families, and occludin.[30,31] Importantly, nitric oxide (NO) production from endothelial cells promotes a healthy endothelium with vasodilatory, antioxidant, and anti-inflammatory affects.[32] In inflammatory conditions, certain molecules like TNF-α can decrease NO production by reducing gene expression of endothelial NO synthase, resulting in impaired vasorelaxation in the context of atherosclerosis.[33] Moreover, numerous risk factors for atherosclerosis including hypercholesterolemia, smoking, diabetes, and hypertension, are also associated with dysfunction of the endothelium.[34,35]

The outermost layer of the aorta is called the tunica adventitia and consists primarily of fibroblasts in a collagen and elastin-rich matrix. Other cell types found in this layer include pericytes, leukocytes, mesenchymal stem cells, and mast cells.[36] In response to certain stimuli (*i.e.* TGF-β, PDGF, mechanical stress, inflammation), fibroblasts can become activated and differentiate into myofibroblasts, expressing alpha-smooth muscle actin (α-SMA) and capable of contractility and ECM synthesis, mediating vascular repair.[37-40] This layer also provides a conduit for the vasa vasorum, small blood vessels which deliver oxygen and nutrients to large vessels.[41] Importantly, adventitial fibroblasts are activated in the early stages of atherosclerosis,

with MCP-1 and collagen type I and III expression detected in adventitial fibroblast with the introduction of hyperlipidemia in apoE$^{-/-}$ mice prior to lesion formation.[42]

1.2.3 Role of the Tunica Media: Vascular Smooth Muscle Cells

The tunica media is the largest of the three aortic layers and is comprised mainly of smooth muscle cells and elastin fibers. The primary function of smooth muscle cells is contraction, with the use of the calcium and ATP-dependent actin-myosin contraction mechanism.[43] Healthy smooth muscle cells express a unique repertoire of contractile proteins, known as markers, that allow for their identification and characterization.[44,45] As these cells are specialized for contraction and ultimate regulation of vascular tone and blood pressure at a physiological state, the rate of proliferation and synthesis of mature smooth muscle cells are very low.[46] When the media experiences pathological conditions, smooth muscle cells can differentiate into synthetic or macrophage-like cells, termed phenotypic-switching.[47,48] The tunica media is rich in proteoglycans and elastic fibres within the ECM.[49] The media is for the most part a homogeneous population of vascular smooth muscle cells, but some data suggest that this is not the case for all mammals, as avian species contain two morphologically distinct populations of VSMC; contractile and neointima like.[50,51]

1.3 Atherosclerosis

1.3.1 Prevalence, cause, sex differences, and clinical outcomes of atherosclerosis

Atherosclerotic cardiovascular disease, an inflammation-driven vascular pathology culminating with the manifestation of fatty plaques within hardened arteries, is the major cause of coronary heart disease (CHD) and stroke, and one of the leading causes of death in the industrialized world. According to the American Heart Association (AHA), CHD caused 382,

820 deaths in 2020 and stroke accounted for 1 in every 21 deaths in the United States that year. Put together, cardiovascular disease resulted in 19.05 million deaths worldwide in 2020. Increased systolic blood pressure is also commonly associated with atherosclerosis, and according to AHA data from 2017 to 2020, 46.7% of Americans had hypertension.[52]

Inflammation of the vessels can cause endothelial cells to express adhesion molecules (VCAM-1) which facilitate rolling of monocytes along the endothelium, and migration into the intima via cues from chemoattractant molecules.[53] With the uptake of lipids, monocyte-derived macrophages turn into the hallmark lipid-laden foam cells.[54] Recent evidence suggests that VSMC proliferate and migrate towards the intima where they undergo phenotypic switching to macrophage-like cells and contribute to about half the total foam cell population.[55] Further accumulation of these foam cells advances plaque growth and could potentially occlude arteries, or dislodge causing thrombosis and myocardial infarction or stroke.

The most common risk factors for atherosclerosis include high blood cholesterol and lipoprotein levels, high blood pressure, and smoking.[56] Sex differences are also at play in atherosclerosis. The incidence of atherosclerosis is higher in men at an earlier age, whereas in women, coronary artery disease increases with the decline of estrogen. Additionally, common risk factors for atherosclerosis have a larger impact in woman than men.[57] In LDLR-deficient mice, estrogen was found to be protective in atherosclerosis independent of plasma cholesterol level changes.[58] Furthermore, after 14 weeks of high fat feeding, female *Ldlr*$^{-/-}$ mice developed significantly more atherosclerosis in the aortic root than males.[59] Importantly, deletion of CD36 in endothelial cells of *Ldlr*$^{-/-}$ female mice showed reduced atherosclerosis burden, whereas global ablation protected against atherosclerosis in both sexes.[59] Therefore it is critical to acknowledge sex differences in atherosclerosis studies involving *Ldlr*$^{-/-}$ mice.

Medical treatments for atherosclerosis include statins (lowers cholesterol), Aspirin (to prevent clotting), nitrates (relax blood vessels), beta blockers and diuretics (lower blood pressure), calcium channel blockers (in combination with beta blockers), and Ranolazine (treat angina). Surgical interventions for atherosclerosis include coronary artery bypass, angioplasty and stent placement, endarterectomy, or fibrinolytic therapy.

1.3.2 Plaque formation: Role of VSMC and Macrophages

As mentioned, VSMC and macrophages take up lipids and turn into the characteristic foam cells within the atheroma. The atheroma initiates with the recruitment of circulating monocytes under inflammatory conditions, promoting the differentiation of these cells into macrophages.[60] Macrophages are critical cells in initiating and resolving inflammation and their activity is directed by inflammatory cues to activate or dampen the inflammatory process. An imbalance between activation and deactivation can result in cellular and tissue damage.[61] Phagocytosis, the engulfment of foreign particles or cellular debris, is a critical response of the innate immune system and is one of the main roles of macrophages. However, in atherosclerosis, macrophages maladaptively take up lipids and transform into foam cells, and without a proper negative feedback mechanism, the disease exacerbates as foam cells become in engorged in lipids. In the plaque, macrophages have been described as classically activated (M1) and proinflammatory or alternatively activated (M2) and protective against tissue damage based on their expression of certain markers. However, *in vivo* data suggests that a broad spectrum of intermediate phenotypes exist, with each performing various functions.[62] Accumulation of macrophages within the plaque diminishes their migratory capacity, and upon their death within the plaque, they release lipids and tissue factors, giving rise to a pro-thrombotic necrotic core.

The inefficient efferocytosis and clearance of apoptotic cells further worsen the development of the necrotic core, a hallmark of unstable plaques susceptible to rupture.

VSMC are differentiated contractile machines that react to physiological cues in order to maintain homeostatic vascular tone. In atherosclerosis, these cells proliferate via clonal expansion of a few cells and migrate towards the site of plaque and synthesize extracellular matrix proteins forming the cap of the plaque.[63] However, lineage-tracing studies have demonstrated that these cells also commence to express a macrophage-like phenotype with the expression of CD68, and cooperatively take on the role of foam cells.[64] These phenotypic switch of smooth muscle cells is described by their decrease in contractile proteins (α-SMA, calponin, SM22), and an increase in ECM-remodelling enzymes, secretory organelles, and proinflammatory cytokines.[65] Switching phenotypes is strictly modulated by transcription factor expression, namely KLF-4, myocardin, and serum response factor (SRF).[66,67] Progression from diffuse intimal thickening (DIT) in pre-atherosclerosis to pathological intimal thickening (PIT) in early atherosclerosis is a dynamic process which involves the phenotypic switching and proliferation of VSMC.[10] DITs are considered to be the precursors for atherosclerotic plaques and under unfavourable conditions have the potential to progress to PITs, therefore highlighting an important role of VSMC in the initiation of atherosclerosis. Functional VSMC are required for stability of the plaque by maintaining the fibrous cap. On the other hand, VSMC death will drive atherosclerosis. Furthermore, VSMC apoptosis has been identified as a key player in plaque instability.[68] Thus, VSMCs are an integral part of atherosclerosis from its initiation to its sequelae, or hopefully, to its resolution. This thesis aims to describe the atherosclerotic role of ADAM17 in VSMC and macrophages.

1.4 ADAMs: origin, structure, function

A disintegrin and metalloproteinases (ADAMs) are a diverse group of proteases with a ride range of functions. These ~750 amino acid proteins, similar in structure to SVMPs, were originally found as being involved in sperm-egg interactions. Since then, ADAMs have been implicated in numerous basic cellular processes such as cell-cell interactions, extracellular matrix remodelling, signal transduction, and notably, ectodomain shedding of ligands and receptors.[69] Therefore, it is no surprise that ADAMs also have roles in pathologies such as cancer, neurodegeneration, chronic inflammation, and cardiovascular disease.[70-73]

1.4.1 Origin of ADAMs within the metzincin superfamily

ADAMs, along with snake venom metalloproteinases (SVMPs) and ADAMs containing thrombospondin motifs (ADAMTS), comprise the adamalysin subfamily within the metzincin superfamily of metalloproteases.[74] This enzyme family also contains the astacins and the reputable matrix metalloproteinases (MMPs). ADAMs were initially introduced as fertilin proteins, found on guinea pig spermatozoa membranes in the mid 90s. For containing A Disintegrin And Metalloprotease domain, this gene family was coined ADAM, orthodoxically honouring its emergence in the disciplines of snakes and fertility.[75] To date, 21 ADAM proteins have been identified in the human genome and 34 in mice.[76]

1.4.2 Structure of ADAMs

All catalytic ADAMs utilize a zinc atom coordinated by three histidine residues at the active site of their metalloproteinase domain which is essential for catalysis. Unlike MMPs, ADAMs do not contain hemopexin domains but do have a disintegrin and cysteine rich domain, a signature shared by SVMPs and ADAMTS as well.[76] In most ADAMs, the N-terminus contains

a signal peptide directing and localizing the enzyme to perform its specific function, followed by the pro-domain, which maintains enzymatic latency. This is achieved via a "cysteine switch" mechanism, which blocks the zinc active site in the metalloproteinase domain by a conserved cysteine residue in the pro-domain.[77]

Found originally in snake venom, disintegrin domains contain the hallmark RGD (Arginine-Glycine-Aspartic acid) sequence, which via integrin binding may inhibit platelet aggregation. However, in most ADAMs (except ADAM15), this sequence is replaced by an ECD (Glutamic acid-Cysteine-Aspartic acid) or xCD (x representing any amino acid) sequence.[78]

The cysteine-rich domain of ADAMs provides unique adhesive capabilities and regulation of protease-specific function. This should not be confounded with the "cysteine-switch" mechanism localized to the pro-domain.[79] This domain also contains highly variable regions (HVR), which may function as a protein-protein interface and mediate substrate recognition.[80]

These three domains—metalloproteinase, disintegrin, and cysteine-rich—collaboratively form the characteristic C-shaped arm of ADAMs. This arm is linked to the transmembrane domain through an epidermal growth factor (EGF)-like region. The EGF-like region, in conjunction with the cytoplasmic tail, plays a crucial role in transducing extracellular signals into the cell, facilitating mRNA expression, post-translational modifications (PTM), and potentially enhancing substrate binding efficiency. [76,81]

ADAMs are transported to the Golgi complex post-synthesis and trafficked through the endoplasmic reticulum for further maturation, which involves convertase or furin-mediated

cleavage of the pro-domain.[82] Unlike their family members, ADAM9 and ADAM12 lack transmembrane and cytoplasmic tails making them soluble ADAMs.[83,84]

1.4.3 Physiological Functions of ADAMs

Initially discovered on spermatozoa membrane, it is no surprise that a majority of the ADAMs have physiological functions in fertility. ADAMs 1, 2, 3, 6, 7, 18, 20, 21, 22, 28, 29, 30, 32, and 33 are involved in embryonic development or reproduction.[76] ADAMs 8, 9, 10, 11, 12, 15, 17, and 19 have broader physiological functions as well as implications in some diseases. In short, ADAMs play a role in cell adhesion, migration, development, and signalling by cleavage of ligand or receptor ectodomains, which can then act on cells in a paracrine or autocrine fashion.[85] Many ADAMs have also been implicated in central nervous system functions, inflammation, and the cardiovascular system.

These functions are tightly regulated by four inhibitor proteins with cross-specificity that bind to the metalloproteinase domain of ADAMs and prevent proteolysis, named Tissue Inhibitors of Metalloproteinases (TIMPs).

1.4.4 Origins and function of ADAM17

TNF-α was discovered to be synthesized as a membrane protein which requires proteolysis for its release.[86] In the presence of hydroxamic acids (which in inhibits metalloproteinases), this release was blunted, identifying the TNF-releasing enzyme as a metalloproteinase.[87] This convertase was then purified and cloned in 1997 and coined TNF-α-converting enzyme, or TACE.[13] It was enrolled as a new member of the ADAM family due to structural homology to disintegrin metalloproteinases, and was consequently renamed ADAM17. Since then, researchers have identified over 80 substrates for this protease, with roles in cytokine activation, growth

factor shedding, and cleavage of many cell surface receptors.[88] To emphasize the importance of this protease in physiology, ADAM17 knock-out mice have skin lesions, an open-eye phenotype, and are not viable, and this defect is linked to the ameliorated release of TGF-α.[89]

ADAM17 is a Type 1 transmembrane protein with a similar structure to other membranous ADAMs as well as Class III snake venom metalloenzymes (Figure 1.2).[90] ADAM17 is trafficked through the endoplasmic reticulum and the Golgi complex before it reaches the plasma membrane.[91] Interestingly, maturation and enzymatic activity of ADAM17 is mediated by iRhom1/2 proteases and may also play a role in selectivity for some ADAM17 targets.[92,93] Endogenous inhibition of ADAM17 at the membrane is mediated by TIMP3.[94,95]

ADAM17 has over 80 documented substrates and is by far the most extensively studies ADAM for its implication in heart disease, cancer, inflammation, and neurodegeneration. Proteolysis by ADAM17 is usually done at the membrane-adjacent part of the protein, which includes epidermal growth factor receptors (EGFR) ligands, proinflammatory cytokines, and other cell surface receptors. After cleavage by ADAM17, these molecules can bind to their receptor or ligand on the same cell (autocrine) or to neighbouring cells (paracrine). For its role in orchestrating inflammation through TNF-α and other mediators, ADAM17 has been implicated as an attractive therapeutic target in multiple diseases. For example, Etanercept is a commonly used pharmaceutical drug for rheumatoid arthritis which works by blocking the actions of TNF-α. Treatment of cells with a PKC stimulator, or phorbol ester (PMA), leads to increased ADAM17 activity.[96] Understanding the principles of ADAM17 inhibition or activation is not enough to robustly and efficiently treat a disease in the case of this protein. The available data indicates that the activity of ADAM17 exhibits inherent cell-type specificity. Consequently,

elucidating the precise role of this protease in a cell-specific context is imperative for achieving a more comprehensive and functionally relevant understanding.

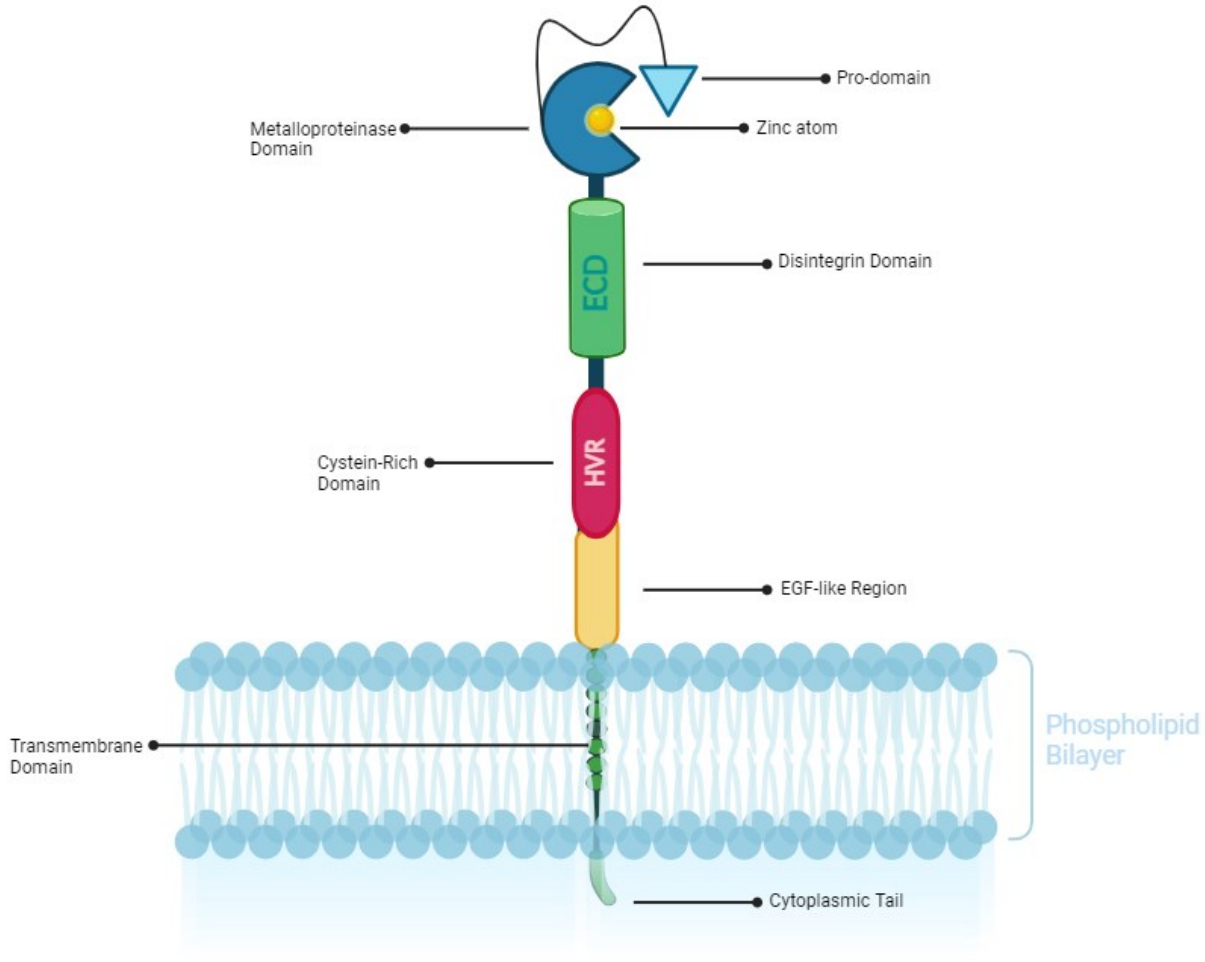

Figure 1.2 Structure of ADAM17

ADAM17 is a Type I transmembrane protein which sheds the ectodomain of numerous cell surface receptors and ligands.

1.4.5 ADAM17: Expression in Healthy vs. Diseased Aorta and Animal Studies

ADAM17 exhibits high expression levels on immune cells, endothelial cells, reproductive organs, and the liver. Its molecular actions are profoundly context-dependent, varying on a cell-to-cell basis, a theme that will be emphasized throughout this thesis. The expression of ADAM17 in the healthy aorta is typically maintained at a relatively low and balanced level. As it sheds various cell surface receptors and ligands, ADAM17 has an important role in normal tissue homeostasis, so its activity is strictly regulated. However, in the context of a chronic inflammatory disease, atherosclerosis, the expression of ADAM17 is elevated in response to this stimulus. One study has shown the expression of ADAM17 is associated with lesions in atherosclerosis-prone sites, and that levels of soluble TNFR1 and TNFR2, substrates of ADAM17, rose with atherosclerosis.[97] In another study with 298 participants with established vascular atherosclerosis, circulating ADAM17 substrates were used to develop a risk score which significantly increased the prediction accuracy of the Framingham *Recurring-Coronary-Heart-Disease-Score*.[98] Along with ADAM9 and ADAM15, ADAM17 level was increased in macrophages in advanced human plaques in the aortic, carotid, and femoral arteries.[99] Furthermore, it was shown that microparticles (MPs), released from activated or dying cell membranes, from endarterectomized human plaques contained mature and active ADAM17, and displayed increased processing of pro-TNF and TNFR1.[100] In contrast, ADAM17^{+} MPs (MPs expressing ADAM17) were not found in healthy human internal mammary arteries. Finally, increased ADAM17 mRNA expression and activity was associated with resistance to atherosclerosis in LDLR null mice.[101] All together, these studies implicate ADAM17 as a potential target in the pathogenesis of atherosclerosis.

One study using ADAM17 hypomorphic mice found that ADAM17 deficiency promoted atherosclerosis, and this was due to enhanced TNFR2 signalling which prompted proliferation and reduced apoptosis of macrophages and VSMC.[17] Another study using a more targeted approach to knock-out ADAM17 in myeloid and endothelial cells of mice found contrasting effects, where the macrophages knockout had increased plaque area and the endothelial cells had reduced plaque burden, highlighting an important cell-specific function of ADAM17.[102] In another model using rabbits, lentivirus-mediated ADAM17 silencing led to decreased plaque area along with more stable plaques.[103] It is notable to mention that the lipid profiles between mice and rabbits are convincingly different. The lipoprotein profiles of rabbits are LDL-rich like that of humans, whereas mice have HDL as the predominant lipoprotein.[104,105] Furthermore, cholesteryl ester transfer protein (CETP), responsible for the transfer of cholesteryl esters from HDL to apoB, is abundant in rabbits and not found in mice.[106-108] However, the point still stands that ADAM17 has broad function in the context in which it is analyzed. The intricate involvement of ADAM17 in atherosclerosis, as evidenced by its complex and cell type-dependent effects, underscores the need for further exploration in this field. This thesis will examine the role of ADAM17 in vascular smooth muscle cells and macrophages, with respect to its capacity to modulate lipid loading and efferocytosis, key aspects of plaque formation.

1.5 Lipid Metabolism in Atherosclerosis

1.5.1 Foam cell formation: cholesterol uptake, efflux, and esterification

Macrophages and activated VSMC which have engulfed excessive amounts of cholesterol and other lipids comprise the hallmark foam cells of atherosclerotic plaques. Foam cell formation involves a balance of three processes: the uptake, esterification, and expulsion of cholesterol. Each process is carried out by a specific set of lipid transporters and enzymes which

are conserved between macrophages and VSMC but expressed to different degrees. Most of the cholesterol in the plasma membranes of cells is located within the inner leaflet adjacent to the cytosol. Excess cholesterol does not accumulate here but is esterified into cholesteryl ester (CE) and stored in hydrophobic lipid droplets. Acyl-CoA cholesterol acyltransferase (ACAT) is responsible for CE formation from free cholesterol.

Uptake of cholesterol in the form of aggregated or oxidized LDL in the atherosclerotic plaque is mediated by scavenger receptors, rather than the LDL receptor which takes up LDL from the bloodstream by binding to apoB-100. The LDL receptor, or LDLR, is tightly regulated by a feedback mechanism in response to accumulation of cholesterol via PCSK9-mediated degradation[109]. Conversely, scavenger receptors can bind to modified lipoproteins and are not regulated by a feedback mechanism in response to excess cholesterol loading. This is because, naturally, they act as pattern recognition receptors (PRR) as part of the immune system. Therefore, these scavenger receptors are responsible for the maladaptive formation of foam cells in atherosclerosis. In pro-atherogenic conditions, endothelial cells express high amounts of LOX-1, which transfers luminal oxLDL into the intima, where infiltrated macrophages and VSMC sense and bind to these particles.[54] The main scavenger receptors involved in foam cell formation are SR-A1, CD36, and LOX-1. The modification of LDL in the sub endothelium is a diverse process resulting in multiple different forms of modified LDL. The rate of native LDL accumulation in mouse peritoneal macrophages is relatively low, whereas modified forms of LDL bind specifically and are actively internalized leading to foam cell formation. Some of which include oxidized LDL, acetylated LDL, glycated LDL, and aggregated LDL, which can be induced through free radicals, hydroperoxides, and advanced glycation end-products (AGEs), leading to the covalent modification of the apoB protein and lipid moeities.[7] Important for our *in*

vitro atherosclerosis model, oxLDL can bind to SR-A1, CD36, and LOX-1 leading to the formation of foam cells, as well as induce cellular efflux via ABCA1/G1 and SR-B1.[110] Glycated LDL also induces foam cell formation though consequently raises its susceptibility to oxidative modification, making it more atherogenic.[111,112] Increased AGEs on LDL in diabetic patients have been shown clinically, making it a candidate model for *in vitro* studies related to atherosclerosis and diabetes.[112] Aggregated LDL leads to massive accumulation of free cholesterol in THP-1 macrophages without stimulating ROS or ER stress.[113] Notably, aggregated LDL is mainly taken up by lipoprotein receptor-related protein (LRP) in VSMC, limiting the analysis of other receptors in foam cell formation.[114,115] Acetylated LDL has minimal induction of mitochondrial stress as compared to oxLDL, as well as better efflux capacity due to the fact that oxLDL accumulates within lysosomes.[116] However, intracellular accumulation of acetylated LDL is primarily due to SR-A1/2, whereas only an approximate 30% of oxLDL uptake is due to this pathway.[117,118] CD36 represents a receptor specific for the uptake of oxidized LDL.[119] Thus, atherosclerosis involves multiple forms of lipogenic stimuli which have specificities for certain receptors involved in foam cell formation.

Cholesterol efflux out of cells under hyperlipidemic conditions is essential in maintaining whole body cholesterol homeostasis. The process of cholesterol efflux is mainly mediated through high-density lipoprotein (HDL), a particle responsible for the movement of cholesterol out of peripheral cells, as well as macrophages and VSMC in the arterial wall. Cholesterol can leave macrophages passively by aqueous diffusion or via SR-B1, but the bulk of efflux in cholesterol-loaded cells is mediated through the active pathway via ABCA1 and ABCG1 cholesterol efflux transporters.[120] People with Tangier disease have extremely low plasma levels of HDL due to a mutation in the *Abca1* gene, increasing the progression of atherosclerosis in

these individuals and emphasizing the predominance of ABCA1 in cholesterol efflux.[121-123] In both macrophages and smooth muscle cells, ABCA1 expression is induced by liver X receptor (LXR).[124,125]

1.5.2 Reverse Cholesterol Transport

Management of cholesterol is crucial in maintaining a healthy balance of lipids between our peripheral tissues and liver, and reverse cholesterol transport (RCT) mediates this process. To ensure cells do not over accumulate cholesterol, which would promote atherogenesis, RCT ensures that surplus cholesterol is removed from peripheral cells, like macrophages in the arterial wall, and transported back to the liver for catalysis and fecal excretion. This phenomenon explains why HDL has been coined as 'good' cholesterol, as it is a critical acceptor of cholesterol from peripheral tissues. Cholesterol and phospholipid poor apoA-1 (very small HDL) complexes with ABCA1 to promote the majority of cholesterol efflux whereas ABCG1 expels cholesterol onto larger cholesterol-containing HDL.[126] RCT has been proposed as beneficial in atherosclerosis, however determination of RCT capacity by measuring static amounts of HDL cholesterol is not useful for such a dynamic and active process, and a conglomeration of methods including cholesterol efflux capacity, ApoA-1, and plasma cholesterol turnover should be assessed. Albeit HDL infusion trials have shown favourable outcomes on coronary atherosclerosis.[127,128] SR-B1 has been shown to passively and bidirectionally transport cholesterol between HDL, phospholipid acceptors, and other cells.[129,130] Loss of macrophage SR-B1 increased atherosclerosis, whereas overexpression in the liver decreased atherosclerosis and positively regulated RCT in macrophages.[131,132]

1.5.3 Role of ADAM17 in lipid metabolism

Though the role of ADAM17 is still an area of ongoing research, some data suggests that ADAM17 may indirectly influence lipid metabolism. The activity of ADAM17 has been shown to occur in cholesterol-rich membrane microdomains, or lipid rafts, and that cholesterol depletion increases the shedding of ADAM17 substrates.[133] This was verified by demonstrating that metalloproteinase inhibition resulted in increased ADAM17 substrates in lipid rafts, and may represent the tight regulation of ADAM17 substrates in these microdomains. HDL incubation with various cells increased the shedding of TNF and its receptors, implying that HDLs might affect lipid raft structure.[134] Purified ApoA-1 increased TNF shedding in an ABCA1-dependent manner, implicating ADAM17 in ABCA1 expression. In accordance with this, HDL increased ADAM17 expression and activity in macrophages.[23] Furthermore, they found that ABCA1 expression was supressed in ADAM17-deficient macrophages due to a lack of TNF-α shedding. Finally, it was shown that ADAM17 may cleave CD36, a scavenger receptor involved in apoptosis that plays a substantial role in foam cell formation.[20] More research is required to fully understand the role of ADAM17 in lipid metabolism, which will be highlighted in this thesis, though evidently ADAM17 does have an indirect role in lipid homeostasis.

1.6 Efferocytosis in Atherosclerosis

1.6.1 Macrophage-mediated efferocytosis

Efferocytosis is an intricately orchestrated cellular event that mediates the phagocytic clearing apoptotic cells and is crucial for maintaining tissue homeostasis. Approximately 0.4% of the cells in an adult human will die each day.[135,136] During efferocytosis, macrophages down-regulate the expression of proinflammatory cytokines and shift towards anti-inflammatory and reparative phenotype, and in defective efferocytosis this process is dysregulated.[137] Apoptotic cells (AC) release chemokines, lipids, and nucleotides which lead to mobilization of

efferocytotic immune cells.[138-141] If unchecked, secondary necrosis can occur and trigger an immune response, which is how efferocytosis prevents further inflammation. The most significant apoptotic signal is phosphatidylserine on the outer leaflet of the cell membrane.[142] Phagocyte receptors directly binding to AC include stabilin 1 and 2, TIM 1, 3, and 4, BAI1, and LRP1.[136] Receptors that work through linking molecules include TYRO3, AXL, MERTK, CD36, and αVβ3 and αVβ5 integrins, and the most significant linking molecules are AXL ligand, protein S and MFG-E8.[143,144] Western diet-fed *Mertk*$^{-/-}$*Ldlr*$^{-/-}$ mice have increased lesion and necrotic core size and reduced production of pro-resolving mediators, highlighting the importance of MERTK in efferocytosis.[145,146] After ingestion, AC derived sterols induce LXR activation and ABCA1 expression, allowing for efflux of the surplus cholesterol.[147] LXR also stimulates the release of anti-inflammatory cytokines IL-10 and TGF-β to further resolve inflammation.[148,149]

1.6.2 Impaired efferocytosis in atheroma and plaque regression

Research suggests that mechanisms in atherosclerosis are responsible for diminishing the total potential capacity of efferocytosis. CD47, the 'don't eat me signal', has been identified as a interacting with SIRPα on macrophages and inhibiting the efferocytotic process.[150] One study found that long noncoding RNA myocardial infarction associated transcript (MIAT) was elevated in advanced, unstable plaques, and that this acted as a micro RNA to induce expression of CD47.[151] Using CD47-blocking antibodies, efferocytosis was enhanced and atherosclerosis was ameliorated in multiple mouse models, and the authors described how TNF-α was a significant driver of impaired efferocytosis.[152] Proteolytic cleavage of MERTK and LRP1 in atherosclerosis have shown to reduce macrophage clearance of AC and contributed to plaque necrosis and

blunted resolution.[153,154] In general, as plaques grow larger, they contain less pro-resolving mediators which contributes to impaired efferocytosis.[155]

1.6.3 Role of ADAM17 in efferocytosis

ADAM17 demonstrates an important role in efferocytosis through cleavage of MerTK and CD36, two receptors responsible for binding to apoptotic stimuli. ADAM deficiency in macrophages was found to upregulate CD36-dependent apoptotic cell uptake.[20] Soluble CD36 is decreased in the media of these cells, implying proteolytic cleavage by ADAM17. Therefore, ADAM17 impairs efferocytosis in macrophages. ADAM17 was found to shed MERTK on murine macrophages through a ROS/PKC/MAPK pathway.[156] Furthermore, through an angiotensin II pathway, ADAM17 cleavage of MERTK was found to hinder efferocytosis.[21] Interestingly, isoflurane treatment of bone marrow-derived macrophages or alveolar macrophages boosted efferocytosis of apoptotic neutrophils, and this was associated with increased surface expression of MERTK and decreased surface expression of ADAM17, and these effects of isoflurane were reversed by an AMPK inhibitor.[157] Finally, in aged macrophages, enhanced ROS leads to ADAM17-mediated cleavage of MerTK, impairing efferocytosis.[158] Therefore, a significant role of ADAM17 in efferocytosis is mediated by its interactions with MERTK and CD36.

1.7 Rationale

ADAM17 has been shown to be upregulated in atherosclerotic plaques, which along with its shedding of inflammatory mediators, implies a role of the protease in this chronic inflammatory process.[97] Moreover, ADAM17 has been shown to influence HDL-mediated RCT and induce expression of *Abca1*, highlighting its role in lipid metabolism.[23] This is important in

atherosclerosis development as foam cell formation is a central to atherosclerotic plaque formation, which can involve both VSMC and macrophages. Finally, ADAM17 has been shown to influence efferocytosis by cleavage of key apoptotic cell recognition receptors.[20,21] Therefore, this thesis aims to study the role of ADAM17 in VSMC and macrophages in atherosclerosis as they are crucial in foam cell development, and the latter in efferocytosis.

1.8 Hypothesis

We hypothesize that deletion of ADAM17 in vascular smooth muscle cells (VSMC) of *Ldlr*$^{-/-}$ mice will result in an increased plaque area by enhancing foam cell formation. This effect may be mediated through a deficiency in TNF-α-induced ABCA1 expression, coupled with heightened CD36 levels (due to the absence of cleavage by ADAM17), ultimately leading to an elevated lipid loading. *In vitro*, ADAM17-deficient VSMC and BMDM will have increased lipid content in response to oxLDL through a lack of ABCA1-mediated efflux and augmented uptake via CD36. In macrophages, ADAM17 deficiency may increase efferocytosis through preservation of the MerTK and CD36 receptors, making ADAM17 pro-atherosclerotic.

Objectives

1. Phenotypic characterization of plaque area in the control and VSMC-specific ADAM17 knock-out mice (*Ldlr*$^{-/-}$*/Adam17*^{SMC}) after 5 months of high cholesterol diet feeding.

- Serum cholesterol profiles and weight gain measurements over 5 months of feeding
- Plaque area formation in the aorta and aortic arch (along with necrotic core quantification)
- Inflammatory staining of the aortic wall (macrophages and neutrophils)

2. Defining the modulation of lipid metabolism in response to ADAM17 deficiency in VSMC and bone marrow-derived macrophages (BMDM).

- Analysis of lipid loading (scavenger receptor-mediated uptake and HDL-mediated efflux) in both cell types in response to oxidized LDL
- Analysis of VSMC transformation into macrophage-like cells
- Female primary VSMC will be utilized as the *Myh11* promoter essential for ADAM17 deletion in smooth muscle cells is Y chromosome-linked and only in males (this will support the male VSMC lipid loading and transformation data)

3. Defining the efferocytotic capacity of macrophages and VSMC in response to ADAM17 deficiency.

- Quantify ability of ADAM17-null macrophages and VSMC to bind apoptotic Jurkat cells
- Analyze MerTK expression in response to oxLDL and inflammatory stimuli in macrophages

CHAPTER 2

MATERIALS AND METHODS

2.1 Animals

Low-density lipoprotein receptor (LDLR) null mice were purchased from Jackson laboratory and were used to breed our experimental mice models. *Ldlr*$^{-/-}$ mice were bred with mice genetically manipulated with the flox sequence flanking the *Adam17* gene to generate *Ldlr*$^{-/-}$/*Adam17*$^{flox/flox}$ mice. Next, these mice were bred with mice expressing a MerCreMer recombinase enzyme under the control of *Myh11* promoter, allowing conditional deletion of *Adam17* in smooth muscle cells (SMC), giving rise to the *Ldlr*$^{-/-}$/*Adam17*$^{flox/flox}$/*Myh11*$^{cre/ERT2}$ (*Ldlr*$^{-/-}$/*Adam17*$^{SMC)}$. Our control groups include the *Ldlr*$^{-/-}$and *Ldlr*$^{-/-}$/*Adam17*$^{flox/flox}$. All mice are of the C57BL/6 genetic background and the mouse colonies are maintained at the University of Alberta Animal Facility in specific pathogen-free (SPF) and viral antibody-free (VAF) facilities. All experiments were performed in accordance with ARRIVE (Animal Research: Reporting of *in vivo* Experiments), University of Alberta ACUC (Animal Care and Use Committee), and CCAC (Canadian Council of Animal Care) guidelines.

Table 2.1 Control and Experimental Mice Genotypes

Genotype	Description
Ldlr$^{-/-}$	LDLR control
Ldlr$^{-/-}$/*Adam17*$^{f/f}$	Flox control
Ldlr$^{-/-}$/*Adam17*$^{f/f}$/*Myh11*$^{Cre/ERT2}$	Smooth Muscle Cell KO
Ldlr$^{-/-}$/*Adam17*$^{f/f}$/*Lyz2*^{Cre}	Macrophage KO (Breeding)

2.2 Genotype Verification

Tail clippings were used for DNA extractions followed by polymerase chain reaction (PCR) to verify the genetic background of individual mice post-breeding. Tails were placed in 175µL of tail digestion buffer (50mM Tris pH 8.0, 100mM EDTA pH 8.0, 100mM NaCl, and 1% SDS) and 6µL of Proteinase K (Thermo Scientific™ EO0491) overnight in 1.5mL Eppendorf tubes. Briefly, tails were treated with NaCl to salt out protein, and centrifuged at 14, 000 rpm. The supernatant containing genetic material was precipitated with isopropanol and centrifuged at 14, 000 rpm and finally washed and spun again with 70% ethanol. DNA pellets were dissolved in 50µL of TE buffer (10mM Tris HCl and 0.1 mM EDTA) and used directly for PCR. Master mix (Thermo Scientific™ F-170) was used for constituting 80% of the total volume for each PCR reaction, and 8% of each. Double-distilled water (ddH_2O) was used to bring PCR mix up to the final volume (15-32% depending on the number of primers required for each gene) of 30µL. Next, 2µL of DNA sample was added to each PCR mix and subjected to the corresponding PCR program on a Bio-Rad S1000™ Thermal Cycler. Agarose gel electrophoresis (1% agarose in 1x TAE) was used to determine fragment sizes along with appropriate controls and Gene Ruler 100 base pair (bp) DNA ladder (Thermo Scientific™ SM0243) and visualized by an ImageQuant LAS 400 system (GE Healthcare).

Table 2.2 Primer Sequences for *Ldlr*, *Adam17*, and *Myh11* PCR Reactions

Primer	Sequence 5' ⟶ 3'	Type	Gene
19799 Common	TAT GCA TCC CCA GTC TTT GG	Forward	
19800 Wild type	CTA CCC AAC CAG CCC CTT AC	Reverse	*Ldlr*
oIMR7770 Mutant	ATA GAT TCG CCC TTG TGT CC	Reverse	
13799	TCC CCC AGC TAG ATT GTT TG	Forward	*Adam17*
13800	AGG ACC CAG GTT CAG TTC CT	Reverse	
12026	TGA CCC CAT CTC TTC ACT CC	Transgene Forward	
12028	AGT CCC TCA CAT CCT CAG GTT	Transgene Reverse	*Myh11-cre/ERT2*
21165	CAG CCA ACT TTA CGC CTA GC	Internal Positive Control F.	
21167	TCT CAA GAT GGA CCT AAT ACG G	Internal Positive Control R.	

Table 2.3 PCR Program Cycles for *Ldlr*, *Adam17*, and *Myh11*

Ldlr	*Adam17* and *Myh11-cre/ERT2*
i. 94°C 8min	**i.** 94°C 8min
ii. 94°C 20 sec	**ii.** 94°C 20 sec
iii. 65°C 30 sec -0.5° C/cycle	**iii.** 65°C 30 sec -0.5° C/cycle
iv. 68°C 15 sec	**iv.** 68°C 40 sec
v. Go to ii, 10 times	**v.** Go to ii, 10 times
vi. 94°C 15 sec	**vi.** 94°C 15 sec
vii. 60°C 30 sec	**vii.** 60°C 30 sec
viii. 72°C 40 sec	**viii.** 72°C 40 sec
ix. Go to vi, 28 times	**ix.** Go to vi, 28 times
x. 72°C 2min	**x.** 72°C 2min
xi. 4°C hold	**xi.** 4°C hold

2.3 PCR-Mediated Detection of *Adam17* Deletion in Mice

DNA was extracted by tail clippings as previously described and used for detection of *Adam17* deletion post-TMX treatment *in vivo* by PCR. Primers were obtained from Integrated DNA Technologies, Inc. and PCR Master Mix composed as previously described. An "*Adam17* flox" and "*Adam17* null" PCR program was run for each sample. The PCR products were then run on agarose gels as previously described and bands were visualized via ImageQuant LAS 400 system (GE Healthcare). Null bands (indicating *Adam17* gene excision) were found at 400 bp, floxed *Adam17* at 1000bp, and wild-type *Adam17* at 850bp.

Table 2.4 Primer Sequences for *Adam17* Flox and Null PCR Reactions

Primer	Sequence 5'⟶ 3'	Type
ALEA 287597799	GGG AGA GCC ACA CCT TGA CC	Null Reaction
S13 287597800	ATG TTC CCC CAG CTA GAT TGT TTG CC	Common
A9 287597801	TAC TGG TGG GGA GGG GGA GAG ATT ACG AAG GC	Flox Reaction

Table 2.5 PCR Program Cycles for *Adam17* null and flox Reactions

***Adam17* null**	***Adam17* flox**
i. 94°C 4min	**i.** 94°C 4min
ii. 94°C 30 sec	**ii.** 94°C 30 sec
iii. 71°C 45 sec	**iii.** 66°C 45 sec
iv. 72°C 60 sec	**iv.** 72°C 60 sec
v. Go to ii, 35 times	**v.** Go to ii, 35 times
vi. 72°C 2min	**vi.** 72°C 2min
vii. 4°C hold	**vii.** 4°C hold

2.4 Mouse Model for Atherosclerosis

Using our transgenic C57BL/6 mice, we carried out a protocol for induction of atherosclerosis which was applied to all genotypes. To induce genetic ablation of *Adam17* in VSMCs, tamoxifen (TMX) (Sigma-Aldrich® 10540-29-1) was injected at 8 weeks of age dissolved in olive oil (commercially bought) for 5 consecutive days with a dose of 100mg/kg/day using a 1mL syringe and 27G x ½ Precision Glide™ Needle. TMX induces Cre-mediated flox cleavage in *Myh11* expressing VSMC, allowing for conditional deletion of *Adam17*. HCD

feeding was initiated at 10 weeks of age; 1-week post-TMX to allow for recovery or continued regular chow diet (21% protein, 11.3% fat, and 53.4% carbohydrate) for 3 or 5 months. HCD (Inotiv TD.96121) consists of 17.3% protein, 48.5% carbohydrate, 21.2% fat, and ~1.3% cholesterol. HCD was irradiated and replaced on a weekly basis. Mice were weighed weekly to assess and ensure weigh gain throughout the course of high cholesterol feeding.

Figure 2.6 Atherosclerosis Mouse Model, Tamoxifen, and High Cholesterol Feeding

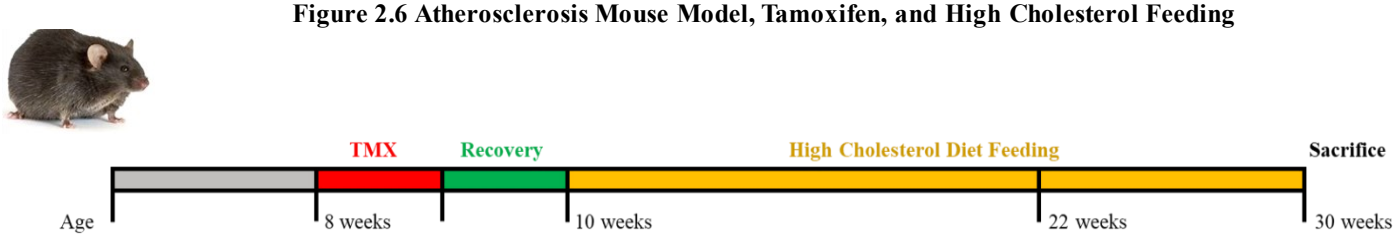

Abbreviations: TMX, tamoxifen.

Figure 2.7 Animal Regular Chow Diet Formula

Ingredient	%
Protein	21.0
Fat	11.3
Nonfibrous carbohydrate	53.4
Fibre (Crude)	4.6
Minerals (Ash)	5.9

Table 2.8 Animal High Cholesterol Diet Formula

Ingredient	g/Kg
Casein	195.0
DL-Methionine	3.0
Sucrose	341.46
Corn Starch	150.0
Anhydrous Milkfat	210.0
Cholesterol	12.5
Cellulose	39.0
Mineral Mix, AIN-76 (170915)	35.0
Calcium Carbonate	4.0
Vitamin Mix, Teklad (40060)	10.0
Ethoxyquin, antioxidant	0.04

2.5 Tissue and Plasma Collection

Mice of each genotype were euthanized by removal of the heart under isoflurane gas at the 3-month or 5-month time points. For plasma collection, two incisions were made on each carotid artery while the mouse was anesthetized in a supine position. A 1mL syringe was used to collect 500µL of blood from each mouse, transferred to 1.5mL Eppendorf tube, then centrifuged at 2000 x g for 15 minutes. The plasma (supernatant) was then carefully pipetted out into a new tube and stored at -80°C for future analyses. Hearts were excised from each experimental mouse genotype by cutting the aorta as close as possible to the base of the heart. The heart was then placed in phosphate-buffered saline (PBS) to expel residual blood, and in 1M KCl to induce diastole, then finally placed in 10% formalin for storage. Aortas from all genotypes were excised by carefully holding the aortic arch with forceps and cutting down along the spine until the iliac bifurcation. Kidneys were removed. The aorta was then placed in a glass 10cm plate coated with

black silicon elastomer plate (SYLGARD™ 170, Dow Corning, 1696157) containing ice-cold PBS. Perivascular fat was removed using forceps and iris scissors. Minutien pins (Fine Science Tools, 26002-20) were used to pin the aorta in place under a Zeiss Stemi 305 dissecting microscope. Cleaned aortas of mice euthanized at the 3 and 5-month time point were then placed in 10% formalin for plaque area quantification or flash-frozen for molecular analyses. Aortas from the 3-month time point were used for optimal cutting temperature (OCT)- embedding of excised segments of the vessel in vinyl specimen cryomolds (Tissue-Tek® 4566) then flash-frozen in liquid nitrogen and stored in -80°C for future molecular analyses.

2.6 *En face* Plaque Visualization and Quantification

Cleaned aortas from the 5-month time point stored in 10% formalin overnight post-euthanasia were stained with Oil Red-O (Sigma-Aldrich® O0625) solution to visualize lipid deposition along the inner vessel. Aortas were first washed twice for 5 minutes in 78% methanol, then incubated with 0.2% Oil Red-O (ORO) dissolved in 70% methanol and 30% 1M NaOH for 1 hour. After incubation, aortas were washed twice again with 78% methanol in new 1.5mL Eppendorf tubes. Next, aortas were transferred to the elastomer plates and pinned down with minutien pins and cut longitudinally to butterfly open the vessel wall, making sure to keep plaques intact. The aorta was then pinned down to expose the luminal surface, and a ruler was placed parallel to the tissue for reference. Images were captured with an iPhone 8 and quantified for plaque area via Image-Pro Plus software (Media Cybernetics). Plaque area was defined as the total ORO^+-area (red) as a fraction of total luminal area. Aortas were quantified separately based on thoracic area (aortic root to diaphragm) and abdominal area (diaphragm to iliac bifurcation) and expressed as a percentage. We studied a larger group of Ldlr-/-Adam17f/f mice because we used them as controls in the same cages as other types of mice (such as those with ADAM17

knocked out in endothelial and fibroblast cells). We measured and compared the plaque area in all these mice.

2.7 Aortic Valve Fixing, Processing, and Plaque Quantification

Hearts stored in 10% formalin were cut parallel to the base of the heart using a razor blade, removing the apical portion just under each atrium. The heart was then placed into plastic molds (Tissue-Tek® 4557) with a biopsy foam pad (Fisherbrand™ 22038221) to keep it secure and placed in 10% formalin for paraffin-embedding at the histology core of the University of Alberta. The heart was then sectioned from the apical side (5µm thick) continuously until three leaflets of the valve were observed under a microscope. Sections were collected from this point until the tricuspid structure was no longer visible. Sections were then stained with hemotoxylin and eosin (H&E) and Gomori Trichrome to visualize plaque structures. Plaque area was determined via Image-Pro Plus software by quantifying the area of the plaque and expressing it as a percentage of the total aortic ring. Necrotic cores were quantified by measuring the area of the plaque devoid of H&E staining and dividing it by the area of the lesion in which it was found. Necrotic core is expressed as a percentage of the lesion. Lesions lacking a necrotic core were assigned a value of zero.

2.8 Immunofluorescent Staining

i.) Aortic OCT-section staining

OCT-fixed aortic segments were processed and sectioned (5µm thick) onto glass slides at the histology core of the University of Alberta and stored at -80°C until ready to use. For immunofluorescent staining, the cryosection slides were left to thaw for 10 minutes at room temperature (RT) and washed once in PBS. Then the slide was fixed in 4% paraformaldehyde

(PFA) pH 7.4 for 15 minutes at RT and washed three times with PBS in 5-minute intervals. The sections were then permeabilized in 0.2% Triton X-100 for 10 minutes and washed again with the same procedure. At this point, each section on the slide was surrounded with a hydrophobic pen to contain the following solutions. The sections were then blocked in 1% bovine serum albumin (BSA) in PBS for 30 minutes. Primary antibody(s) were diluted in a 1:200 ratio in 1% BSA and stored overnight in the 4°C cold-room. The next day, slides were washed three times with 0.1% PBS-T. Fluorophore-conjugated secondary antibodies (diluted 1:400 in 1% BSA) appropriate for the specific primary antibody used were then incubated on the slides for 1 hour. Sections were then washed three times with 0.1% PBS-T and mounted with ProLong™ Gold antifade reagent with DAPI and a cover slip (Thermo Scientific™ P36931) and imaged under a fluorescent microscope (Olympus IX81).

ii.) in vitro cell staining

Cell cultures were grown on Nunc™ Lab-Tek™ 4 chambered slides (Thermo Scientific™ 154526) for subsequent staining. Similarly, to the procedure mentioned above, slides were fixed in 4% PFA, permeabilized with 0.2% Triton X-100, blocked with 1% BSA, and incubated with primary antibodies (1:200 dilution in 1% BSA) overnight at 4°C. The next day, slides were washed and incubated with the appropriate secondary antibodies (1:400 dilution in 1% BSA) for hour. After a final wash, the chamber was removed with a plastic removal tool and the slide was mounted with DAPI and a coverslip. The slides were then imaged under a fluorescent microscope (Olympus IX81).

2.9 Primary Mouse Smooth Muscle Cell Isolation and Culture

Ldlr$^{-/-}$ mice aged 3-4 weeks old were used for isolation of primary vascular smooth muscle cells. Each isolation used 3-5 mice to achieve a suitable yield to culture. Each mouse was euthanized by cervical dislocation while anesthetized under isoflurane gas. The body was sprayed with 70% ethanol and placed down in a supine position. All tools used were disinfected with 70% ethanol and left in a Germinator™ 500 for 30 seconds prior to working with the mice. The abdominal cavity was opened all the way to the chest cavity and the whole aorta was excised and rapidly cleaned of adipose and connective tissue in ice-cold, sterile PBS (100U/mL penicillin, 100µg/mL streptomycin, and 250 ng/mL Fungizone) in a black elastomer plate under a dissecting microscope. The aorta was then incubated in digestion buffer (2mg/mL BSA, 1mg/mL collagenase type II, 0.774 U/mL elastase, and 1mg/mL soybean trypsin inhibitor in HBSS) at 37°C for 10 minutes in a 35mm culture plate. The aorta was then transferred to fresh 1x Hanks' balanced salt solution (HBSS) in a 35mm culture plate where the adventitial layer was carefully removed using two forceps. The stripped aorta was then cut with a razor blade into 2mm x 2mm pieces in a 10cm tissue culture plate and then transferred into a second 35mm culture plate with digestion buffer for 2 hours in a 37°C Heracell™ 150 (Thermo Scientific™ 50116048) humidified incubator until cells were visibly sloughing off the cut pieces. The enzyme solution was deactivated by adding an equal volume of Dulbecco's modified eagle medium (DMEM, Gibco™ 11330032) supplemented with 20% fetal bovine serum (FBS, Canadian Origin, 12483020) (DMEM/F-12). The solution was then placed in a 5mL tube and centrifuged at 300 x g for 5 minutes to pellet the cells and then resuspended in DMEM/F-12 (with 100U/mL penicillin, 100µg/mL streptomycin, and 20% FBS). The cells were plated on a 35mm culture dish coated with 0.1% gelatin and left to grow in humidified incubator with 5% CO_2 at 37°C.

Cell culture media was replaced with fresh media (10% FBS) after 48 hours. Cells were treated with 15nM siRNA (control or *Adam17* siRNA) with Lipofectamine™ RNAiMAX Transfection Reagent (Thermo Scientific™ 13778075) for 6 hours. Passages 3-5 were used for all experiments and serum-deprived (0.5% FBS) for 24 hours prior to any treatments. Oxidized LDL (oxLDL) was used as an atherogenic stimuli at 20µg/mL for 72 hours to induce foam cell formation. There are other forms of modified LDL that are relevant to atherosclerosis *in vivo*, though for the purposes of our study, oxLDL is a suitable atherogenic model to study the manipulation of scavenger receptors and efflux transporters. These concentrations for VSMC are based on previous studies from our lab.[159]

2.10 Primary Bone Marrow-Derived Macrophage Isolation and Culture

Ldlr$^{-/-}$ mice used for isolation of BMDM were euthanized by cervical dislocation while anesthetized by isoflurane and soaked in 70% ethanol prior to dissection. All tools were disinfected with 70% ethanol and left in a Germinator™ 500 for 30 seconds prior to working with the mice. After removing the skin, the legs were removed with forceps and scissors into a 10cm culture plate with DMEM. The muscles were removed with a razor blade by gently scraping along the bone, and the femurs and tibia were left to soak for 5 minutes in a dish of 70% ethanol in a Nuaire©-425-400 biosafety cabinet. The bones were then transferred to a third 10cm dish with 1x PBS and the marrow was flushed out of the bones using a 10mL syringe and 25-guage needle into a 10mL Falcon® tube and centrifuged at 300 x g for 5 minutes. The supernatant was discarded, and the pellet was resuspended in DMEM supplemented with 10% FBS, 30% L929 conditioned media, and 1% Penicillin/Streptomycin (P/S) (Gibco™ 15140122) and passed through a cell strainer (VWR® 76327-102) then plated onto a 10cm culture dish (VWR® 10062-880) and grown in a humidified incubator with 5% CO_2 at 37°C for one week. Cell culture media

was replaced with fresh media (10% FBS, 20% L929 conditioned media) after 48 hours. Cells were treated with 15nM siRNA (control or *Adam17* siRNA) with Lipofectamine™ RNAiMAX Transfection Reagent (Thermo Scientific™ 13778075) for 18 hours. Passage 1 cells were used for all experiments and serum-deprived (0.5% FBS, 20% L929 conditioned media) for 24 hours prior to any treatments. Oxidized LDL (oxLDL) was used as an atherogenic stimuli at 10µg/mL for 48 hours. The oxLDL concentration and duration is reduced for macrophages as they readily take up this atherogenic stimuli. Therefore, to prevent unnecessary expenditure and time in culture, cells are analyzed after 48 hours with half the oxLDL content as in VSMC. These concentrations for BMDM have been used by previous members of our laboratory.[159]

2.10.1 L929 Conditioned Media Preparation

L929 conditioned media containing colony-stimulating factor (CSF-1) is required for macrophage proliferation during isolation and growth of bone-marrow derived macrophages (BMDM). L929 cells (ATCC, C3H/An) were grow in DMEM (Gibco™ 11995065) on 10cm culture plates until confluence. The media was then collected after 3 days into a 10mL syringe and filter through a 0.22µm filter (Millex® SLGSR33SS) into 50mL Falcon® tubes which were stored at -20°C.

2.11 RNA Extraction from Cultured Cells

VSMC or BMDM cultured in 6-well plates (VWR® CA62406-163) were washed twice with ice-cold 1x PBS. On ice, 500µL of Invitrogen TRIzol® Reagent (Cat. 1559608) was added to each well and the cells were scraped and transferred to 1.5mL RNase free Eppendorf tubes, vortexed thoroughly, and centrifuged at 12, 000 x g for 10 minutes at 4°C. The supernatant was

transferred to new tubes and 200µL of chloroform was added to each tube and shaken vigorously for 15 seconds, then incubated at RT for 3 minutes. The tubes were then centrifuged at 12, 000 x g for 15 minutes at 4°C. The upper colourless phase was transferred to new tubes, and 500µL of isopropanol was added and stored in -20°C for one week. The tubes were centrifuged again and washed with 75% ethanol. The tubes were centrifuged a final time at 7, 500 x g for 5 minutes at 4°C and the pellet was air dried, then dissolved in 12µLof RNase free water. A NanoDrop™ 2000/2000c spectrophotometer was used to quantify total RNA concentration using 1.5µL of sample.

2.12 Quantitative Real-Time PCR

Quantified RNA samples from cell cultures were reverse transcribed into complementary deoxyribonucleic acid (cDNA). Briefly, one microgram of total RNA and 1µg/µL Random Hexamers (Invitrogen™ 48190-011) were used for first strand synthesis using SuperScriptII (Invitrogen™ 18064-014) and a PCR machine running the RT70 program (70°C for 10 minutes). Reaction mix per sample is listed in **Table 2.5.** cDNA is then produced by RT40 program (40°C for one hour) at a concentration of 50ng/mL and stored in -20°C. cDNA was diluted by 100x and a LightCycler 480 II system (Roche©) and Probes Master kit (Roche© 04887301001) were used for TaqMan RT-PCR. Probes and assay IDs of all genes are listed in **Table 2.6.** Brain or heart tissues were used to create standards ranging from 0.0625ng/µL to 2ng/µL. Samples were loaded into a 384-well white plate (Roche© 04729749001) and covered with a clear adhesive seal.

Table 2.9 Reaction Mix per Sample for cDNA Synthesis

Stock Concentration	Component	Final Concentration	Invitrogen™ Cat. #
5X	RT buffer	-	18064-14
0.1M	Dithiothreitol	10mM	18064-14
100mM	Dinucleotide triphosphate	5mM	10297-018
40U/µL	RNaseOUT	2U/µL	10777-019
200U/µL	SuperScriptII	10U/µL	18064-14

Table 2.10 TaqMan RT-PCR Probes, Alias, and Assay IDs

Alias	Gene Name	Assay ID
18S	18 Svedberg ribosomal RNA	Mm04277571_s1
Adam17	A disintegrin and metalloproteinase 17	Mm01231071_m1
Abc-A1	ATP-binding cassette transporter A1	Mm00442646_m1
Abc-G1	ATP-binding cassette transporter G1	Mm00437390_m1
Srb1/Scarb1	Scavenger receptor class B type 1	Mm00450236_m1
Olr1	Oxidized low-density lipoprotein receptor 1	Mm00454582_m1
Cd36	Cluster of Differentiation 36	Mm00432403_m1
Sra1/Msr1	Macrophage scavenger receptor 1	Mm00446214_m1
MerTK	Proto-oncogene tyrosine-protein kinase Mer	Mm00434920_m1
Tnfα	Tumor necrosis factor alpha	Mm00443258_m1
Il1β	Interleukin 1 beta	Mm00434228_m1
Il6	Interleukin 6	Mm00446190_m1
Il10	Interleukin 10	Mm01288386_m1
Svep1	Sushi, von Willebrand factor type A, EGF and pentraxin domain containing 1	Mm01346904_m1

2.13 Protein Extraction from Cultured Cells

VSMC or BMDM cultured in 6-well plates (VWR® CA62406-163) were washed twice with ice-cold 1x PBS. On ice, 100µL CelLytic™ M lysis buffer (Sigma-Aldrich® C2978) containing 20µM BB-2516 and 10mM 1,10-pheanthrolinewas, and a 1:100 ratio of Phosphatase Inhibitor Cocktail 2 (Sigma-Aldrich® P5726), Protease Inhibitor Cocktail 3 (Sigma-Aldrich® 539134), and Phosphatase Inhibitor Cocktail 4 (Sigma-Aldrich® 524628), added to each well

and the cells were scraped and transferred to 1.5mL Eppendorf tubes, vortexed, and placed on ice. The cells were then snap-frozen with methanol and dry ice several times before centrifugation at 12, 000 x g for 10 minutes at 4°C, and the supernatant was collected into new tubes. DC™ Protein Assay Kit (Bio-Rad 5000112) was used to determine protein concentration in 96-well plates and absorbance was measured at 750nm.

2.14 Western Blotting

About 20µg of protein was run in each lane of a 6 or 10% SDS-polyacrylamide gel (Bio-Rad 1610156) prepared with suitable protein ladders (Thermo Scientific™ 26619 or 26616) for about 1.5 hours at 120 volts. The protein was then transferred to a polyvinylidene fluoride (PVDF, Pierce™ 24585) membrane by wet transfer at 250 mA for 2 hours and 10 minutes. The membrane was then blocked in 3% BSA (in 1x TBS, pH 7.4) for 30 minutes at RT. Primary antibodies were incubated at dilutions of 1:1000 in 3% BSA for most antibodies overnight at 4°C. The membranes were then washed three times with 1x TBST for three minutes each and incubated with HRP-linked secondary antibodies (1:5000) in 3% BSA for one hour at RT. The blots were washed again before incubating with Clarity Max™ Western ECL Substrate (Bio-Rad 1705062) to expose target proteins. An ImageQuant LAS 400 system (GE Healthcare) was used to expose the target bands under the chemiluminescence setting. Band intensity was quantified using ImageJ software (NIH, Java™). The Pierce™ Reversible Protein Stain Kit for PVDF Membranes (Cat. 24585) was used for MEMCODE protein staining (loading control), destaining, and stripping the blots. Restore™ Western Blot Stripping Buffer was used according to manufacturers instructions. Briefly, Stripping Buffer was warmed up to 37°C in a water bath and incubated with membranes for 15-20 minutes.

2.15 Jurkat Cell Culture

Clone E6-1 of the Jurkat-FHCRC cell line (ATCC, TIB-152) were grown in RPMI Medium 1640 (Gibco™ 11875093) supplemented with 10% FBS and 1% P/S (Jurkat complete media) in 25cm^2 cell culture flasks (Nest® Scientific 707001). Cells were left to grow in 5-7mL of media and replaced every 48 hours and cell density was maintained between 2 x 10^5 and 1 x 10^6 cells/mL by counting via a hemocytometer (Marienfeld© 0630030).

2.15.1 Staurosporine-Induced Apoptosis

Jurkat E6-1 cells were cultured as previously described in complete RPMI media. 1 x 10^6 cells were plated onto four 35mm culture dishes in 4mL volume. Each plate was treated with either 0, 2, 5, or 10µM Staurosporine A for one hour in a humidified incubator. The cells were then transferred to 5mL tubes and centrifuged at 500 x g for 5 minutes, and the pellets were resuspended in 100µL of CelLytic buffer with inhibitor cocktail and placed on ice for 30 minutes with rigorous vortexing every 10 minutes. The tubes were then centrifuged at 12, 000 x g for 10 minutes at 4°C, and the supernatant was collected into new tubes. DC™ Protein Assay Kit (Bio-Rad 5000112) was used to determine protein concentration in 96-well plates and absorbance was measured at 750nm. 30µg of protein from each sample was run on each lane of a 10% SDS-gel, transferred to a PVDF membrane, and blotted for cleaved caspase-3 (17/19 kDa), stripped, and then blotted for full length caspase-3 (35 kDa) as a proxy for apoptosis.

2.16 Efferocytosis

These experiments were done by following a protocol by Matthew C. Gage titled "*Measuring Apoptotic Cell Engulfment (Efferocytosis) Efficiency*".[160] However, instead of using UV light to induce apoptosis in Jurkat cells, we used 5µM Staurosporine A (Abcam© ab120056)

treatment for one hour in a humidified incubator. In brief, Jurkat cells were centrifuged at 500 x g for 5 minutes and resuspended at about 2 x 10^6 cells/mL onto a 10cm culture dish. Then, 10µL of 1mg/ml Calcein-AM (Invitrogen™ C1430) dissolved in DMSO was added to the dish to fluorescently label the cells and left to incubate for 2 hours at 37°C and 5% CO_2. The cells were then collected in a 15mL tube and washed several times with warm 1x PBS and centrifugation, and then resuspended in 10mL of Jurkat complete media onto a new 10cm dish. The cells were then incubated with saline (for controls) or 5µM Staurosporine A (in DMSO) for one hour in the incubator to induce apoptosis, as measured by caspase-3 cleavage. At this point, siRNA treated macrophages (or VSMC) were already plated onto 4 chambered slides. The Jurkat cells were then collected and resuspended in either macrophage or VSMC complete media and 1 x 10^5 cells were added to each well of the 4 chambered slides containing the siRNA treated phagocytic cells. The cells were left to incubate for various time points, and then were immediately washed thoroughly with 1x PBS 5 times to wash off any loosely bound Jurkat cells. Cells were then fixed in 4% PFA pH 7.4, for 15 minutes. The immunofluorescence procedure as mentioned previously was utilized here to counterstain the phagocytic cells (CD68 for macrophages and calponin for VSMC) to assist in visualization. Cells were then imaged under a fluorescent microscope at 200x and 400x magnification and efferocytosis efficiency was quantified by counting the number of Jurkat cells (green) as a fraction of the total number of phagocytic cells (red) and expressed as a percentage.

2.17 Histological Staining

Oil Red-O staining of primary cultured cells was utilized to visualize neutral lipids and quantify lipid loading in response to oxLDL treatment. VSMC were treated with 20µg/mL oxLDL for 72 hours and BMDM with 10µg/mL for 48 hours. After siRNA (control or *Adam17*

siRNA) and insult (saline or oxLDL) of cultures in 4 chambered slides, the cells were rinsed twice with 1x PBS and fixed in ice-cold 4% PFA for 20 minutes. The cells were rinsed twice and left to air dry for 2-3 minutes, then incubated with 0.5% ORO solution in isopropanol mixed in a 3:2 ratio with ddH_2O and filtered through a 0.22-micron filter for 15 minutes at RT. The cells were then thoroughly rinsed 5-6 times with ddH_2O to remove any non-specific staining. A 1:2 dilution of Harris Hematoxylin (Sigma-Aldrich® HHS16) solution in ddH_2O for about 30 seconds was used as a background stain. The cells were rinsed twice and mounted with Histomount (Thermo Scientific™ 008030) and cover slip and imaged under a Leica brightfield microscope at 400x and 630x magnification. Lipid content was quantified via Image-Pro Plus software by measuring red pixel count (ORO^+ stain) and normalizing to cell count per frame (field of view of an image taken by the fluorescent microscope at 400x magnification).

2.18 Plasma Lipoprotein Cholesterol Measurements

Plasma samples were extracted from mice as previously described, aliquoted, and stored in -80°C until required. Plasma from 5-month regular chow and HCD fed mice from *Ldlr*$^{-/-}$ and *Ldlr*$^{-/-}$*/Adam17*^{SMC} genetic backgrounds were analyzed for lipoprotein cholesterol fractions at the Lipidomics Core Facility (Faculty of Medicine and Dentistry at the University of Alberta) by fast-protein liquid chromatography (FPLC). Briefly, 12µL of EDTA-treated plasma was injected via autosampler into an Agilent 1200 HPLC instrument with a Superose 6 Increase 10/300 GL gel-filtration FPLC column, separating the intact lipoproteins by size. An in-line assay for total cholesterol (Cholesterol-SL reagent, Sekisui Diagnostics, Charlottetown, Canada) was performed at 37°C using a post-column reaction and products measured in real-time at 505nm and analyzed via Agilent Chemstation software. The fluorescence of quinonimine is used to calculate the initial cholesterol content using the following equation:

Cholesterol Esters → Cholesterol + Fatty Acids CO Cholesterol + O_2 →

Cholest-4-ene-3-one + H_2O_2 Peroxidase 2 H_2O_2 + 4-aminoantipyrine + p-hydroxybenzoate →

Quinonimine (505nm) + 4 H_2O

2.19 Cholesterol Efflux Assay

Cholesterol Efflux Assay Kit was performed as per manufacturer's instructions (Sigma-Aldrich® MAK192). BMDM and VSMC treated with siRNA (control or *Adam17*) were detached by 0.25% trypsin (Sigma-Aldrich® T4049) incubation for 2 minutes, stopped with complete media, and centrifuged at 300 x g for 5 minutes. The cells were resuspended in complete media and seeded onto 96-well tissue culture plates (Sigma-Aldrich® P8366) at a density of 1 x 10^5 cells/well and left to attach in a humidified incubator at 37°C and 5% CO_2 overnight. Briefly, the cells were labelled with FBS-free media containing the Labeling Reagent for 1 hour covered in tin foil in the incubator. The cells were then incubated for 12-16 hours in Equilibration Buffer in the incubator protected from light. Human serum (Sigma-Aldrich® H4522) containing 40% Serum Treatment Reagent was incubated for 20 minutes on ice and centrifuged for 10 minutes at 9000 x g at 4°C to be used as the cholesterol acceptor. The supernatant was then diluted 50x in FBS-free media and added to the cells for 4 hours. The cell media was then transferred to a white 96-well plate with opaque bottoms and fluorescence was measured (F_m, λ_{Ex} = 485/ λ_{Em} = 523nm) in endpoint mode. The cell monolayer was solubilized with Cell Lysis Buffer and shaken for 30 minutes at RT, then transferred to a fresh white 96-well plate with opaque bottoms and fluorescence was measured (F_c, λ_{Ex} = 485/ λ_{Em} = 523nm) in endpoint mode. The following formula was used for calculating efflux capacity, C:

$$C = [Fm/ (Fm + Fc)] \times 100\%$$

Fm = fluorescent intensity of supernatant

Fc = fluorescent intensity of cell lysate

2.20 Scavenger Receptor-Mediated Endocytosis Quantification

1,1'-Dioctadecyl-3,3,3',3'-Tetramethylindocarbocyanine Perchlorate (Dil)-conjugated oxLDL (Invitrogen™ D282) was used to measure scavenger receptor-mediated endocytosis in primary cultured cells. VSMC and BMDM in 4 chambered slides (pre-treated with siRNA) were incubated with 10μg/mL Dil-oxLDL for 24 hours in minimal media. Slides were rinsed with 1x PBS 3 times and fixed in 4% PFA for 15 minutes, then washed 3 times with 1x PBS for 3 minutes and mounted with coverslip and DAPI. Slides were imaged using the Cy3 filter on an Olympus IX81 fluorescent microscope at 200x and 400x magnification. Scavenger receptor-mediated endocytosis was quantified via ImageJ software by calculating red pixel integrated intensity (Dil-oxLDL$^+$ area) and normalized to DAPI count per frame (field of view of an image taken by the fluorescent microscope at 200x or 400x magnification).

2.21 Transfection of Cultured Cells

siRNA transfection of VSMC and BMDM were conducted in 6-well plates during sub confluence (5 x 10^4 cells/mL and 1 x 10^5 cells/mL, respectively) with Lipofectamine™ RNAiMAX Transfection Reagent in Opti-MEM Reduced Serum Medium (Gibco™ 31985070) as per manufacturers protocol. Cells were washed twice with 1x PBS before adding 15nM of

either control siRNA (Invitrogen™ 4390844) or *Adam17* siRNA (Thermo Scientific™ 4390771) for 6 hours in VSMC and 18 hours in BMDM. Cells were recovered with complete media overnight post-transfection.

2.22 Subcellular Fractionation of Cultured Cells

VSMC and BMDM were cultured in 6-well plates in a humidified incubator and treated with siRNA, then insulted with either saline or oxLDL as previously described, or IL-6/TNF-α (10ng/mL each) for 48 hours. Cells were then placed on ice and washed twice with ice-cold 1x PBS. Then, 50µL of RIPA buffer (50mM Tris-HCl pH 7.4, 150mM NaCl, and 1mM EDTA) containing 20µM BB-2516 and 10mM 1,10-pheanthrolinewas, and a 1:100 ratio of Phosphatase Inhibitor Cocktail 2 (Sigma-Aldrich® P5726), Protease Inhibitor Cocktail 3 (Sigma-Aldrich® 539134), and Phosphatase Inhibitor Cocktail 4 (Sigma-Aldrich® 524628) was added to each well, and three wells were pooled into one round-bottom microcentrifuge tube with a metal bead and each sample was homogenized with a TissueLyser II (QIAGEN) for 2 minutes at 25 Hz. The lysate was transferred to new 1.5mL Eppendorf tubes and centrifuged at 2900 rpm for 10 minutes at 4°C, and the supernatant containing the cytosolic and membrane fractions were further centrifuged at 20 000 x g for 30 minutes. The membrane fraction pellet was resuspended in 40µL of commercial RIPA buffer (Thermo Scientific™ 89900) with inhibitor cocktails and centrifuged a final time at 14 000 x g for 10 minutes. The supernatant was collected as the membrane fraction and quantified as previously described. Fractionation was verified by blotting for markers of nuclear (histone H3), cytosol (caspase 3), and membrane (TLR4) proteins.

2.23 Antibodies

All antibodies are listed in **Table 2.11.**

Table 2.11 List of Primary Antibodies with Dilution Factors and Application

Antibody	Catalogue No.	Supplier	Dilution/Application(s)
ADAM17	EHS008	Kerafast	1:2000/WB
ADAM17	ab39162	Abcam	1:200/IF
Calponin	ab46794	Abcam	1:200/IF
CD68	MCA1957GA	EMD Millipore	1:200/IF
Ly6B.2	MCA771GA	AbD Serotec	1:200/IF
MerTK	ab184086	Abcam	1:200/IF; 1:1000/WB

2.24 Statistics

Data was reported as Mean ± SEM (standard error of the mean). Graphs and statistical analyses were conducted on OriginLab® 2023 software. Comparison between two means was analyzed via unpaired student's t-test. Comparison between multiple groups involving one factor was analyzed via 1-way analysis of variance (ANOVA) followed by Bonferroni post hoc test. Comparison between multiple groups involving more than one factor was analyzed by two-way ANOVA followed by Bonferroni post-hoc test. Statistical significance was recognized at a p value less than 0.05.

CHAPTER 3

RESULTS

3.1 *In vivo Adam17* Deletion in Vascular Smooth Muscle Cells

ADAM17 was knocked-out in VSMC of *Ldlr*$^{-/-}$*/Adam17*^{SMC} mice via TMX-induced Cre recombinase expression under the *Myh11* promoter at 8 weeks of age. PCR reactions on the null (400 base pairs) and flox bands (1000 base pairs) were conducted on DNA extracts from tail clippings of *Ldlr*$^{-/-}$*/Adam17*$^{flox/flox}$ *and Ldlr*$^{-/-}$*/Adam17*^{SMC} **(Figure 3.1).** The flox bands were observed in both genotypes of mice, but the null band was only present in the *Ldlr*$^{-/-}$*/Adam17*^{SMC} mice, thereby demonstrating *Adam17* deletion at the DNA level.

3.2 *In vivo* ADAM17 Deletion in Vascular Smooth Muscle Cells

After 3 months, aortas from *Ldlr*$^{-/-}$*/Adam17*$^{flox/flox}$ *and Ldlr*$^{-/-}$*/Adam17*^{SMC} mice were OCT-embedded and stained for the cytoplasmic domain of ADAM17 and visualized via fluorescent microscopy **(Figure 3.2)**. ADAM17 was detected throughout the adventitia, medial, and intimal layers of the control mice, whereas in the *Ldlr*$^{-/-}$*/Adam17*^{SMC} mice, ADAM17 was markedly knocked-down, with minimal detection in the adventitial and intimal areas, which are comprised mainly of fibroblasts and endothelial cells, respectively. Therefore, our mice are validated to have VSMC-specific ADAM17 deletion at the protein level.

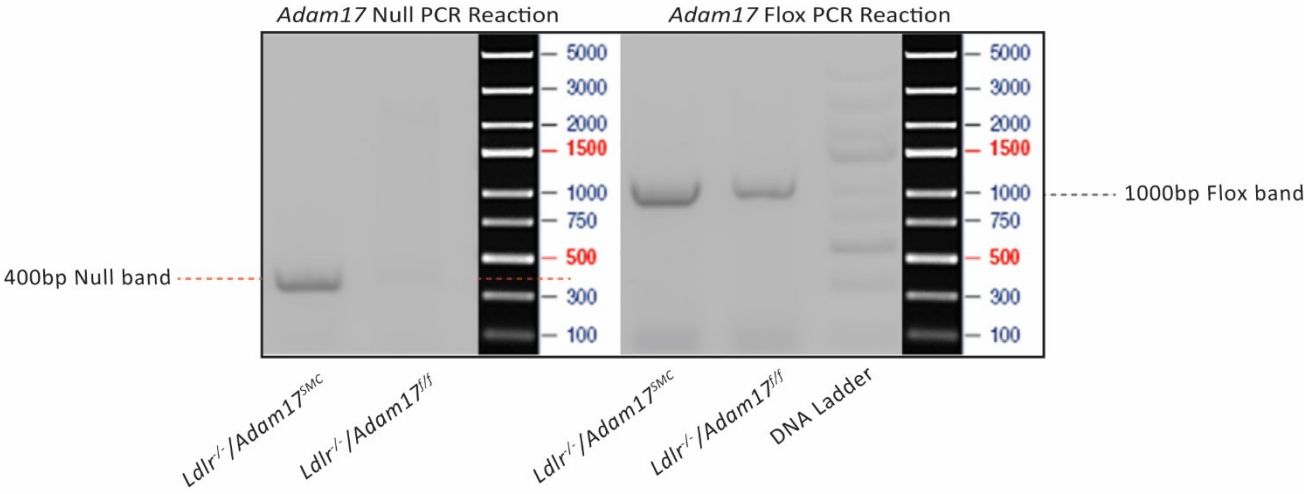

Figure 3.1 *Adam17* knock-out is detected in *Ldlr$^{-/-}$/Adam17^{SMC}* mice tail DNA extracts.

PCR reactions for the 'null' and 'flox' *Adam17* bands between *Ldlr$^{-/-}$/Adam17$^{f/f}$* and *Ldlr$^{-/-}$/Adam17^{SMC}* mice on DNA extracts from tail clipping samples. The flox bands observed in both genotypes are found at 1000 base pairs (bp), while the null band only present in the *Ldlr$^{-/-}$/Adam17^{SMC}* mice at 400 bp.

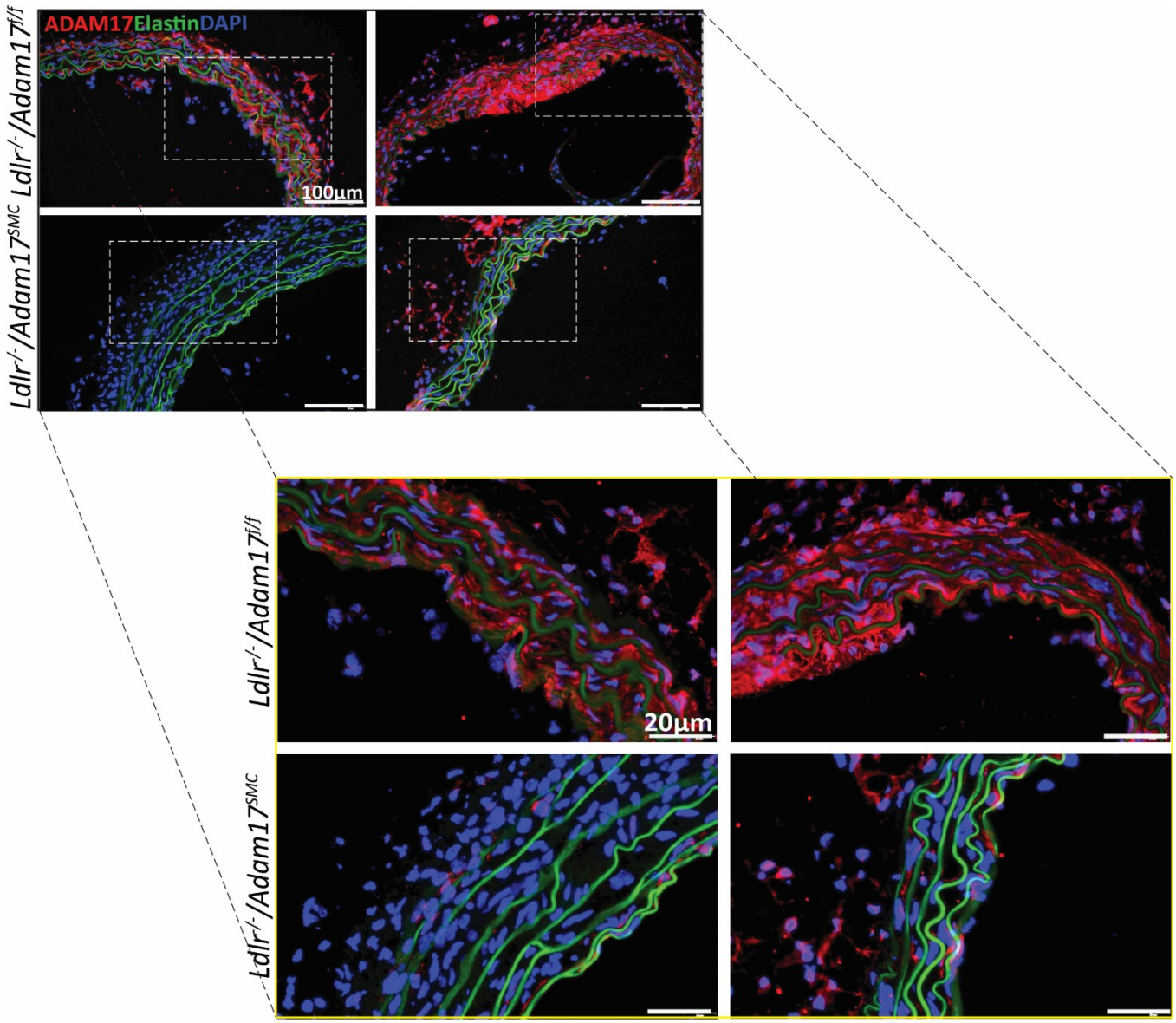

Figure 3.2 ADAM17 is knocked-out in smooth muscle cells of *Ldlr*$^{-/-}$/*Adam17*^{SMC} mice.

Representative immunofluorescent images of 5 µm OCT-embedded cryosections of aortic segments stained for ADAM17 (ab39162, red), elastin (autofluorescence, green), and nuclei (DAPI, blue) between control *Ldlr*$^{-/-}$/*Adam17*$^{flox/flox}$ and VSMC *Adam17*-null *Ldlr*$^{-/-}$/*Adam17*^{SMC} mice at 200x magnification (scale bars=100µm) and at 400x magnification (scale bars=20µm) showing ablation of ADAM17.

3.3 Weight Gain on High Cholesterol Diet

Mice were weighed weekly to ensure weight gain over the course of high cholesterol diet feeding. Both genotypes gained weight because of high cholesterol diet feeding **(Figure 3.3)**. The average starting weight of the *Ldlr*$^{-/-}$ mice was 25 grams (g) to a final weight of approximately 39g, and the *Ldlr*$^{-/-}$*/Adam17*^{SMC} mice started at an average weight of 20g to a final weight of approximately 36g. Two-ANOVA analysis determined no statistical significance between the means. Thus, a high cholesterol diet consisting of 1.3% cholesterol and 21.2% fat induces consistent weight gain in LDLR-deficient mice.

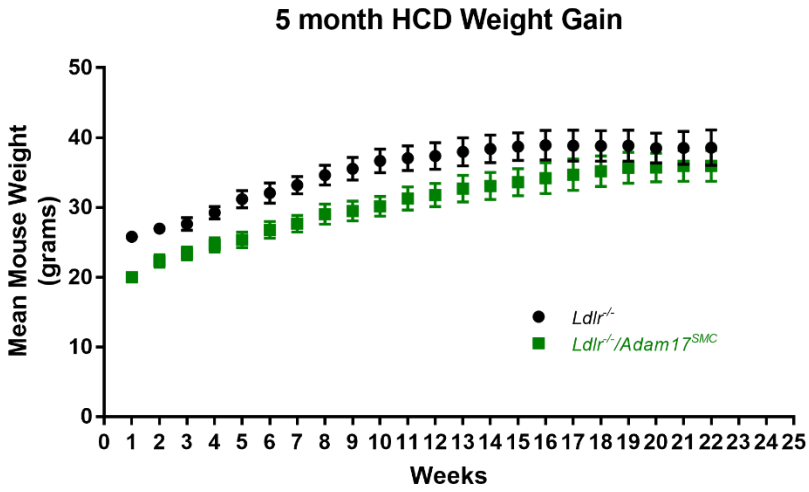

Figure 3.3 Hyperlipemia induces weight gain in LDLR-deficient mice.

Averaged data (n=5/group) of body weights during the 5 months of HCD feeding in *Ldlr*$^{-/-}$ (black) and *Ldlr*$^{-/-}$*/Adam17*^{SMC} (green) mice. Mice consistently gained weight each week over the 5-month feeding course. Averaged values represent mean ±SEM. Two-way ANOVA was used to show no statistically significant difference between the genotypes.

3.4 Plasma Lipoprotein Cholesterol Evaluation

To determine that any differences in aortic plaque area were not due to variations in plasma cholesterol content, plasma lipoprotein cholesterol was analyzed by fast-protein liquid chromatography (FPLC). Post-TMX injections, mice from control and *Ldlr*$^{-/-}$*/Adam17*^{SMC} genotypes fed a regular chow or high cholesterol diet (HCD) for 5 months were euthanized and plasma was collected. Plasma lipoprotein cholesterol fractions showed no difference between the genotypes (**Figure 3.4**), but with the introduction of HCD, low-density lipoprotein (LDL) and very low-density lipoprotein (VLDL) were greatly elevated going from regular chow to HCD in both genotypes. Thus, for the purposes of our study, any differences in plaque area are not associated with changes in plasma lipoprotein cholesterol content.

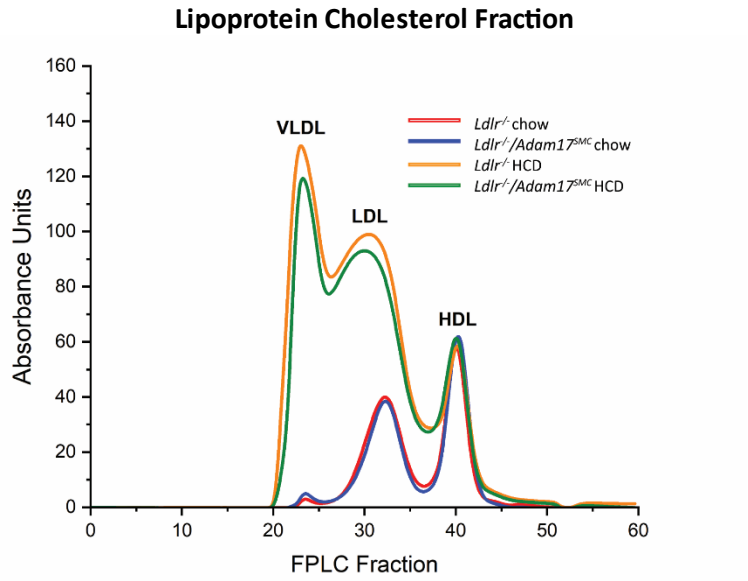

Figure 3.4 ADAM17 deletion in VSMC does not affect lipoprotein distribution.

Plasma lipoprotein cholesterol fast-protein liquid chromatography (FPLC) from *Ldlr*$^{-/-}$*/Adam17*$^{flox/flox}$ and *Ldlr*$^{-/-}$*/Adam17*^{SMC} mice (n=2-5 mice/group/genotype) fed a regular chow (11.3% fat, 53.4% carbohydrate, and 21% protein) or high cholesterol diet (HCD; 1.3% cholesterol, 21.2% fat, 48.5% carbohydrate, and 17.3% protein) for 5 months. Curves represent distributions of cholesterol in VLDL (very low-density lipoprotein), LDL (low-density lipoprotein), and HDL (high-density lipoprotein) populations.

3.5 *Ldlr*$^{-/-}$*/Adam17*^{SMC} Mice Have Augmented Aortic Plaque Area

After verification of *Adam17* deletion and plasma cholesterol homogeneity, we investigated if *Adam17* had any effect on plaque formation in our atherosclerotic model. *Ldlr*$^{-/-}$*/Adam17*^{SMC} mice show significantly increased plaque as compared to *Ldlr*$^{-/-}$ and *Ldlr*$^{-/-}$*/Adam17*$^{flox/flox}$ mice after 5 months of HCD in both thoracic and abdominal segments of the aorta (**Figure 3.5A**). In the abdominal region, *Ldlr*$^{-/-}$ mice developed 10.29±1.5% plaque area as a percentage of the total aortic area, the *Ldlr*$^{-/-}$*/Adam17*$^{flox/flox}$ mice developed 8.11±0.96% plaque area , and *Ldlr*$^{-/-}$*/Adam17*^{SMC} mice developed 20.65±3.24%. In the thoracic regions, these mice acquired 21.29±1.09%, 22.43±1.10%, and 28.82±1.89% plaque area , respectively. In the whole aorta, the mice acquired 15.79±1.07%, 15.27±0.94%, and 23.05±1.54% plaque area , respectively. Mice fed a regular chow diet for 5 months did not develop plaques in any of the genotypes. Aortic plaque area in 11-23 mice/genotype was quantified via Image-Pro Plus Software in thoracic, abdominal, and aortic sections and expressed as a percentage of plaque area over aortic segment area (**Figure 3.5B**). Plaques in the aorta of *Ldlr*$^{-/-}$*/Adam17*^{SMC} showed visually larger atherosclerotic plaques throughout the artery. The control mice displayed smaller and scattered plaques, mostly near the aortic arch and bifurcations of the renal arteries.

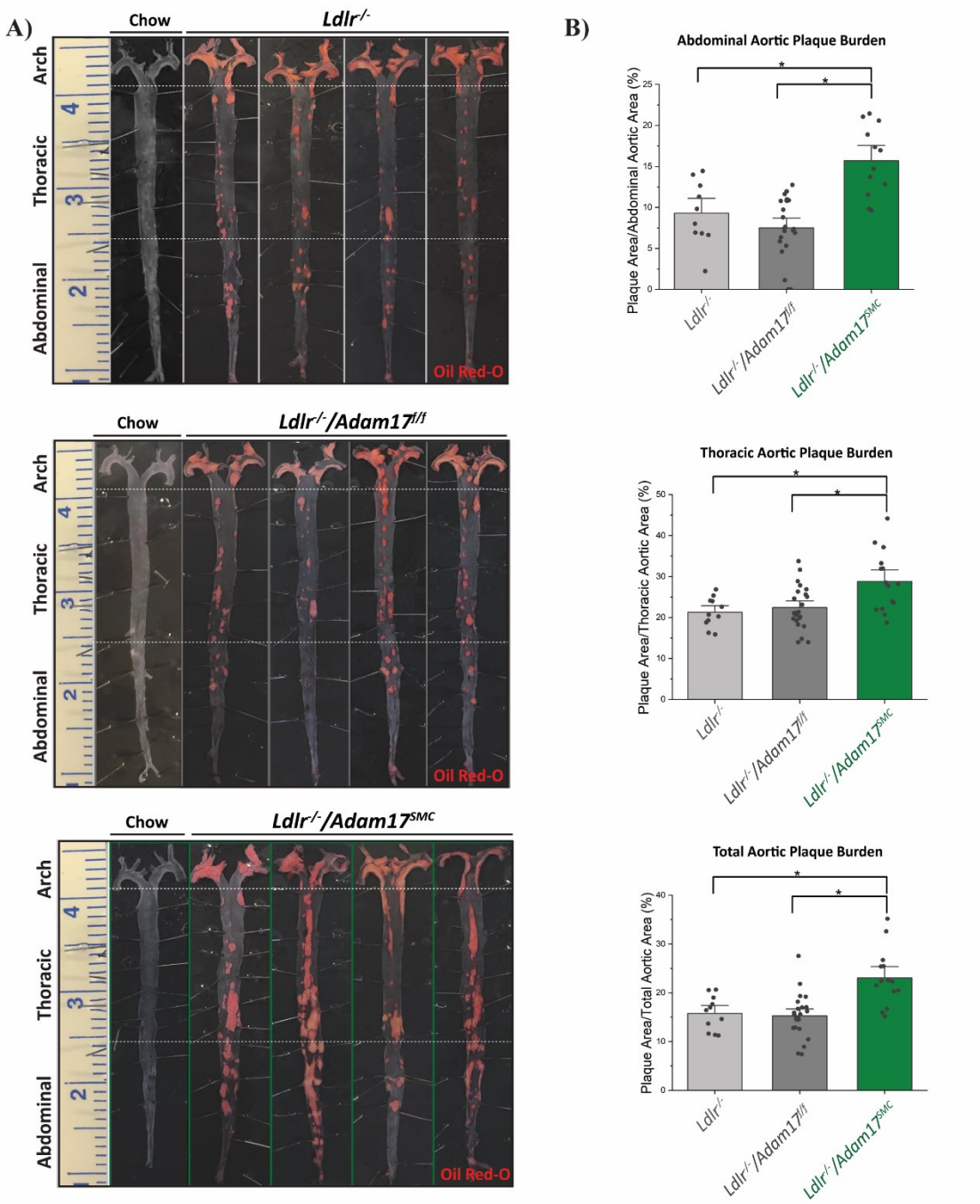

Figure 3.5 Deletion of ADAM17 in VSMC augments aortic plaque area.

A. Oil Red-O staining of aortas of *Ldlr*$^{-/-}$, *Ldlr*$^{-/-}$*/Adam17*$^{flox/flox}$, and *Ldlr*$^{-/-}$*/Adam17*^{SMC} (n=11, 23, and 15, respectively) mice fed a regular chow or HCD for 5 months showing increased plaque area in the *Ldlr*$^{-/-}$*/Adam17*^{SMC} mice. Dashed white lines represent segmentation of the aorta into the arch, thoracic, and abdominal sections. **B**. Quantification of plaque area in thoracic, abdominal, and total aortic segments by calculation of plaque area (red) divided by aortic segment area (x100) using Image-Pro Plus Software. Statistical analyses used was one-way ANOVA followed by a Bonferroni post-hoc test and significance recognized at the 0.05 level. Averaged data

3.6 *Ldlr*$^{-/-}$*/Adam17*^{SMC} Mice Develop Increased Aortic Root Plaque Area and Necrotic Cores

Aortic tricuspid valves from *Ldlr*$^{-/-}$, *Ldlr*$^{-/-}$*/Adam17*$^{flox/flox}$, and *Ldlr*$^{-/-}$*/Adam17*^{SMC} mice fed a high cholesterol diet for 5 months were paraffin-embedded and stained for Trichrome and H&E (**Figure 3.6A**). Congruent with the aortic data, *Ldlr*$^{-/-}$*/Adam17*^{SMC} mice display elevated aortic valve plaque area compared to the control mice. The *Ldlr*$^{-/-}$, *Ldlr*$^{-/-}$*/Adam17*$^{flox/flox}$, and *Ldlr*$^{-/-}$*/Adam17*^{SMC} displayed 32.71±2.12%, 31.83±1.79%, and 37.83±0.83% aortic root plaque area, respectively (**Figure 3.6B**). Aortic root plaque area was calculated by measuring lesion area over total aortic root area in serial sections. Furthermore, necrotic cores (area within the plaques containing dead cells and other debris) were larger and more frequent in mice lacking VSMC ADAM17. The aortic roots of *Ldlr*$^{-/-}$, *Ldlr*$^{-/-}$*/Adam17*$^{flox/flox}$, and *Ldlr*$^{-/-}$*/Adam17*^{SMC} displayed 4.93±1.53%, 6.05±2.73%, and 19.33±2.83% necrotic core area, respectively. Necrotic core area was quantified by measuring the areas of the necrotic cores (areas devoid of H&E staining) and dividing it by the area of the lesion in which it was found. Lesions lacking a necrotic core were assigned a value of zero. Therefore, *Ldlr*$^{-/-}$*/Adam17*^{SMC} exhibit elevated plaque area in the aortic valves along with more vulnerable plaques characterized by the size and frequency of necrotic cores.

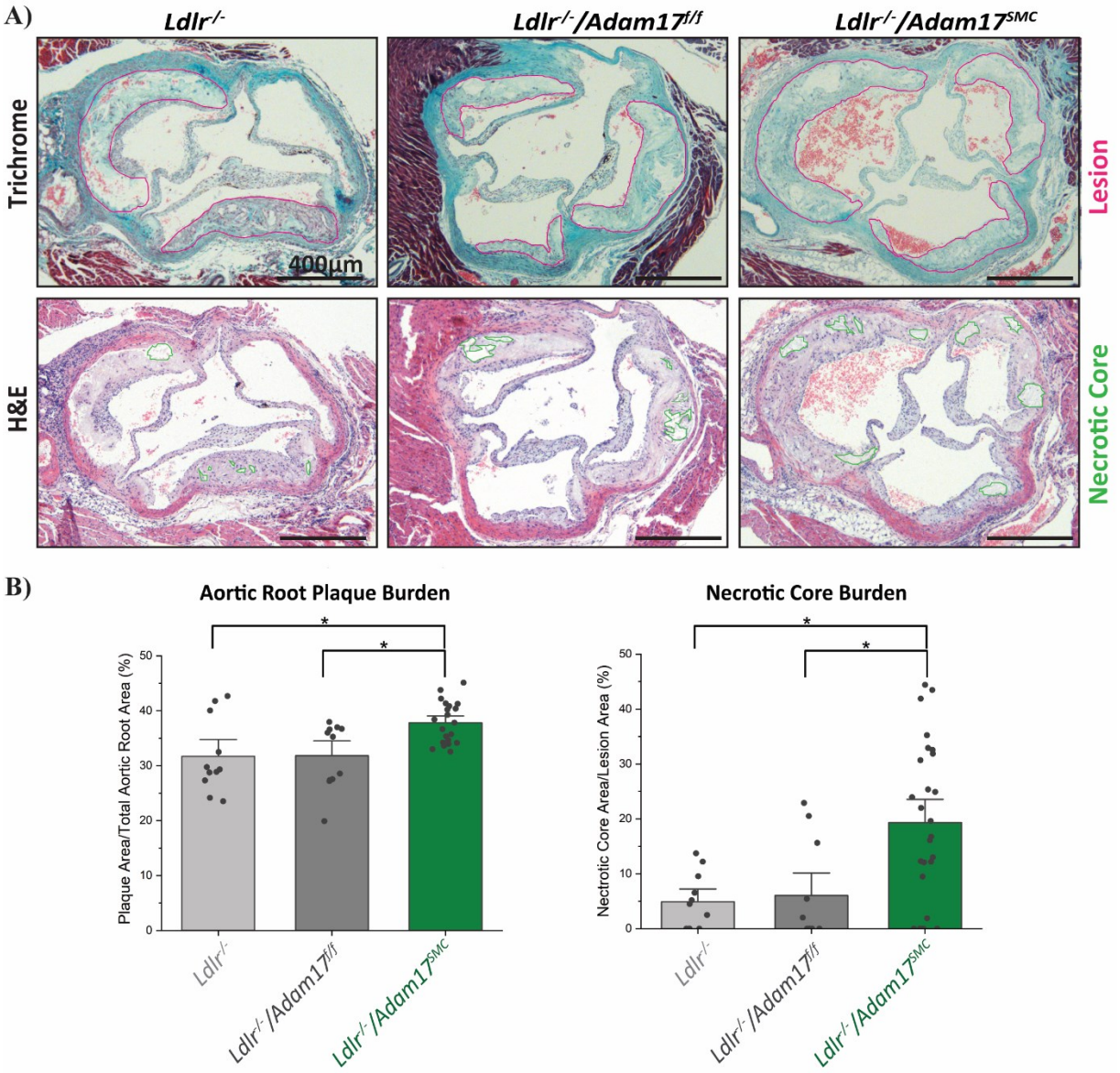

Figure 3.6 Deletion of ADAM17 in VSMC augments aortic valve plaque area and instability.

A. Aortic tricuspid valves from *Ldlr*$^{-/-}$, *Ldlr*$^{-/-}$*/Adam17*$^{flox/flox}$, and *Ldlr*$^{-/-}$*/Adam17*^{SMC} mice fed a high cholesterol diet for 5 months showing increased plaque area and instability in the *Ldlr*$^{-/-}$*/Adam17*^{SMC} mice. 5μm sections of formalin-fixed hearts were placed on microscopy glass slides and stained for trichrome (lesions outlined in pink) and H&E (necrotic cores outlined in green) and imaged with a light microscope (scale bars=400μm). **B.** Aortic root plaque area was calculated 3-4 serial sections (n=4-9 valves/genotype). Necrotic core size was calculated by measuring the area of the necrotic cores (areas devoid of H&E staining) and dividing it by the area of the lesion in which it was found. Lesions lacking a necrotic core were assigned a value of zero (n=5-9valves/genotype). Statistical analyses used was one-way ANOVA followed by a Bonferroni post-hoc test and significance recognized at the 0.05 level. Averaged data represent mean±SEM.

3.7 Augmented Inflammatory Markers in Aortas of *Ldlr$^{-/-}$/Adam17^{SMC}* Mice

Inflammation was assessed in the diseased aorta by immunofluorescent staining of macrophage markers. At 3 months of HCD feeding, the aortas from control and *Ldlr$^{-/-}$/Adam17^{SMC}* mice were OCT-embedded and cryosections stained for pan-macrophage marker CD68. CD68 was detected mainly in the plaque regions rather than medial or adventitial layers of the artery. In the stained cryosections, it is evident that the atherosclerotic plaques are more prominent. Thus, CD68^{+} area was higher in the aortas of the *Ldlr$^{-/-}$/Adam17^{SMC}* as the plaques were larger at the 3-month time point compared to the control mice (**Figure 3.7A**). Furthermore, *in vivo* CD68 staining did not appear to be associated with viable cells. These data suggest increased macrophage or VSMC-derived macrophage-like cell accumulation within the atherosclerotic plaques of *Ldlr$^{-/-}$/Adam17^{SMC}* mice.

We also assessed inflammation in the diseased aorta by immunofluorescent staining of neutrophil markers. At 3 months of HCD feeding, the aortas from control and *Ldlr$^{-/-}$/Adam17^{SMC}* mice were OCT-embedded and cryosections stained for neutrophil marker Ly6B. Ly6B expression was detected in the *Ldlr$^{-/-}$/Adam17^{SMC}* group, but not in the control mice after 3 months of HCD feeding. Ly6B staining was observed within the plaques, though to a lesser extent than CD68 expression in plaques. Furthermore, neutrophils were observed within the tunica media between the layers of elastin, and most prominent in heavily diseased plaques, conversely to the macrophages, which were not detected in the medial layers of the atherosclerotic artery. It is important to note however that Ly6B is also expressed by monocytes. In conclusion, Ly6B^{+} staining was augmented in the tunica media of *Ldlr$^{-/-}$/Adam17^{SMC}* compared to the control mice, suggesting increased neutrophil content in the aortic wall (**Figure 3.7B**).

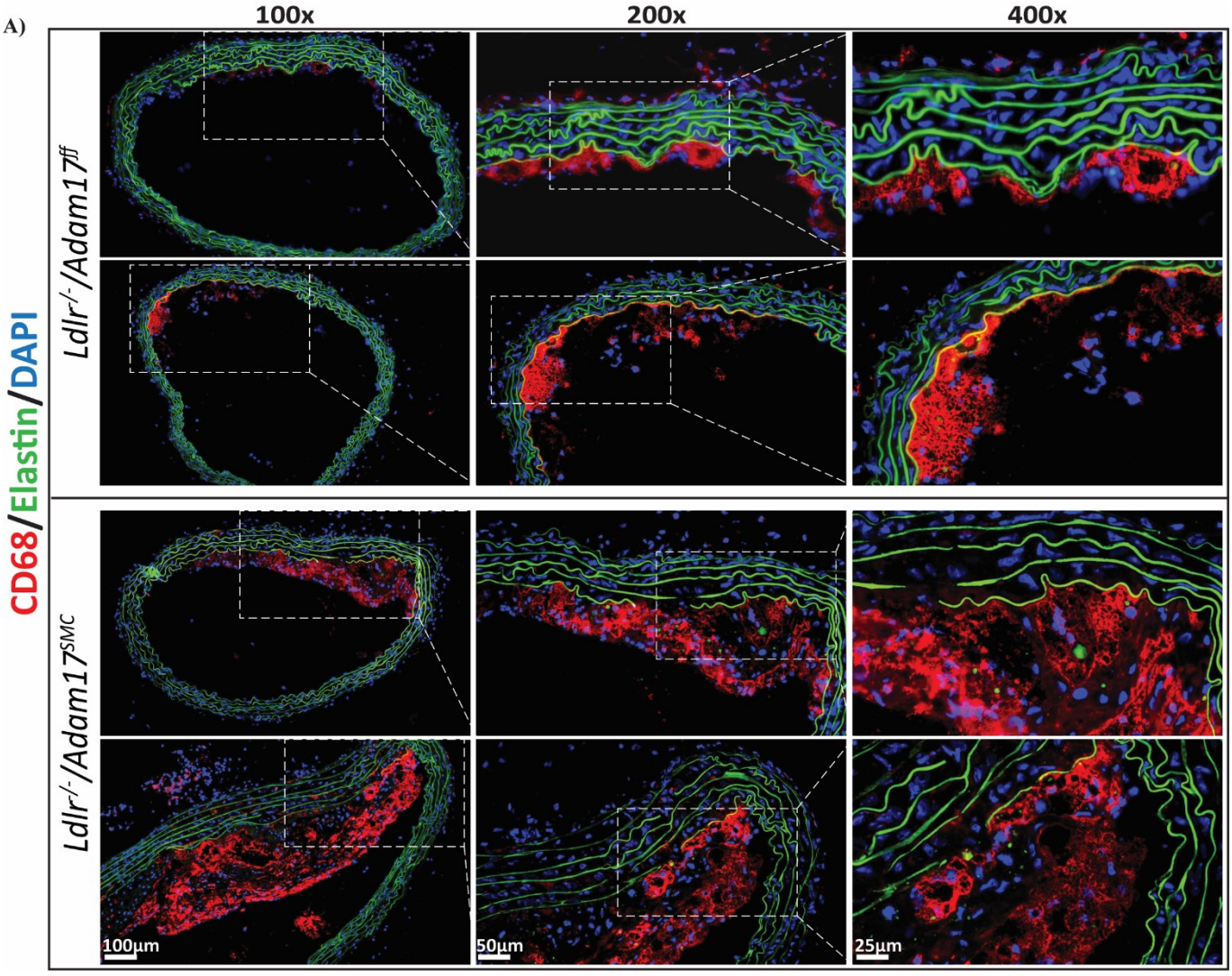

Figure 3.7A ADAM17 deletion in VSMC increases CD68+ area.

Representative immunofluorescent images of 5µm OCT-embedded cryosections of aortic segments stained for CD68 (MCA1597, red), elastin (autofluorescence, green), and nuclei (DAPI, blue) showing increased macrophage content in the *Ldlr*$^{-/-}$*/Adam17*^{SMC} mice. Fluorescent microscopy images were taken at 100x magnification (scale bar=100µm), 200x (scale bar=50µm), and 400x (scale bar=25µm) showing accumulation of macrophages within the atherosclerotic plaques.

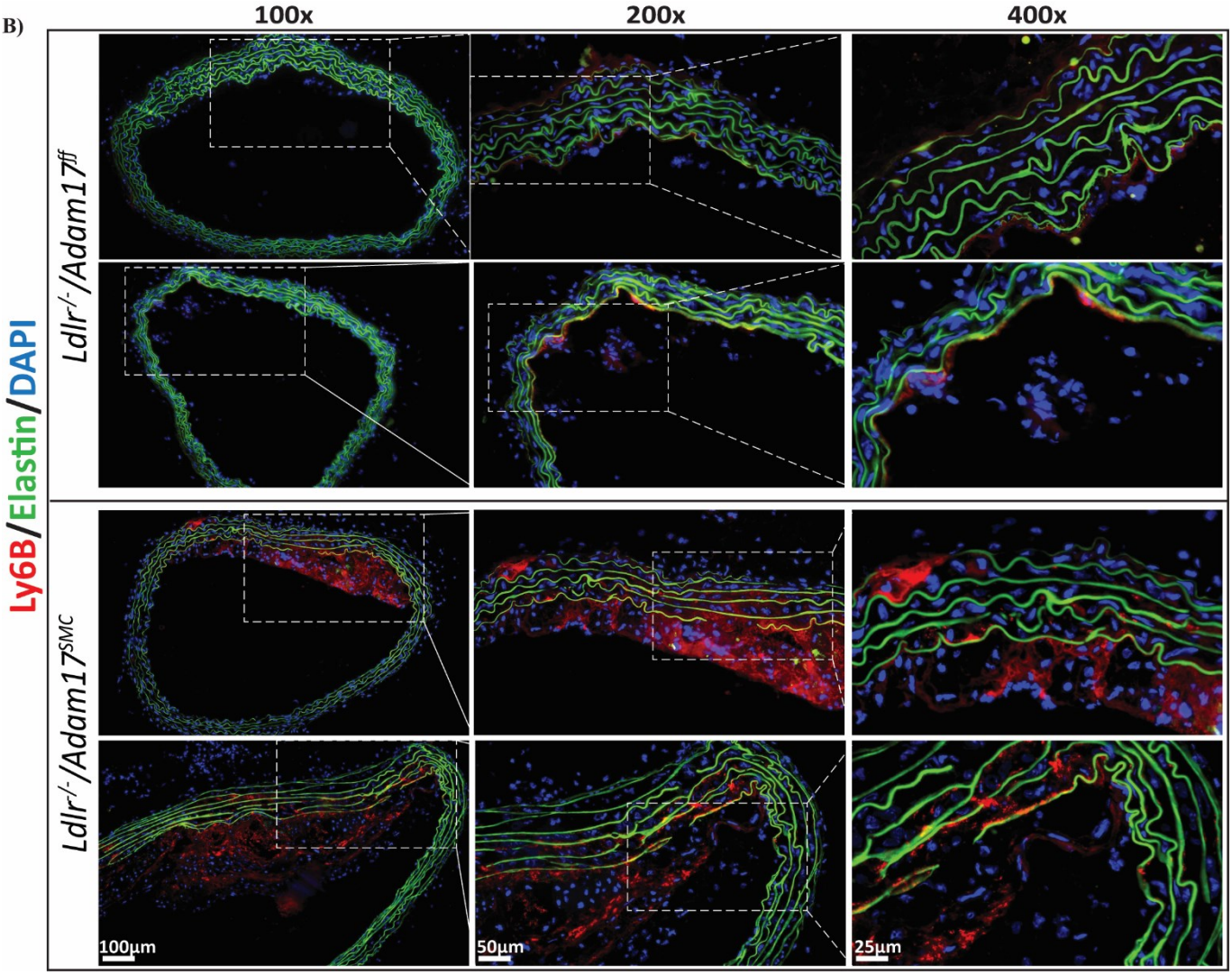

Figure 3.7B ADAM17 deletion in VSMC increases Ly6B+ staining in the tunica media.

Representative immunofluorescent images of 5µm OCT-embedded cryosections of aortic segments stained for Ly6B.2 (MCA771G, red), elastin (autofluorescence, green), and nuclei (DAPI, blue) showing increased neutrophil staining in the *Ldlr*$^{-/-}$*/Adam17*^{SMC} mice, noticeable between the medial elastin layers. Fluorescent microscopy images were taken at 100x magnification (scale bars=100µm), 200x (scale bars=50µm), and 400x (scale bars=25µm) showing accumulation of neutrophils within the atherosclerotic plaques and the medial layer of the aortas.

3.8 ADAM17 is Effectively Knocked Down in Cultured VSMC

To study the effect of ADAM17 in VSMC, we used *Adam17*-specific siRNA (along with Lipofectamine) to knock-down *Adam17* in primary vascular smooth muscle cells *in vitro* ($Adam17^{KD}$). VSMC was isolated from $Ldlr^{-/-}$ mice which would provide a similar atherogenic environment as in our *in vivo* studies. Negative control siRNA (siRNA with sequences that do not target any gene transcripts) treated cell were used alongside all experiments as controls. Protein was visualized using an ADAM17 antibody specific for the cytoplasmic domain (**Figure 3.8**). On average, this siRNA achieves an approximate 95-96% knock-down of ADAM17, providing $Adam17^{KD}$ VSMC for our study.

3.9 $Adam17^{KD}$ in VSMC Augments Lipid Content

To understand the effect of ADAM17 loss on lipid loading, we used primary vascular smooth muscle cells transfected with control and *Adam17* siRNA and treated them with 20μg/ml oxidized LDL (oxLDL) for 72 hours. Oil Red-O staining was used to visualize intracellular neutral lipids. Control cells treated with saline were used to verify that the ORO^{+} staining was only observed with the addition of oxLDL. Interestingly, the $Adam17^{KD}$ cells had significantly higher oxLDL content than the control cells after 72 hours (**Figure 3.9**). ADAM17 inhibition led to a 2.2-fold increase in lipid content per cell. Saline treated cells did not contain ORO^{+} staining. However, these data do not show the rate of cholesterol uptake or efflux, but it represents that $Adam17^{KD}$ VSMC contain an elevated lipid content in hyperlipidemic conditions. Thus, ADAM17 deletion in VSMC augments intracellular lipid load in response to oxLDL.

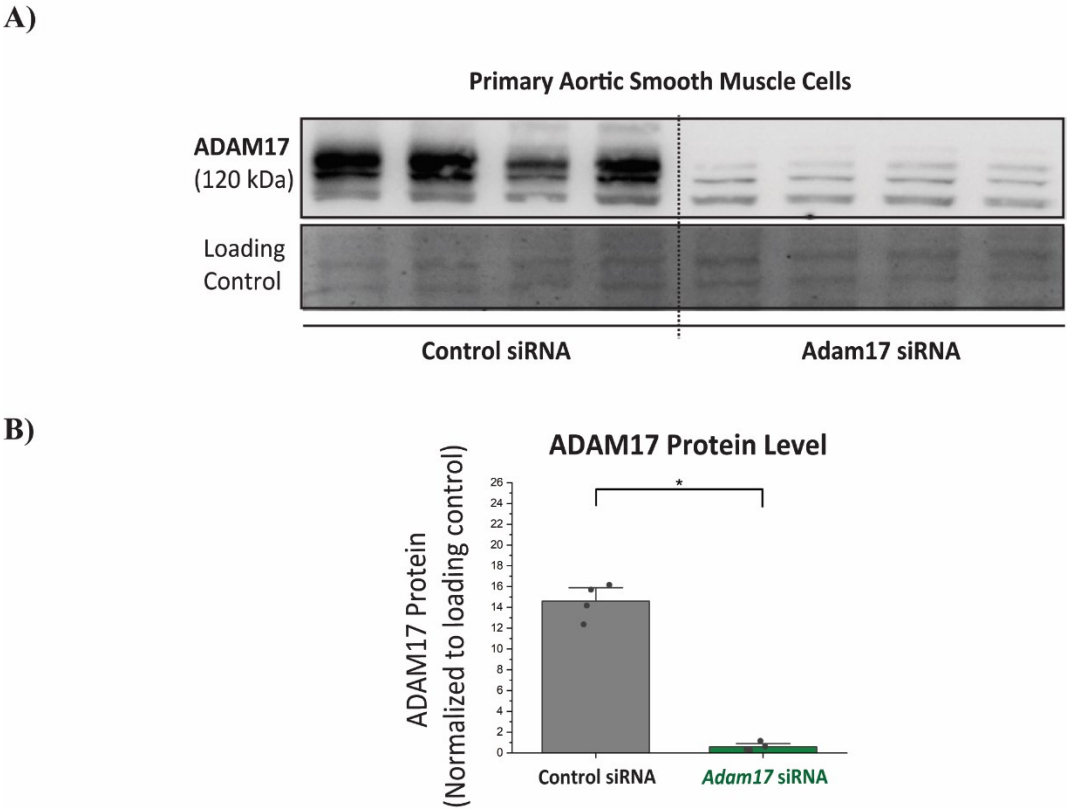

Figure 3.8 ADAM17 protein is knocked-down with *Adam17*-specific siRNA in VSMC.

A. Western blot for ADAM17 of primary cultured VSMC lysates with control (negative siRNA) and *Adam17*-specific siRNA (15nM for 6 hours) loaded with 20ug protein/lane showing sufficient knockdown of ADAM17. ADAM17 primary antibody (EHS008) specific for the cytoplasmic domain of ADAM17 was detect at approximately 120 kDa. **B.** Quantification of ADAM17 knockdown in cultured VSMC. Unpaired student t-test was used to determine significance at the 0.05 level. Averaged data represent mean±SEM.

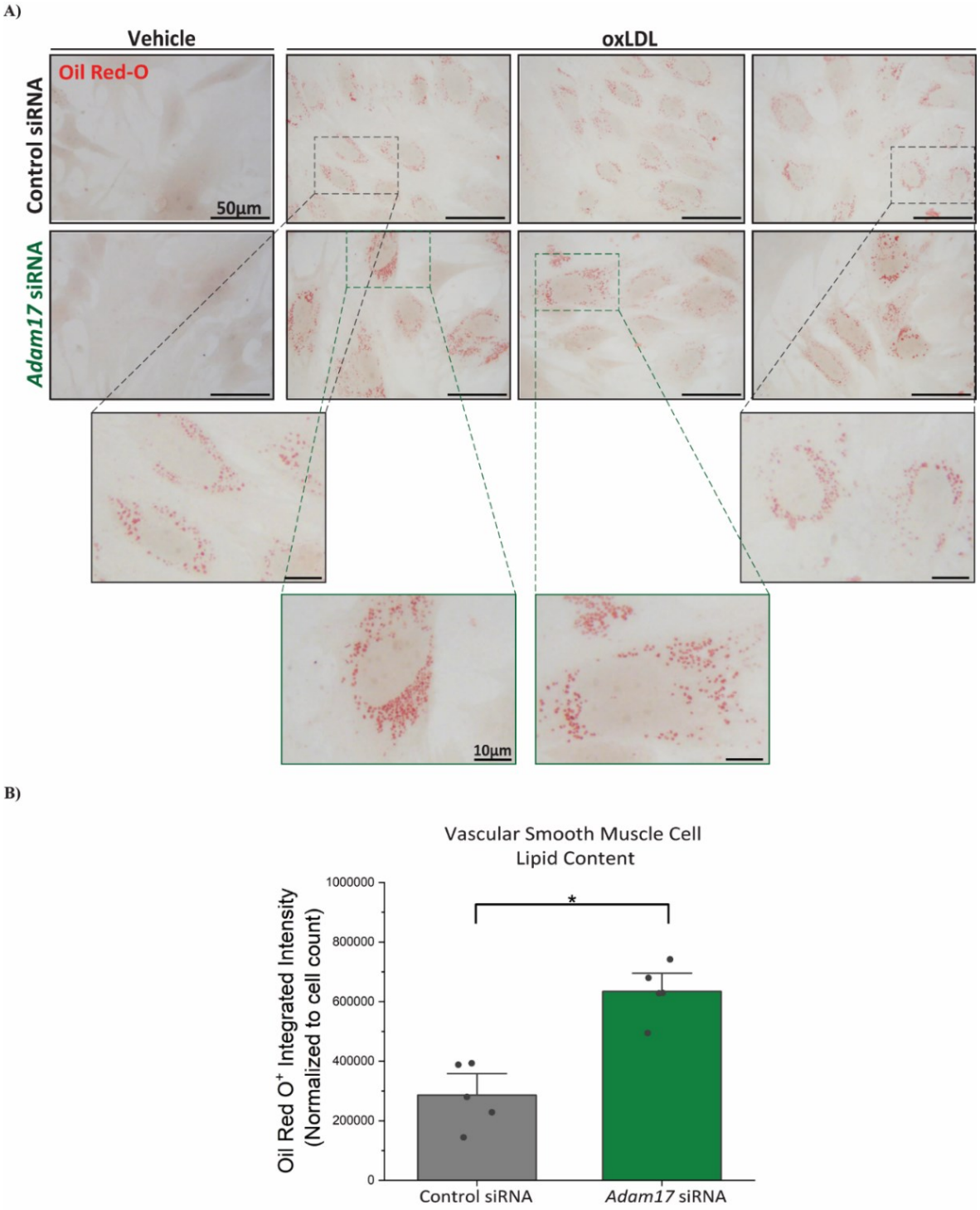

Figure 3.9 ADAM17 knockdown in VSMC augments lipid loading in response to oxLDL.

A. Primary VSMCs (from 3-4 4-week-old *Ldlr*$^{-/-}$ mice) treated with 20μg/ml oxidized LDL and stained with 0.5% ORO (scale bars=50μm and 10μm) showing increased lipid content in the *Adam17*^{KD} VSMC. **B.** ImageJ was used to calculate red pixel integrated intensity (n=5-6 images/group) and normalized to cell count per frame. Unpaired student t-test was used to determine significance at the 0.05 level. Averaged data represent mean±SEM.

3.10 *Adam17*^{KD} VSMC Have Augmented Scavenger Receptor-Mediated Lipid Loading

To determine if the increased lipid loading seen in the Oil Red-O stained *Adam17*^{KD} VSMC was due to increased lipid uptake, we used fluorescently labelled oxLDL (Dil-oxLDL) treatment. VSMC treated with Dil-oxLDL will accumulate the Dil dye within the cytosol, which therefore allows for tracking of scavenger receptor-mediated endocytosis of oxLDL. *Adam17*^{KD} VSMC showed significantly increased uptake of Dil-oxLDL after 24 hours as compared to the control siRNA treated cells (**Figure 3.11**). ADAM17 inhibition in VSMC led to a 1.5-fold increase in scavenger receptor-mediated lipid loading. There was no fluorescence detected in the vehicle treated groups. Therefore, these data suggest that the increased lipid loading in VSMC in response to oxLDL is in part due to elevated scavenger-receptor mediated lipid loading. Female *Adam17*^{KD} VSMC also showed a significant increase in scavenger receptor-mediated lipid loading **(Figure 3.12)**. We interpret this as increased levels of scavenger-receptors on the membranes of *Adam17*^{KD} vascular smooth muscle cells. The main scavenger receptors to investigate and which are mainly implicated in atherosclerotic foam cell formation include SR-A1, CD36, and OLR1. Compared to the lipid loading data, the uptake results show only a modest increase, providing rationale to investigate efflux as well.

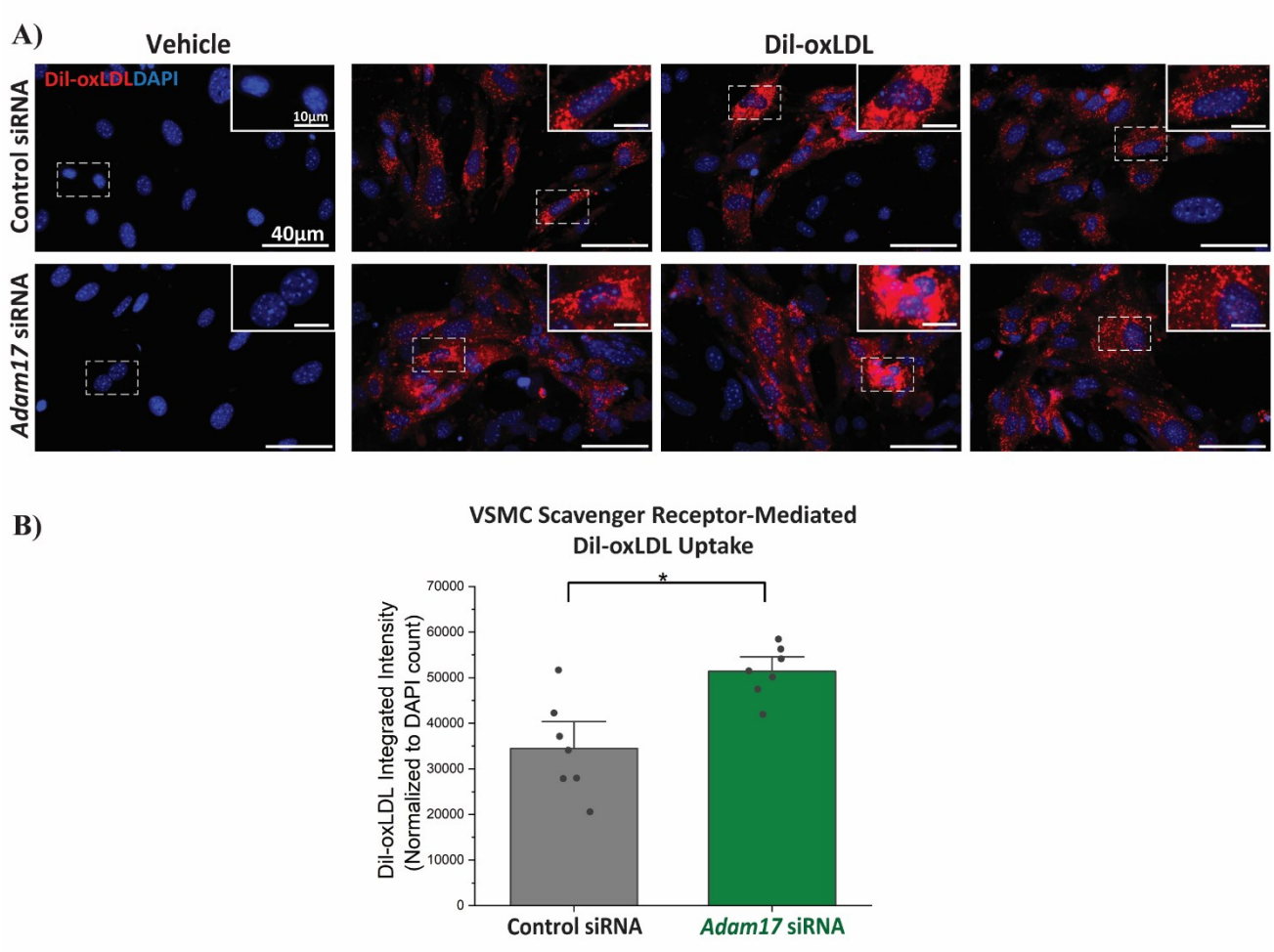

Figure 3.10 ADAM17 knockdown in VSMC augments scavenger receptor-mediated lipid loading.

A. Primary VSMCs treated with vehicle or 10μg/ml Dil-oxidized LDL (Dil-oxLDL) for 24 hours at passages 4-6 on 4-chambered (scale bars=40μm and 10μm for the inset) showing increased scavenger receptor-mediated lipid loading in the *Adam17*^{KD} cells. **B.** ImageJ was used to calculate red pixel integrated intensity (n=7 images/group) and normalized to DAPI count per frame. Each data point represents data from one frame at 400x magnification. Unpaired student t-test was used to determine significance at the 0.05 level. Averaged data represent mean±SEM.

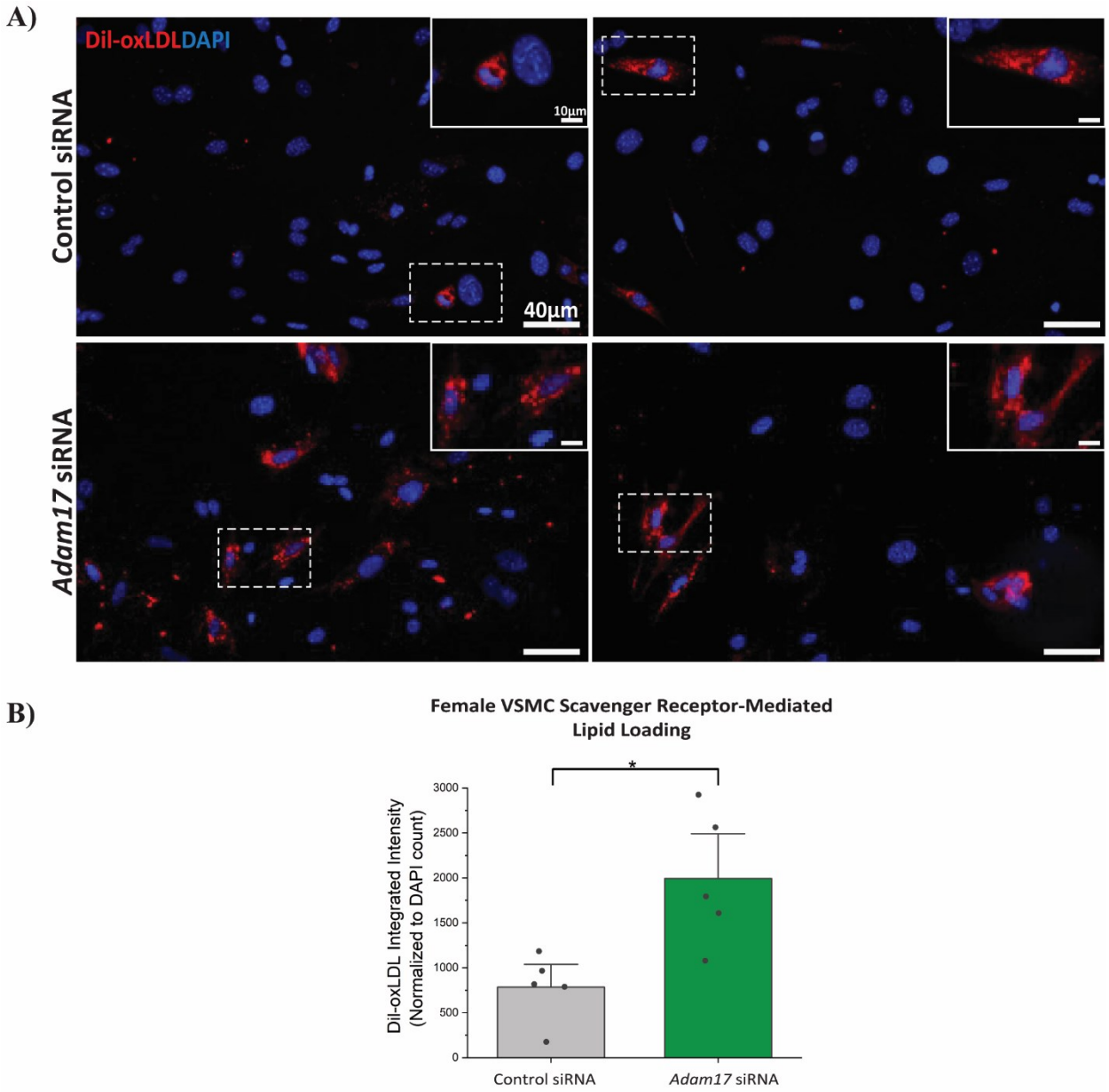

Figure 3.11 Female *Adam17*^{KD} cells also show elevated scavenger receptor-mediated lipid loading.

A. Primary female VSMCs treated with 15nM control or *Adam17* siRNA for 6 hours and incubated with vehicle or 10µg/ml Dil-oxidized LDL (Dil-oxLDL) for 24 hours at passages 4-6 on 4-chambered (scale bars=40µm and 10µm for the inset) showing increased scavenger receptor-mediated lipid loading in the *Adam17*^{KD} cells.. **B.** ImageJ was used to calculate red pixel integrated intensity (n=5 images/group) and normalized to DAPI count per frame. Each data point represents data from one frame at 200x magnification. Unpaired student t-test was used to determine significance at the 0.05 level. Averaged data represent mean±SEM.

3.11 *Adam17*^{KD} in VSMC Reduces Cholesterol Efflux

As reported, ADAM17 has the potential to play a role in cholesterol efflux by modulation of the ABCA1 cholesterol efflux protein.[23] Therefore, we performed a cholesterol efflux assay (MAK192, Sigma-Aldrich) on primary *Ldlr*$^{-/-}$ VSMCs treated with control or *Adam17*-specific siRNA. Interestingly, *Adam17*^{KD} VSMCs also displayed reduced cholesterol efflux (**Figure 3.13**). Control siRNA treated VSMC displayed approximately 8% cholesterol efflux, while *Adam17* siRNA led to a decrease in cholesterol efflux to ~6% cholesterol efflux. Importantly, these data, along with the scavenger receptor-mediated uptake data, indicate that ADAM17 modulates the efflux and uptake capacity of VSMC, resulting in increased lipid content via two mechanisms.

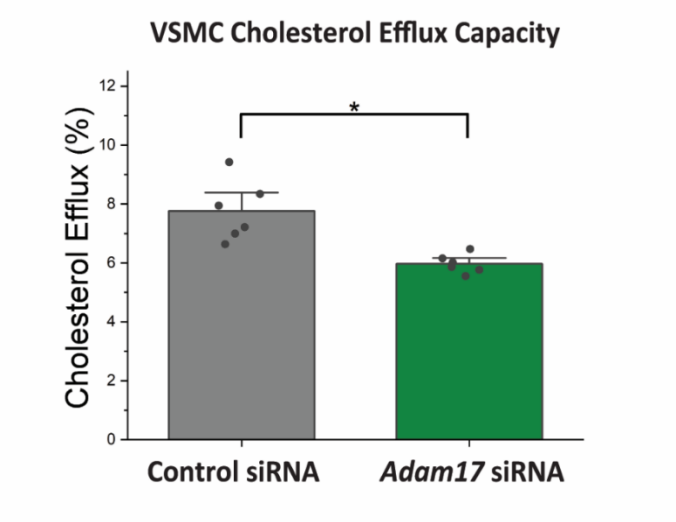

Figure 3.12 ADAM17 knockdown in VSMC reduces cholesterol efflux.

Primary cultured VSMCs (isolated from 3-4 *Ldlr*$^{-/-}$ mice at approximately 4 weeks of age) treated with 15nM control or *Adam17* siRNA for 6 hours were transferred to 96-well plates and the efflux assay (MAK192, Sigma-Aldrich) was performed as per manufacturers instructions. These data show decreased cholesterol efflux capacity in the *Adam17*^{KD} VSMC. Cholesterol efflux was calculated by fluorescence intensity of the supernatant divided by the sum of the fluorescence intensity of the supernatant plus cell lysate. Unpaired student t-test was used to determine significance at the 0.05 level. Each data point is one well in a 96-well plate. Averaged data represent mean±SEM.

3.12 Lipid Transporter RNA Expression in Vascular Smooth Muscle Cells

To determine if *Adam17* had any role in modulating the RNA expression of any lipid transporters in VSMC, we utilized Taqman RT-PCR to amplify and quantify mRNA expression of key lipid transporters (**Figure 3.14**). Cell cultures of VSMC were transfected with siRNA and treated with either vehicle (saline) or 20μg/ml oxLDL for 72 hours. We found that mRNA expression of ABCA1, the primary cellular cholesterol efflux transporter, was significantly reduced in the $Adam17^{KD}$ cells as compared to the controls following oxLDL treatment. There were no significant differences between saline and the oxLDL groups or between the control and *Adam17* siRNA groups in any of the other lipid transporters analyzed. However, expression of OLR1 and SRA1 seemed to increase with oxLDL in the $Adam17^{KD}$ groups but decreased in the control siRNA groups, as expected with addition of cholesterol Therefore, our key finding here is that ADAM17 knockdown in VSMC augments lipid uptake and reduces efflux, leading to increased lipid content. *Abca1* mRNA data suggest that reduced expression of this lipid transporter is the culprit for reduced cholesterol efflux in the $Adam17^{KD}$ group.

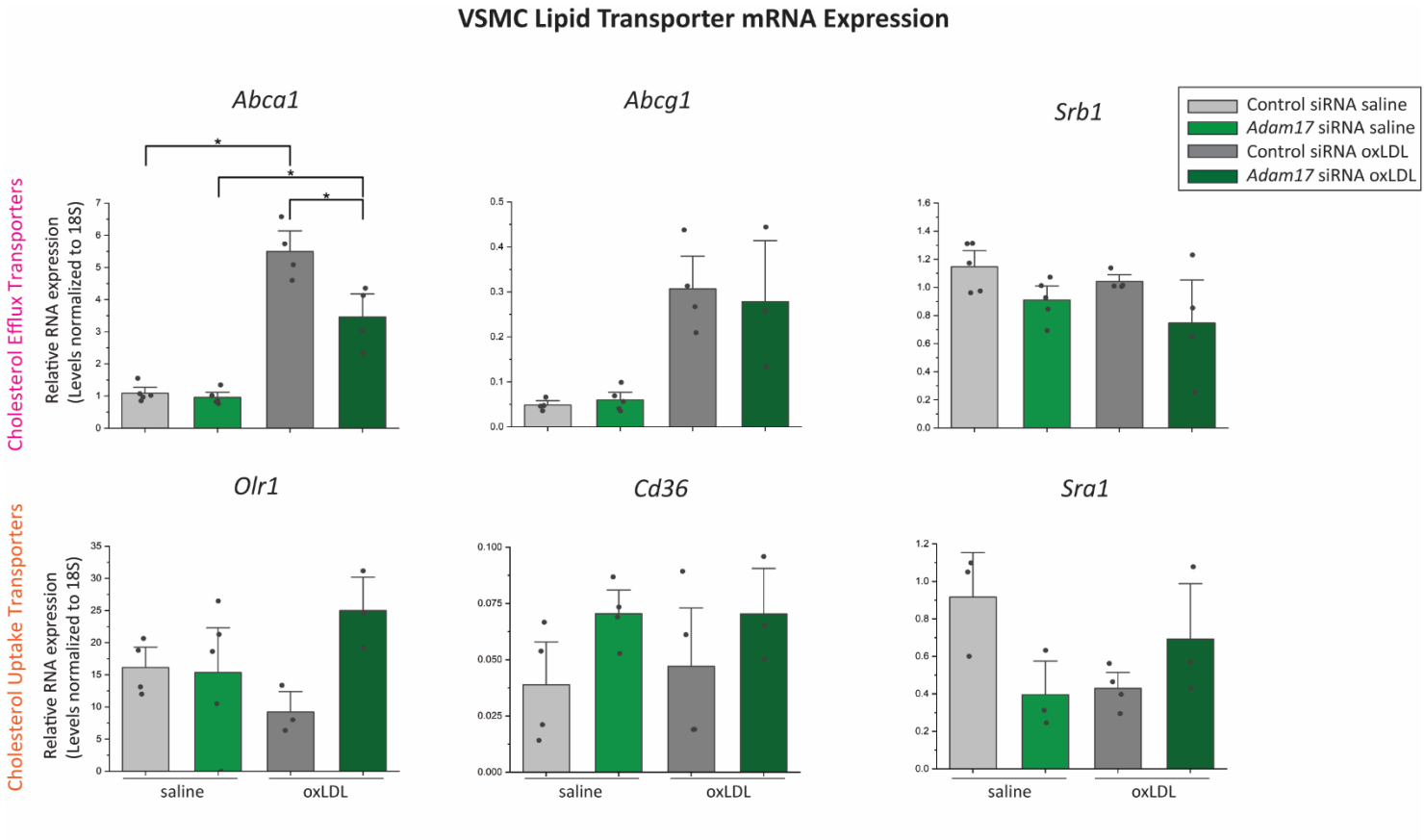

Figure 3.13 ADAM17 knockdown in VSMC reduces oxLDL-mediated *Abca1* expression.

Real-time quantitative PCR analysis of cholesterol transport proteins in VSMC cell lysates treated with control or *Adam17* siRNA and saline or 20µg/ml oxLDL for 72 hours. Statistical significance determined via Two-Way ANOVA followed by Bonferroni means comparison test. Averaged data represent mean±SEM.

3.13 *Adam17*^{KD} in VSMC Augments Transformation to a Macrophage-like Phenotype

Contractile VSMC are known to undergo phenotypic transformation into macrophage-like cells and eventually foam cells in the milieu of atherosclerosis. For our experiments, we used oxidized LDL and *Ldlr*$^{-/-}$ primary vascular smooth muscle cells to provide an atherogenic environment like *in vivo* atherosclerotic conditions, stimulating the transition of VSMC towards foam cells. *Adam17*^{KD} VSMC demonstrated higher conversion towards macrophage-like foam cells when treated with oxLDL, and this was true for both female and male VSMC (**Figure 3.15**). Compared to the vehicle treated cells, both control and *Ldlr*$^{-/-}$*/Adam17*^{SMC} groups had decreased calponin expression in the presence of oxLDL. Intriguingly, sub-populations of VSMC were observed to transform into CD68-expressing cells, while other cells remained expressing calponin. These subpopulations were larger and more frequent in the *Adam17* siRNA treated cells. Thus, we interpret these observations as an accelerated transformation of *Adam17*^{KD} VSMC to macrophage-like cells in hyperlipidemic conditions.

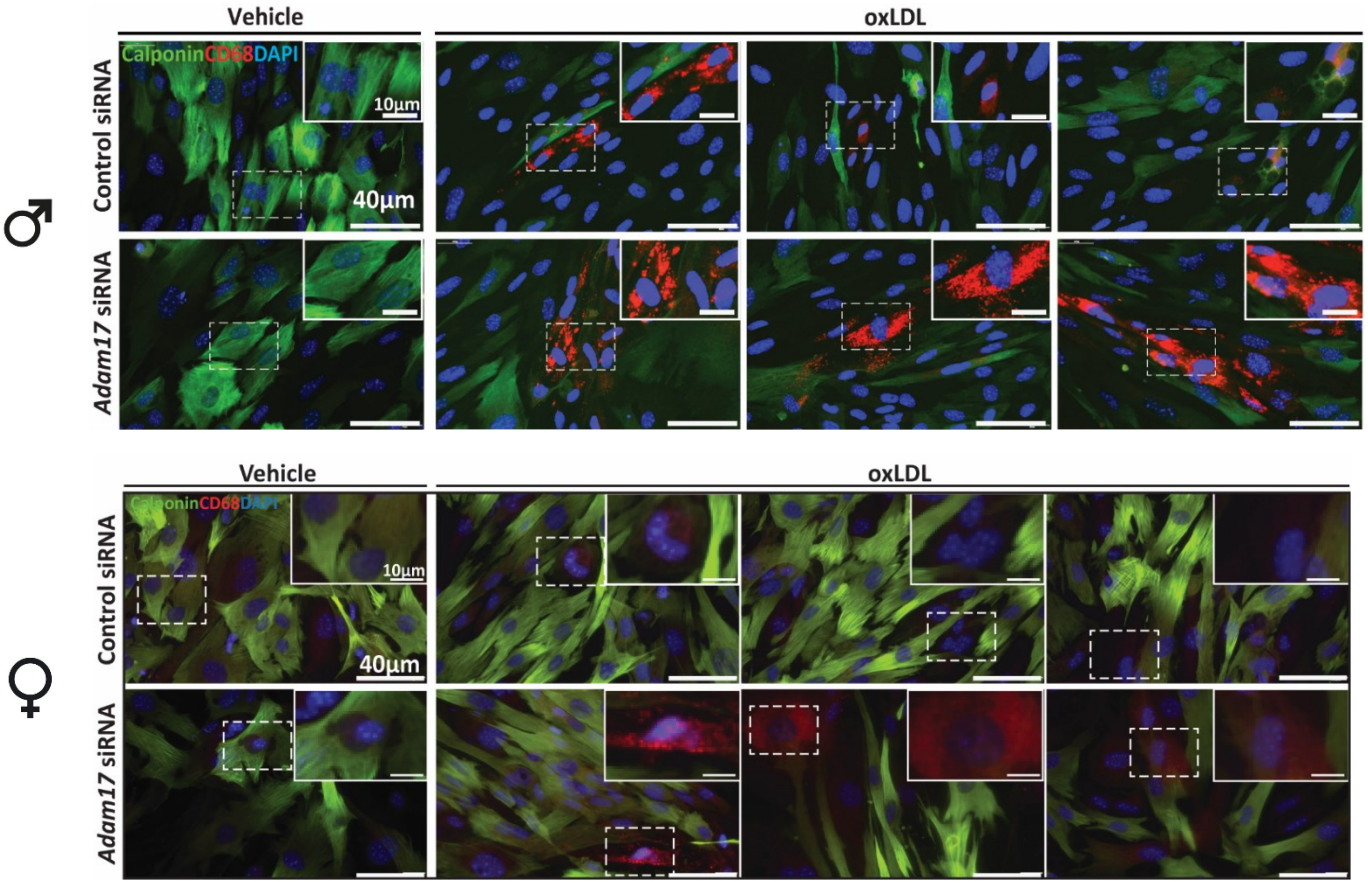

Figure 3.14 ADAM17 knockdown in VSMC augments conversion to macrophage-like cells.

Primary cultured male and female VSMCs were prepared and treated with siRNA and oxLDL as mentioned prior and stained for VSMC-marker, calponin (ab46794), and macrophage-marker, CD68 (MCA1957) to visualize conversion of contractile VSMCs to foam cells (scale bars=40μm and 10μm for the inset). *Adam17*^{KD} VSMCs have increased conversion towards macrophage-like cells.

3.14 VSMC Do Not Contribute to Clearance of Apoptotic Jurkat Cells

In this study, we investigated the capacity for VSMC to contribute to efferocytosis. As expected, we did not see the process of efferocytosis in VSMC. We noticed that apoptotic and even non-apoptotic Jurkat cells were seen remaining within the cell monolayer (**Figure 3.16**). We interpret these as non-specific attachments to matrix deposited by VSMC, rather than initiation of efferocytosis. Furthermore, the Jurkat cells were seen to not be associated with VSMC in many cases, but in areas between cells. The protocol used for this experiment is designed to study the efferocytotic capacity of professional phagocytes (*i.e.* macrophages), in which non-apoptotic Jurkat cells are not recognized by the phagocyte and are subsequently washed off.[160] Therefore, we conclude that VSMC do not recognize and initiate efferocytosis in response to apoptotic stimuli.

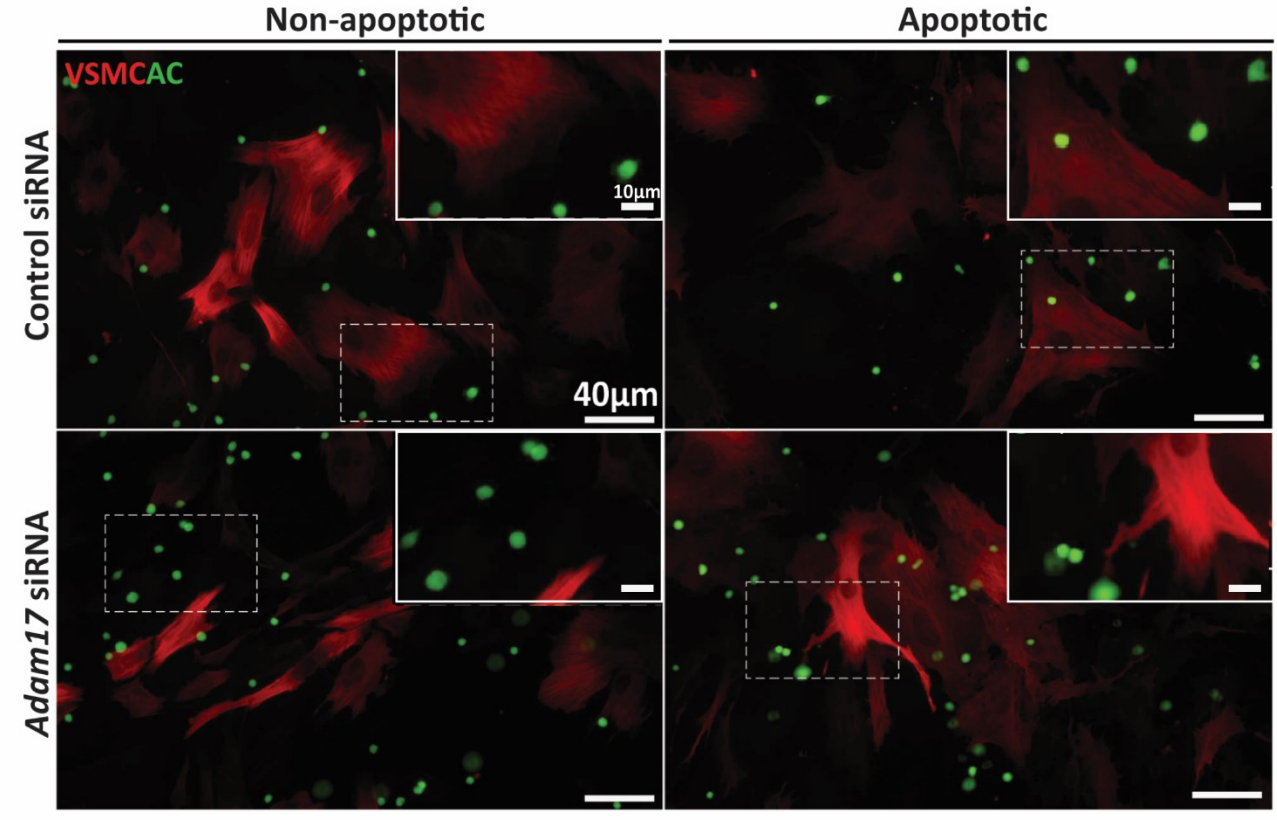

Figure 3.15 VSMC do not perform efferocytosis in response to apoptotic stimuli.

Non-apoptotic (0µM Staurosporine A/1hr.) and apoptotic (5µM/1hr.) Jurkat cells incubated on control or *Adam17*^{KD} VSMC (scale bars=40µm and the inset 10µm). Jurkat cells can be seen bound to areas between cells, possibly to the extracellular matrix synthesized by the VSMC. Cells are stained with VSMC-marker calponin (red) and Jurkat cells are labelled with Calcein-AM (green). These data imply that VSMC do not perform efferocytosis of apoptotic Jurkat cells.

3.15 VSMC Do Not Express MerTK on the Cell Membrane

MerTK is a membrane-bound protein crucial for recognition of apoptotic cells and initiation of efferocytosis. As our VSMC did not appear to be able to initiate efferocytosis, MerTK should not be expressed in these cells as their primary function is contractility. During our investigation into the mRNA expression of lipid transporters in VSMC, we also analyzed *MerTK* expression in these cells. Interestingly, we noticed that our mRNA data showed expression of MerTK in VSMC relative to 18S control mRNA (**Figure 3.17A**). We then sought to determine if we could detect MerTK expression in VSMC at the protein level. After staining for MerTK in VSMC treated with siRNA and 10ng/ml IL-6 + 10ng/ml TNF-α (to induce expression of MerTK), we did not detect expression of MerTK on the cell membrane (**Figure 3.17B**). We did however detect some nuclear staining of MerTK, but this was only a few cells in a field of 1 x 10^5 smooth muscle cells. Thus, we conclude from this experiment that VSMC do express MerTK in their transcriptome, but active, membranous MerTK is not apparent in these cells in baseline or inflammatory conditions.

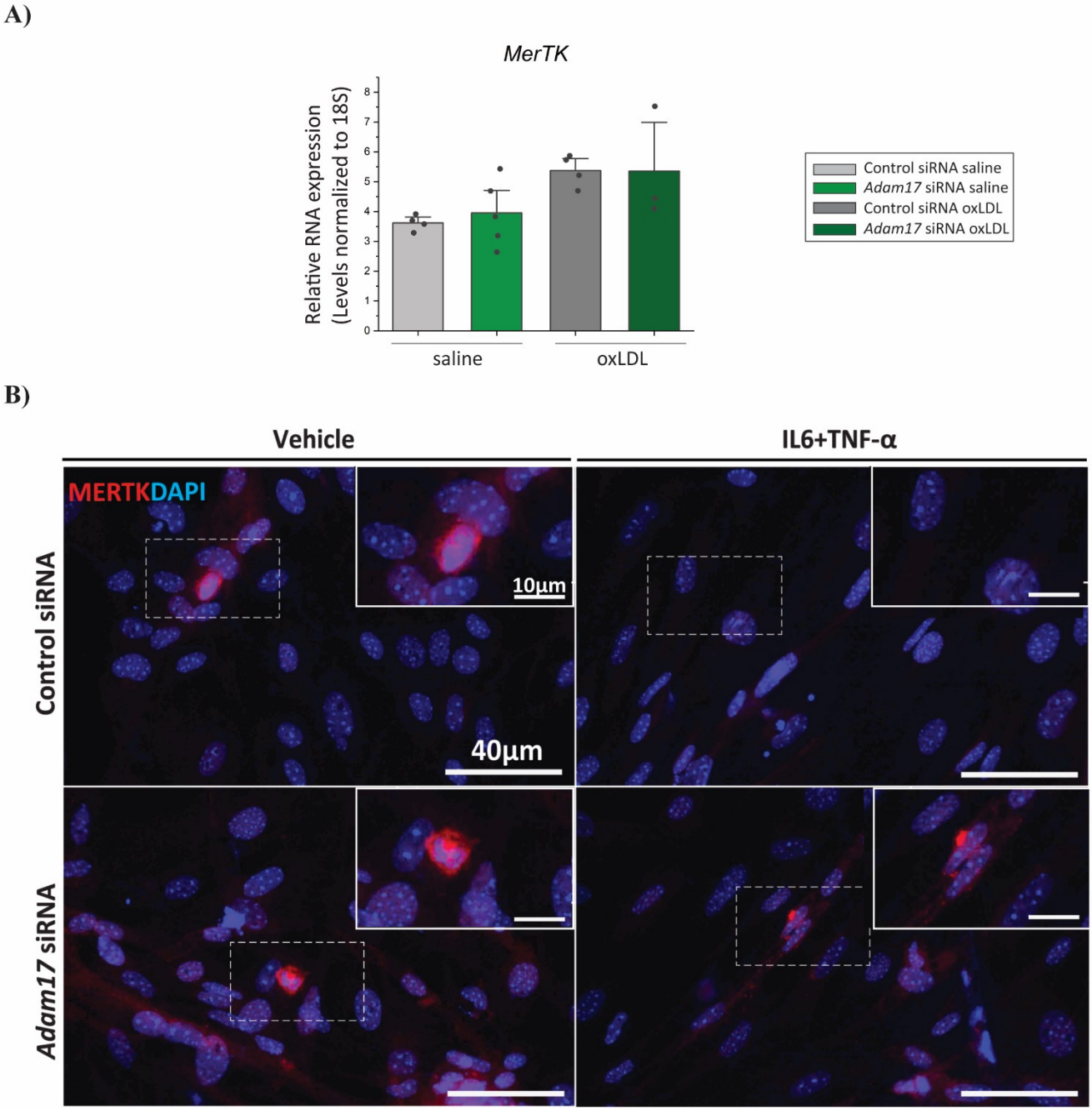

Figure 3.16 VSMC do not express MerTK on the cell membrane.

A. Real-time quantitative PCR analysis of *MerTK* in VSMC cell lysates treated with control or *Adam17* siRNA and saline or 20µg/ml oxLDL for 72 hours. Two-Way ANOVA followed by Bonferroni means comparison test was conducted. Averaged data represent mean±SEM. **B.** Immunofluorescent staining of MerTK in VSMC treated with siRNA and IL-6/TNF-α showing minimal expression of MerTK around the nuclei of a small number of cells (scale bars=40µm and the inset 10µm).

3.16 ADAM17 is Knocked Down in Bone Marrow-Derived Macrophages (BMDM)

To study the effect of ADAM17 in BMDM, we used *Adam17*-specific siRNA (along with Lipofectamine) to knock-down ADAM17 in primary bone marrow-derived macrophages *in vitro*. BMDM was isolated from *Ldlr*$^{-/-}$ mice which would provide a similar atherogenic environment as they would in the *in vivo*. Control siRNA was used alongside all experiments as controls. Protein levels were visualized using an ADAM17 antibody specific for the cytoplasmic domain (**Figure 3.18**). This data shows that on average, approximately 90% of ADAM17 protein levels are decreased compared to control siRNA treated BMDM, providing a sufficient knock-down of ADAM17 for our studies.

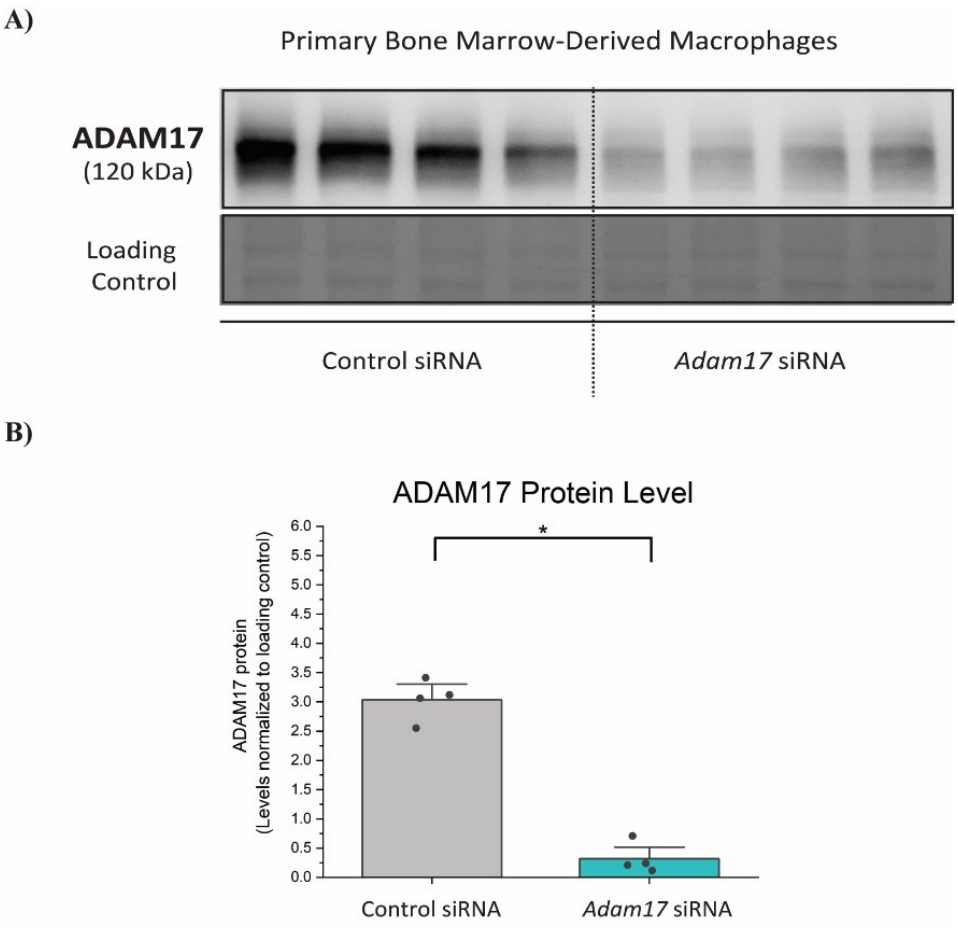

Figure 3.17 ADAM17 protein is knocked-down with *Adam17*-specific siRNA in BMDM.

A. Western blot showing ADAM17 knockdown in primary cultured BMDM lysates with control (negative siRNA) and *Adam17*-specific siRNA (15nM for 18 hours) loaded with 25ug protein/lane. ADAM17 primary antibody (EHS008) specific for the cytoplasmic domain of ADAM17 was detect at approximately 120 kDa. **B.** Quantification of ADAM17 knock-down in cultured VSMC. Unpaired student t-test was used to determine significance at the 0.05 level. Averaged data represent mean±SEM.

3.17 *Adam17*^{KD} in BMDM Augments Lipid Content

To understand the effect of ADAM17 on lipid loading in macrophages, we transfected cells with control and *Adam17* siRNA and treated them with 10μg/ml oxidized LDL (oxLDL) for 48 hours. Oil Red-O staining was used to visualize neutral lipids between the cells. Control cells treated with saline were used to verify that the ORO^{+} staining was only observed with the addition of oxLDL. Along with the VSMC, the *Adam17*^{KD} macrophages also had significantly higher oxLDL content than the control cells after 48 hours (**Figure 3.19**). ADAM17 inhibition in BMDM led to a 1.49-fold increase in intracellular lipid content. ORO^{+} staining was not detected in saline treated cells. Thus, ADAM17 deletion in macrophages augments intracellular lipid load in response to oxidized LDL.

3.18 *Adam17*^{KD} in BMDM Augments Scavenger Receptor-Mediated Lipid Loading

To determine if the increased lipid loading seen in the *Adam17*^{KD} Oil Red-O stained BMDM was due to increased lipid uptake, we used fluorescently labelled oxLDL (Dil-oxLDL) treatment. siRNA treated BMDM were insulted with 10μg/ml Dil-oxLDL for 24 hours and imaged via fluorescent microscopy with DAPI *Adam17*^{KD} BMDM showed significantly increased uptake of Dil-oxLDL after 24 hours as compared to the control siRNA treated cells (**Figure 3.20**). ADAM17 inhibition in BMDM led to a 1.34-fold increase in scavenger receptor-mediated lipid loading. There was no fluorescence detected in the vehicle treated groups. Therefore, these data suggest increased lipid loading in BMDM in response to oxLDL is in part due to elevated scavenger-receptor mediated lipid loading. Thus, we interpret this to imply increased levels of scavenger-receptors on the membranes of *Adam17*^{KD} macrophages, highlighting an important overlapping role of ADAM17 in VSMC and BMDM.

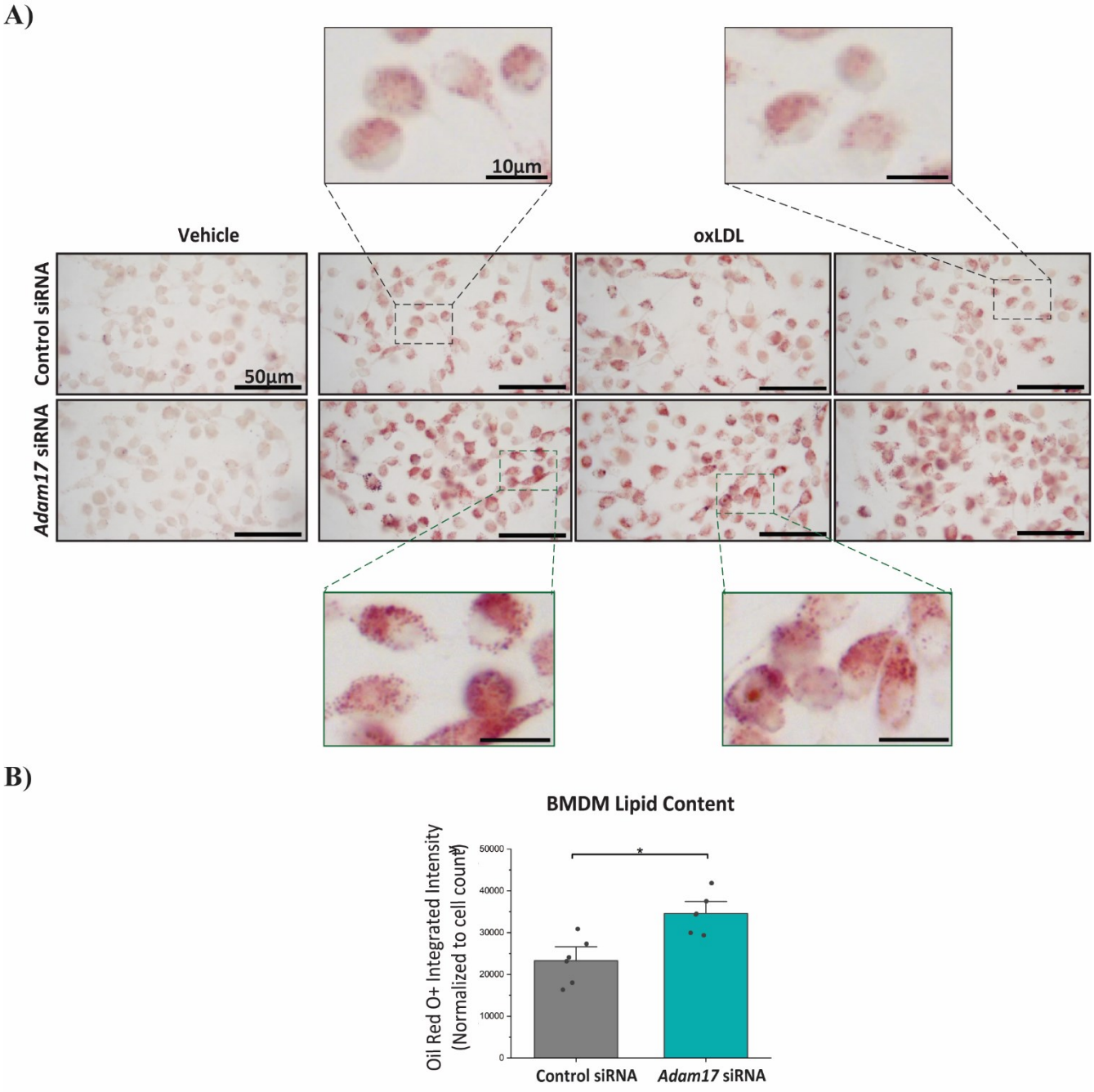

Figure 3.18 ADAM17 knockdown in BMDM augments lipid loading in response to oxLDL.

A. Primary cultured BMDM (isolated from 3-4 *Ldlr*$^{-/-}$ mice) treated with vehicle or 10µg/ml oxidized LDL for 48 hours and stained with 0.5% ORO solution to visualize neutral lipids in red (scale bars=50µm and 10µm for the inset) showing increased lipid content in *Adam17*^{KD} macrophages. **B.** ImageJ was used to calculate red pixel integrated intensity (n=6 images/group) and normalized to cell count per frame. Each data point represents data from one frame at 400x magnification. Unpaired student t-test was used to determine significance at the 0.05 level. Averaged data represent mean±SEM.

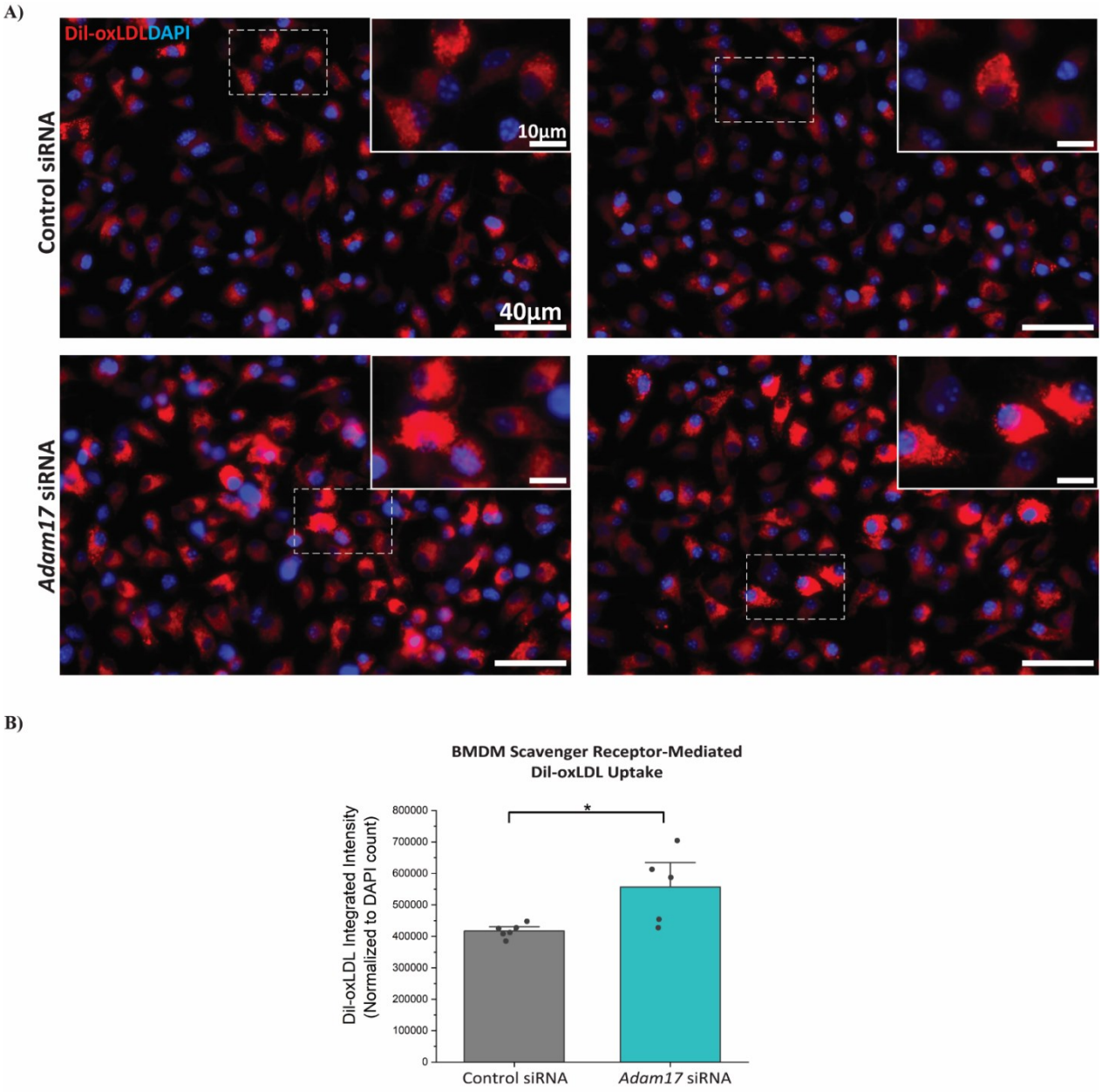

Figure 3.19 ADAM17 knockdown in BMDM augments scavenger receptor-mediated lipid loading.

A. Primary cultured BMDM (isolated from 3-4 *Ldlr*$^{-/-}$ mice) treated with vehicle or 10μg/ml Dil-oxidized LDL (Dil-oxLDL) for 24 hours showing increased scavenger receptor-mediated lipid loading in the *Adam17*^{KD} macrophages (scale bars=40μm and the inset 10μm). **B.** ImageJ was used to calculate red pixel integrated intensity (n=5-6 images/group) and normalized to DAPI count per frame. Each data point represents data from one frame at 400x magnification. Unpaired student t-test was used to determine significance at the 0.05 level. Averaged data represent mean±SEM.

3.19 *Adam17*^{KD} in BMDM Does Not Change Cholesterol Efflux Capacity

It has been reported that ADAM17 can induce cholesterol efflux in macrophages through expression of the ABCA1 transporter.[23] However, we could not detect a decrease in cholesterol efflux in our *Adam17*^{KD} macrophages (**Figure 3.21**), despite observing a decrease in *Abca1* expression with *Adam17* siRNA and oxLDL (**Figure 3.22**). This could be due to the experiment being done at baseline conditions. The research cited above used cyclic AMP-induced cholesterol efflux, which resulted in a more pronounced decrease in efflux compared to the baseline conditions between the wild type and *Adam17*^{KD} macrophages. Therefore, we can not conclude ourselves that ADAM17 inhibition in macrophages decreases cholesterol efflux, but further inquiry is required.

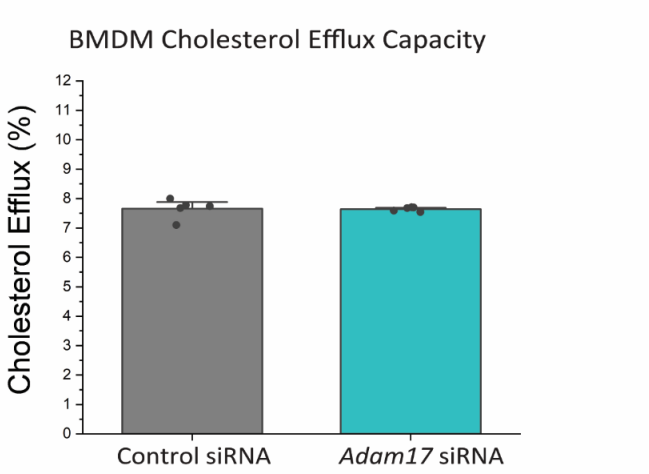

Figure 3.20 ADAM17 knockdown in BMDM does not affect cholesterol efflux.

Primary cultured BMDM (isolated from 3-4 *Ldlr*$^{-/-}$ mice) were transferred to 96-well plates and the efflux assay (MAK192, Sigma-Aldrich) was performed as per manufacturers instructions. These data showed no difference in cholesterol efflux capacity between control or *Adam17*^{KD} macrophages. Cholesterol efflux was calculated by fluorescence intensity of the supernatant divided by the sum of the fluorescence intensity of the supernatant plus cell lysate. Unpaired student t-test was used to determine significance at the 0.05 level. Each data point is one well in a 96-well plate. Averaged data represent mean±SEM.

3.20 Macrophage Lipid Transporter Expression

To determine if *Adam17* had any role in modulating the expression of any lipid transport proteins in macrophages, we utilized RT-PCR to amplify and quantify mRNA expression of key lipid transporters (**Figure 3.22**). Cell cultures of BMDM were transfected with siRNA and treated with either vehicle (saline) or 10μg/ml oxLDL for 48 hours. As in the case with smooth muscle cells, we found that expression of *Abca1* was significantly reduced in the $Adam17^{KD}$ cells as compared to the controls within the oxLDL treated groups. We also observed a significant increase in *Abca1* expression from vehicle to oxLDL in the control siRNA group. We did not see this increase in the $Adam17^{KD}$ cells. Despite these differences, we did not detect a decrease in cholesterol efflux with *Adam17* siRNA (**Figure 3.21**). *Sra1* expression decreased with oxidized LDL in the $Adam17^{KD}$ group, but there was no difference in the control siRNA group. *Srb1* expression increased with oxLDL in the control siRNA group, but not in the $Adam17^{KD}$ group. Furthermore, in the oxLDL treated cells, *Srb1* expression was significantly lower with *Adam17* siRNA compared to the control group. Thus, further investigation is required to determine if this decrease in *Abca1* mRNA leads to a decrease in ABCA1 at the protein level, thereby augmenting lipid loading in these cells.

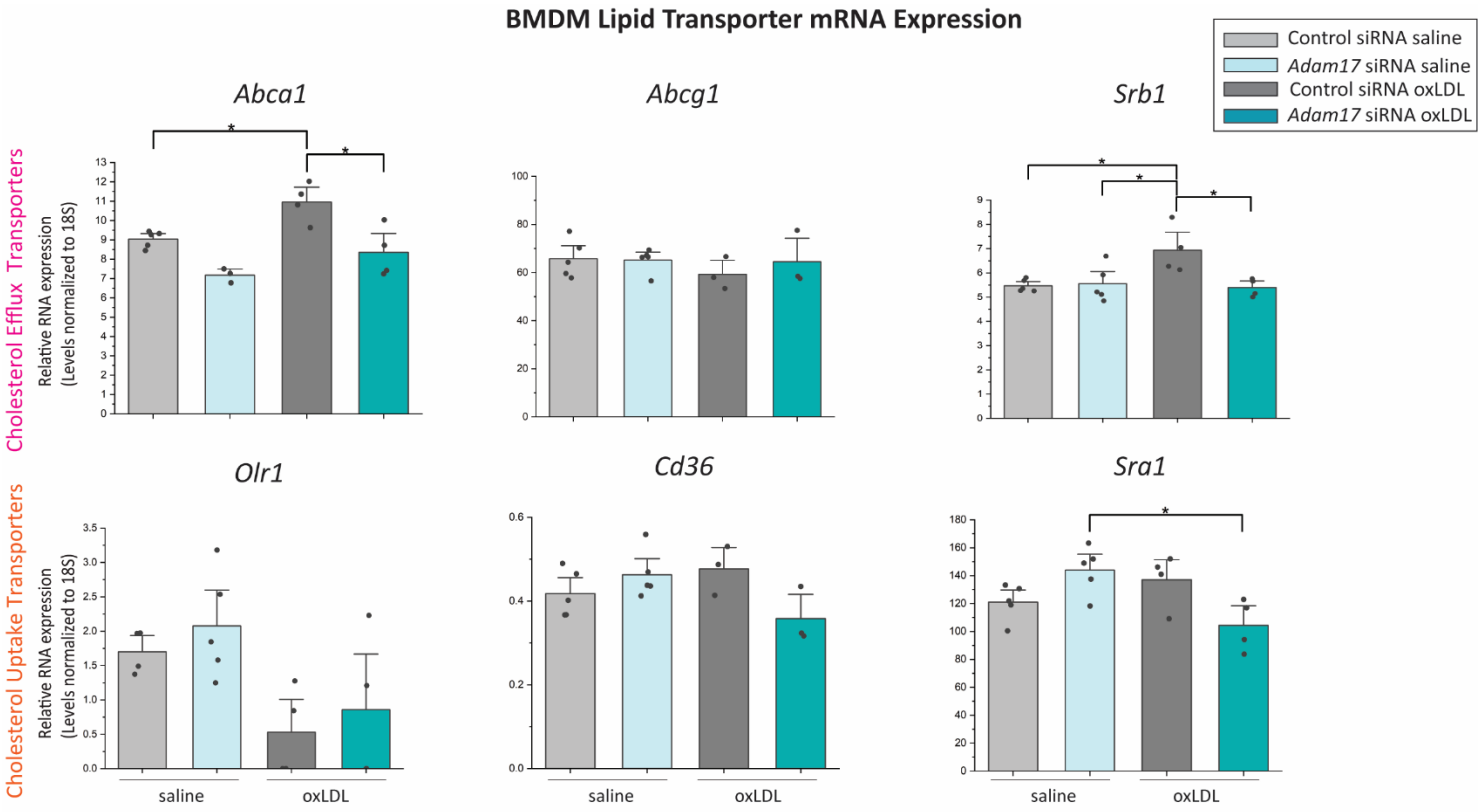

Figure 3.21 ADAM17 knockdown in BMDM reduces oxLDL-mediated *Abca1* expression.

Real-time quantitative PCR analysis of cholesterol transport proteins in BMDM cell lysates treated with control or *Adam17* siRNA and saline or 10µg/ml oxLDL for 48 hours. Statistical significance determined via Two-Way ANOVA followed by Bonferroni means comparison test. Averaged data represent mean±SEM.

3.21 *Adam17*^{KD} in BMDM Augments Efferocytosis

Like the VSMC, *Adam17*^{KD} macrophages have increased lipid content when exposed to oxidized LDL, possibly exacerbating atherosclerosis. However, macrophages also have the capacity for efferocytosis, which could potentially improve plaque area through clearance of dead cell debris within the plaque. Therefore, we investigated the role of ADAM17 on macrophage efferocytosis using the same protocol as with our VSMC. After incubating siRNA treated macrophages with non-apoptotic or apoptotic Jurkat cells, we found that macrophages lacking ADAM17 had increased ability to bind and initiate efferocytosis of apoptotic Jurkat cells (**Figure 3.23**). Control siRNA treated cells exhibited approximately 9% efferocytosis, while the *Adam17*^{KD} BMDM had 2-fold this amount at ~18%. The non-apoptotic Jurkat cells did not bind to the macrophages and were washed off as per our protocol. Thus, ADAM17 loss augmented the ability of macrophages to bind to and recognize apoptotic stimuli.

3.22 *Adam17*^{KD} in BMDM Augments MerTK Expression

MerTK is known to be expressed by macrophages as a key player in the process of efferocytosis. We hypothesized that the increase in efferocytosis that we observed with *Adam17*^{KD} macrophages was due to preservation of the MerTK protein on the surface of macrophages. We therefore insulted siRNA treated macrophages with IL-6 and TNF-α to induce expression of MerTK and stained for the protein via immunofluorescent antibodies. We observed an increase in MerTK positive staining in the *Adam17*^{KD} macrophages (**Figure 3.24**). Furthermore, IL-6 and TNF-α increased MerTK expression in both groups. Interestingly, MerTK was observed as punctuated dots at the junctions of adjacent macrophages, which was not seen when performed on smooth muscle cells. Thus, along with increased efferocytosis, ADAM17

inhibition in macrophages augments surface level expression of the key efferocytotic receptor MerTK.

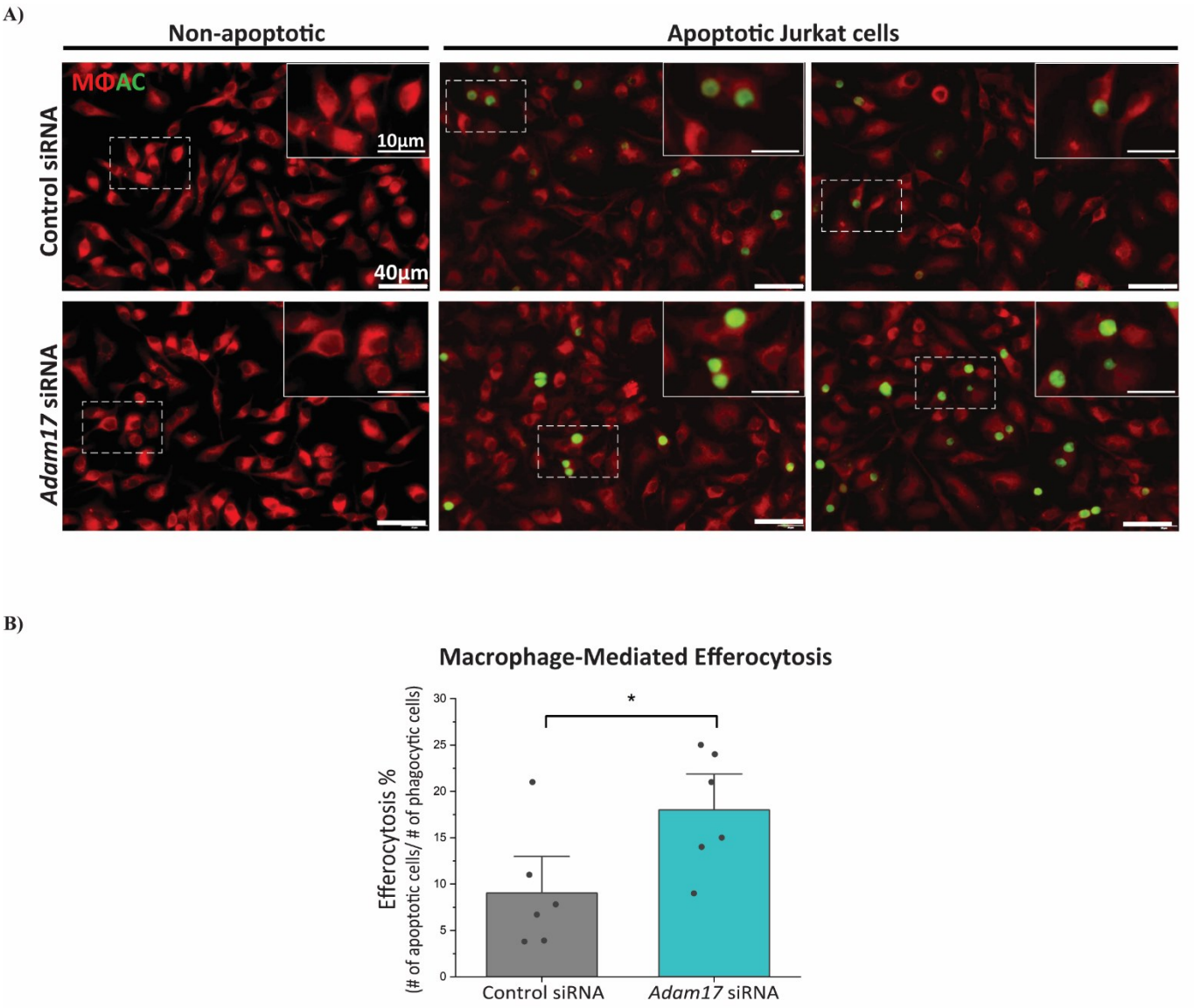

Figure 3.22 ADAM17 knockdown in BMDM augments efferocytosis of apoptotic stimuli.

A. Non-apoptotic (0µM Staurosporine A/1hr.) and apoptotic (5µM/1hr.) Jurkat cells incubated on control or *Adam17* siRNA treated VSMC (scale bars=40µm and the inset 10µm). Jurkat cells (Calcein-Am, green) can be seen bound specifically to the macrophages (CD68, red), with a higher amount bound to the $Adam17^{KD}$ macrophages. **B.** Quantification of efferocytosis by dividing the number of bound Jurkat cells by the total number of macrophages and expressing it as a percentage. Unpaired student t-test was used to determine significance at the 0.05 level. Each data point is one frame at 400x magnification. Averaged data represent mean±SEM.

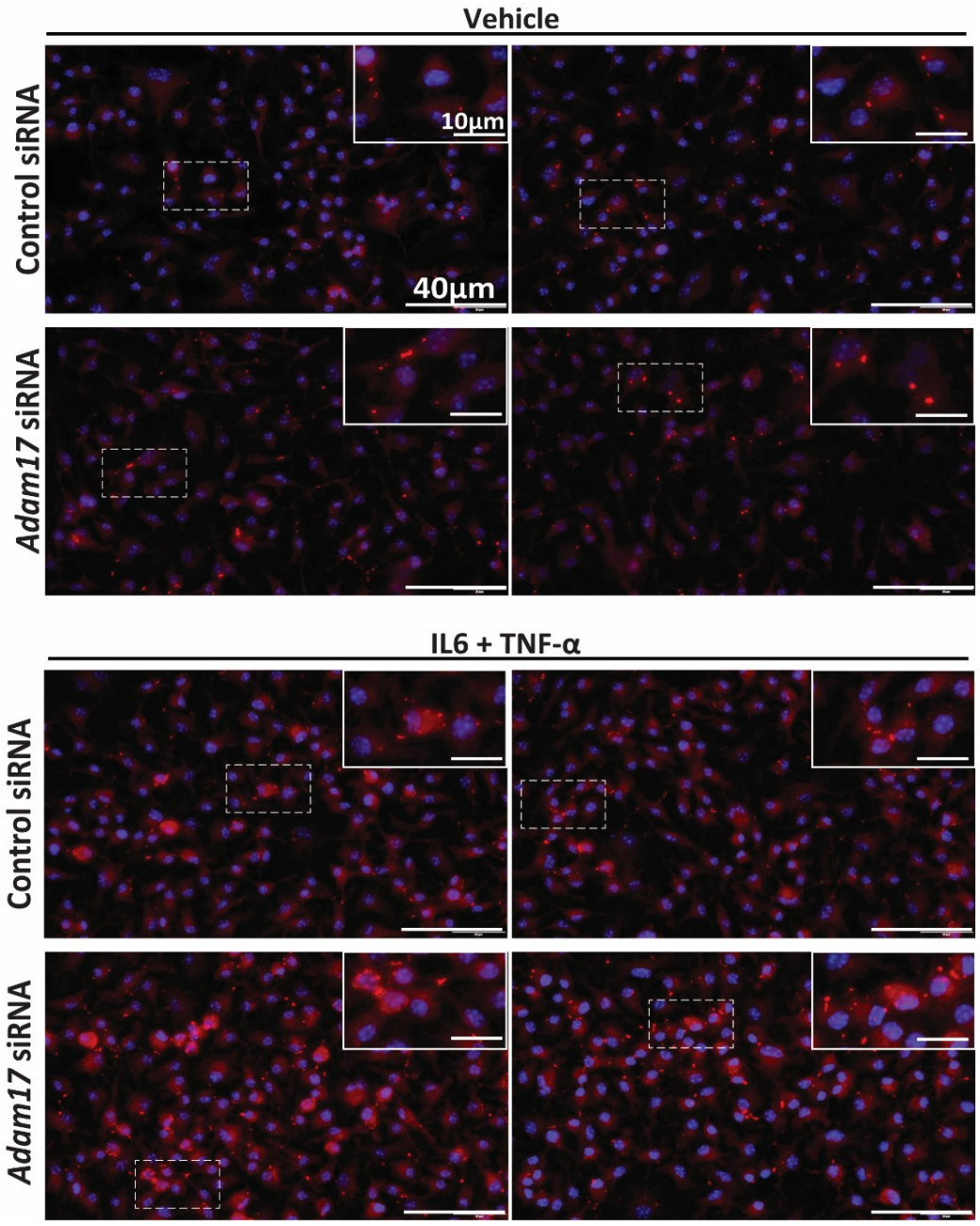

Figure 3.23 ADAM17 knockdown in BMDM augments MerTK expression in response to inflammatory stimuli.

Immunofluorescent staining of MerTK in BMDM treated with siRNA and IL-6/TNF-α (10ng/ml each) showing increased expression of MerTK on the surface of *Adam17*^{KD} macrophages (scale bars=40µm and the inset 10µm).

3.23 *Adam17*^{KD} in BMDM Augments MerTK Protein Levels

We also investigated the mRNA and protein expression of MerTK in macrophages treated with oxidized LDL. In the control siRNA macrophages, *MerTK* RNA expression increased significantly with oxLDL introduction (**Figure 3.25B**). However, this increase was not seen in the *Adam17*^{KD} cells, and the expression was significantly lower than the control siRNA treated cells within the oxLDL group.

Protein expression of MerTK in response to oxLDL was investigated via western blotting. We observed that, in the oxLDL groups, MerTK protein levels were minimally higher in the *Adam17*^{KD} cells compared to the control siRNA treated cells (**Figure 3.25A**). However, these data were not statistically significant, so further experimentation is necessary.

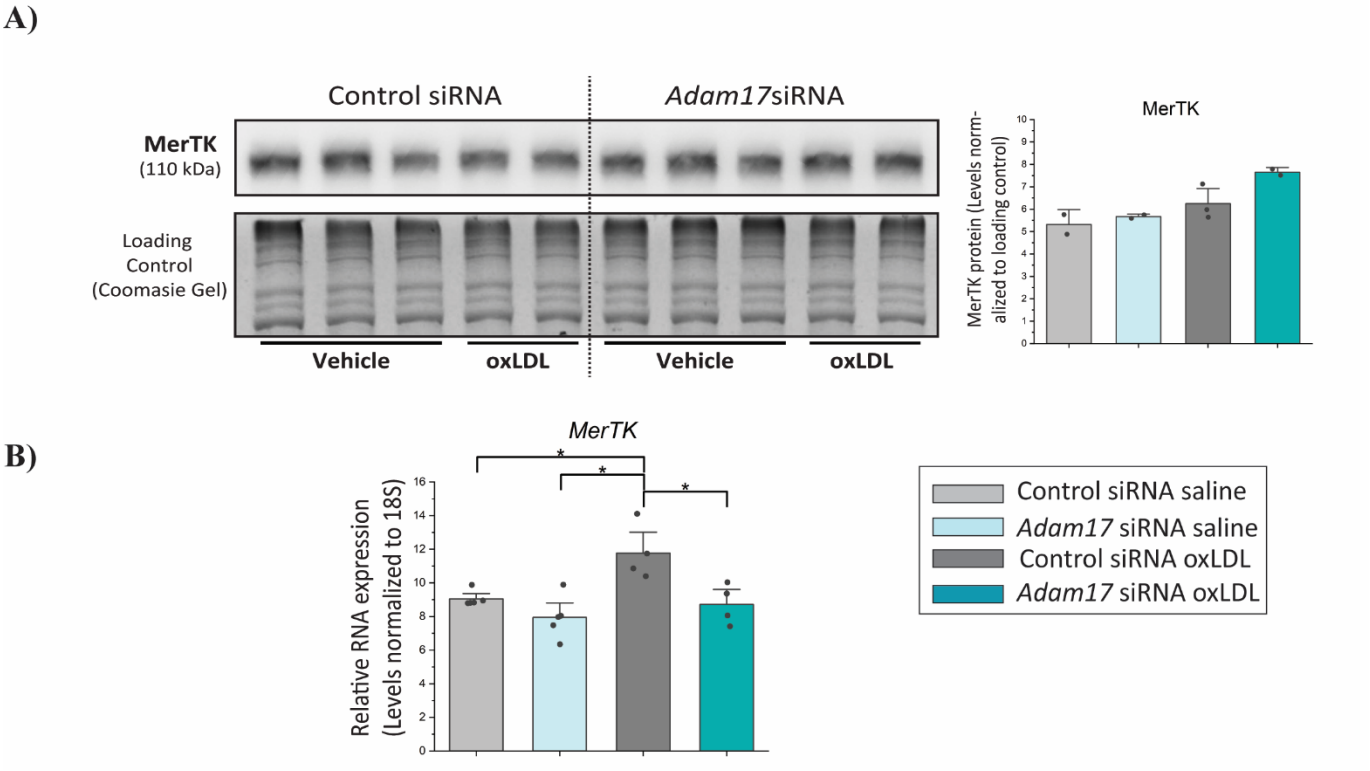

Figure 3.24 MerTK mRNA and Protein Expression in Macrophages

A. Western blot of MerTK (110 kDa) in lysates of primary cultured BMDM with control and *Adam17*-specific siRNA (15nM for 18 hours) loaded with 20ug protein/lane. Cells were also treated with vehicle or 10 µg/ml oxidized LDL for 48 hours. MerTK protein expression was quantified via ImageJ software and normalized to the loading control. Statistical significance was determined via Two-Way ANOVA followed by Bonferroni means comparison test. Averaged data represent mean±SEM. **B.** Relative mRNA expression of *MerTK* in siRNA and oxLDL treated macrophages showing a significant decrease in MerTK RNA expression in the $Adam17^{KD}$ macrophages treated with oxLDL. Statistical significance was determined via Two-Way ANOVA followed by Bonferroni means comparison test. Averaged data represent mean±SEM.

CHAPTER 4

DISCUSSION

Important Findings

With the findings of this study, we propose that VSMC ADAM17 plays a protective role in atherosclerosis. We report that C57BL/6 mice lacking ADAM17 in VSMC have increased aortic plaque area after 5 months of high cholesterol diet feeding. *In vitro*, aortic SMCs lacking ADAM17 display increased scavenger receptor-mediated uptake of oxidized LDL, a possible explanation for the exacerbated phenotype *in vivo*. Moreover, $Adam17^{KD}$ VSMC have reduced cholesterol efflux. In the absence of efficient expulsion, cholesterol accumulates within the smooth muscle cell, disrupting its natural homeostasis. Without a regulatory feedback mechanism, this accumulation may eventually lead to the transformation of the cell into foam cells. We found reduced *Abca1* mRNA levels, which may implicate ADAM17 as having a part in promoting the expression of the efflux transporter. Nevertheless, these cells also exhibit increased scavenger receptor-mediated oxLDL uptake, implicating a broad role in lipid metabolism for this metalloproteinase. Therefore, further inquiry is required into the role of ADAM17 in regulating lipid trafficking.

$Adam17^{KD}$ macrophages exposed to oxLDL also have increased lipid loading, but we were not able to detect a change in efflux capacity. However, scavenger receptor-mediated uptake of oxLDL was observed to be augmented in the $Adam17^{KD}$ cells, in line with the VSMC data as ADAM17 having a protective role. Unlike VSMCs, however, macrophages lacking ADAM17 have increased capacity to recognize and initiate efferocytosis of apoptotic stimuli. Efferocytosis within the plaque can prevent exacerbation of the necrotic core, and possibly prevent instability of the plaque. Therefore, these results could possibly paint ADAM17 as a culprit in atherosclerosis with cell-specific functions, requiring further investigations.

4.1 Mice Lacking ADAM17 in Smooth Muscle Cells Have Increased Atherosclerotic Burden

The observation that mice deficient in VSMC-specific ADAM17 have increased atherosclerotic plaque area in the aorta and aortic valve, along with increased size and frequency of necrotic cores within the plaques prompts a deeper exploration into the role of ADAM17 in atherosclerosis. Notably, the absence of ADAM17 in SMCs resulted in longer and larger atherosclerotic plaques throughout the aorta and aortic root, indicating a potentially pivotal role for ADAM17 in plaque morphology. The aortic valves revealed that with ADAM17 deficiency, the plaques had larger and more frequent necrotic cores. Plaques with large necrotic cores makes them more susceptible to rupture and subsequent release of thrombogenic mediators which can cause myocardial infarction.[161] The diverse outcomes observed in different cell types, such as enhanced plaque stability in rabbits, contrasting effects in myeloid and endothelial cells, and the exacerbated pathology of ADAM17 hypomorphic mice, underscores the nuanced nature of ADAM17 in the atherosclerotic process.[16,17,102] Our research has found a protective effect of ADAM17 in vascular smooth muscle cells which prevents accelerated plaque formation.

Unfortunately, this *Myh11* Cre-driver is expressed on the Y chromosome in mice, therefore our *in vivo* findings are limited to male mice. As such, performed *in vitro* studies using female VSMC, but this may not represent the effects of ADAM17 deletion in female VSMC *in vivo*. It is known that pathologies affecting SMC-dense tissue, including atherosclerosis, display sex-dependent differences.[162] Specifically, *Ldlr*$^{-/-}$ female mice have been shown to develop increased atherosclerosis as compared to males.[163,164] Interestingly, endothelial deletion of CD36 lead to reduced atherosclerosis in female mice as compared to males, but global ablation of CD36 reduced atherosclerosis in both male and female *Ldlr*$^{-/-}$ mice.[59] CD36 has been shown to be cleaved by ADAM17, and it is possible that this may attenuate atherosclerosis progression.[20]

It is possible that similar to the experiment mentioned, there may be sex differences in atherosclerosis progression between male and female mice lacking ADAM17 in VSMC if this can modulate levels of CD36. Therefore, it is necessary to state that although cell cultures of female cells do provide valuable insight into potential mechanism at play, *in vivo* data are the gold standard for reporting sex differences in atherosclerosis.

4.2 Macrophages and Neutrophils in the Aortic Wall

Inflammation in the arterial wall under hypercholesterolemic conditions was assessed by immunofluorescent staining for macrophage and neutrophil markers. Notably, the $CD68^+$ area showed a substantial increase in macrophage content at 3 months of HCD feeding in the *Ldlr*$^{-/-}$*/Adam17*^{SMC} group (Figure 3.5 A). The CD68 area was localized to the plaque regions, with its expression being proportionally related to the size of the lesion. Therefore, since the ADAM17 knock-out mice had larger plaques after 3 months of HCD feeding, the $CD68^+$ area was inevitably increased. Expanding the investigation on inflammation, neutrophils were visualized as well in the atherosclerotic artery. The results demonstrated an elevated expression of Ly6B in the *Ldlr*$^{-/-}$*/Adam17*^{SMC} group compared to control mice. Intriguingly, neutrophils were observed distributed throughout the medial layers of the aorta, with a greater concentration in heavily diseased plaques. In contrast to the macrophages, neutrophils showed significantly less expression within the plaques. A reason for their limited detection in plaques could be a consequence of their short life span in lesional areas compared to other leukocytes.[165,166] However, the presence of Ly6B expression in the aortic wall prompts further questions into how and why the neutrophils appear in the tunica media. One study has notated that neutrophils specifically infiltrate the shoulder regions of plaques in an atherosclerotic mouse model.[167] Furthermore, these neutrophils were shown to accumulate in areas with high monocyte density.

High monocyte density in the *Ldlr*$^{-/-}$*/Adam17*^{SMC} mice may explain why they have increased neutrophil content, and although our mice have increased CD68 expression, this does not implicate a higher monocyte content as well. Typically, neutrophils are thought of as transient mediators to recruit monocytes and macrophages, though this narrative has been challenged. The lifespan of neutrophils at sites of inflammation are determined by growth factors and cytokines, and neutrophils ultimately undergo apoptosis, which is believed to be anti-inflammatory due to macrophage-mediated clearance and resolution.[168] However, in atherosclerosis, if the macrophages are saturated with apoptotic signals and reach maximum engulfment capacity, the neutrophils may become necrotic and propel further inflammation.[169] Due to excessive and accelerated atherosclerotic progression in our *Ldlr*$^{-/-}$*/Adam17*^{SMC} mice , neutrophil clearance may be defective leading to its preservation in the aortic wall. This may highlight a specific role of neutrophils in the aortic as compared to CD68-expressing macrophages and monocytes. Nevertheless, these results contribute to the notion that ADAM17 plays a crucial role in orchestrating an inflammatory response within the atherosclerotic environment.[170-172]

4.3 VSMC Phenotype Switching

As smooth muscle cells are known to transform to macrophage-like cells in atherosclerosis, we sought to investigate whether ADAM17 played a role in this process. We found that *Adam17*^{KD} VSMC had increased expression of macrophage-marker CD68 when insulted with oxLDL as compared to the control cells. We found subpopulations of cells in both control and *Adam17*^{KD} groups with decreased calponin expression and augmented CD68 expression, and these subpopulations were larger and more frequent in the *Adam17*^{KD} group. Transformation into CD68-expressing cells did not occur in the groups treated with only saline, underscoring the importance of oxidized LDL in propelling the atherosclerotic process. These

findings along with the increased lipid loading represents an increased propensity of *Adam17*^{KD} VSMC to phenotype-switch into macrophage-like cells and subsequent foam cells. Cholesterol loading in VSMC promotes transformation to macrophage-like cells via downregulating microRNA (miR)-143/145-myocardin axis, a signalling pathway specific for VSMC differentiation.[173] Interestingly, it has been reported that miR-145 can inhibit ADAM17 activity.[174,175] Thus, as cholesterol loading reduces expression of these key phenotype regulators, the increased oxLDL accumulation seen in *Adam17*^{KD} VSMC (as a consequence of decreased efflux and increased uptake) may decrease miR-143/145 and myocardin expression, accelerating the conversion of smooth muscle cells into a $CD68^{+}$ macrophage-like phenotype.

4.4 Vascular Smooth Muscle Cell Lipid Loading

Our *in vitro* studies indicate a role for ADAM17 in modulating lipid loading in VSMC. The main scavenger receptors in foam cell formation include OLR1, CD36, and SR-A1.[176] In our VSMC culture, we did not detect any significant changes in mRNA expression of scavenger receptors, though they tended to be higher than their control siRNA treated counterparts with oxLDL incubation. Therefore, any changes in scavenger receptor protein levels may be due to ADAM17 mediated cleavage (*i.e.* cell surface shedding of CD36) rather than through a signalling event. It has been reported that CD36, a primary scavenger receptor, is cleaved by ADAM17 on macrophages making them less efficient at CD36-dependent apoptotic cell uptake.[20] In the context of atherosclerosis, if this occurs on the membrane of VSMC transforming to macrophage-like cells or in VSMC-derived foam cells lacking ADAM17, CD36 preservation could accelerate lipid uptake, explaining why these cells have increased lipid content. However, one major limitation of this study is that we do not have the protein level data

of these lipid transporters, which is crucial for a comprehensive understand of the changes in lipid metabolism with *Adam17*^{KD}.

We observed that *Adam17*^{KD} VSMC exhibit reduced cholesterol efflux accompanied by reduced *Abca1* mRNA expression in response to oxLDL treatment. Recently, it has been reported that ADAM17-mediated TNF-α shedding can lead to the expression of ABCA1 via NF-kB, promoting cholesterol efflux in macrophages.[23] This indicates a non-direct role of ADAM17 in lipid metabolism by regulating the expression of ABCA1 through TNF-α processing (Figure 4.1). TNF-α has been previously shown to induce ABCA1 expression in macrophages, but conversely been shown to reduce ABCA1 in human intestinal cells and pancreatic β-cells.[177-180] In this research, we demonstrate that in VSMC, ADAM17 depletion decreases *Abca1* expression, which could contribute to the reduced cholesterol efflux, augmenting foam cell formation. Furthermore, this could contribute to the accelerated transformation to macrophage-like cells and the elevated plaque area seen in the *Ldlr*$^{-/-}$*/Adam17*^{SMC} mice.

4.5 Macrophage Lipid Loading

After the discovery that *Adam17*^{KD} VSMC exhibit increased lipid loading, we sought to investigate if this was also the case in bone marrow-derived macrophages (BMDM), or if ADAM17 had a different role in these cells. According to recent literature, ADAM17 has been shown to boost cholesterol efflux in macrophages through the expression of ABCA1.[23] Though we did see reduced mRNA expression of *Abca1* in *Adam17*^{KD} macrophages treated with oxLDL, we were not able to detect a change in efflux at basal levels compared to control siRNA treated cells. Possibly repeating the experiment with an inducer of cholesterol efflux may lead to results consistent with the literature. In the case of our cultured VSMC, oxLDL incubation led to an approximate 4x increase in RNA expression of *Abca1,* whereas in the BMDM, this increase was

only about 1.2-fold. Although they were treated with different amounts and durations of oxLDL, this could highlight the robust nature of macrophages in the hyperlipidemic environment by maintaining suitable protein levels of ABCA1 even though the TNF-mediated RNA expression may decrease (*i.e.* in the *Adam17*^{KD} cells). In support of this, it has been shown that lipid-loaded SMC have insufficient ability to hydrolyze lysosomal lipids compared to macrophages, subsequently causing reduced expression of *Abca1,* whereas this insufficiency to hydrolyze and efflux cholesterol is not present in marcophages.[181] Moreover, it is well known that macrophages express high levels of ABCA1 compared to VSMC, so a decrease in RNA expression (as a result of ADAM17 knockdown) in macrophages may not reflect as drastic of a change in cholesterol efflux as is seen in the VSMC. In support of this, ABCA1 expression, as well as 27-hydroxycholesterol and LXRα (the key oxysterol and transcription factors required for ABCA1 upregulation) are all lower in arterial SMC compared to macrophages.[182] A recent study has shown that dysfunctional autophagy-mediated cholesterol efflux to HDL is greatly impaired in VSMC as compared to macrophages, which was due to the predominant expression of ABCG1 in VSMC.[183] This could also explain why we didn't observe a decrease in cholesterol efflux in the *Adam17*^{KD} macrophages even though *Abca1* expression was decreased, since autophagy-mediated efflux is not impaired in macrophages and may contribute to overall cholesterol efflux.

Furthermore, we also observed a decrease in *Srb1* expression in *Adam17*^{KD} macrophages treated with oxLDL. It is possible that SR-B1 protein levels may also be reduced in this case, which would lead to reduced RCT and possibly exacerbate foam cell formation. However, SR-B1 has been shown to not contribute to RCT as much as ABCA1 and ABCG1 transporters *in vivo*.[184] Therefore, the participation of SR-B1 in cholesterol efflux may not be as relevant, but SR-B1 has also been shown to mediate binding and removal of apoptotic cells and autophagy,

limiting necrotic core formation and augmenting plaque stability.[185] Therefore, a possible decrease in SR-B1 in *Adam17*^{KD} macrophages may exacerbate plaque formation by insufficient apoptotic cell clearance. A possible explanation for decreased *Srb1* RNA we observed in *Adam17*^{KD} macrophages may be a result of reduced PPAR-γ activity, which is known to upregulate SR-B1.[186,187] PPAR-γ activity is greatly reduced in ADAM17-null embryonic fibroblasts, which could translate into *Adam17*^{KD} macrophages as well, thereby ameliorating *Srb1* expression.[188] However, this assumption requires validation as this study has demonstrated the cell-specific nature and functions of ADAM17.

Consistent with the VSMC, we observed increased scavenger receptor-mediated uptake of oxLDL in *Adam17*^{KD} macrophages. As mentioned, CD36, a primary scavenger receptor, is cleaved by ADAM17.[20] It is possible that through preservation of CD36 in *Adam17*^{KD} cells, macrophages will take up more lipids through this receptor, augmenting foam cell formation (Figure 4.1). In support of this, cell surface levels of CD36 are augmented in macrophages lacking ADAM17.[20]

We did not find any significant changes in mRNA expression of *Olr1* or *Cd36* in oxLDL treated macrophages, but mRNA expression of *Sra1* was significantly reduced with ADAM17 siRNA from saline to oxLDL. If this reduction in RNA expression does indeed lead to reduced SR-A1 protein levels, one would expect that scavenger-receptor mediated lipid loading may be decreased, which has been shown to occur *in vitro*.[189] However, decreased mRNA expression does not imply decreased protein levels. Interestingly, *in vivo* SR-A1 overexpression in bone marrow cells does not increase lesion development, due to increased clearance of modified lipoproteins.[189] However, if SR-A1 protein levels are reduced in *Adam17*^{KD} cells as the mRNA

data suggests, this does not lead to an overall reduction in foam cell formation as shown by our scavenger receptor-mediated uptake data.

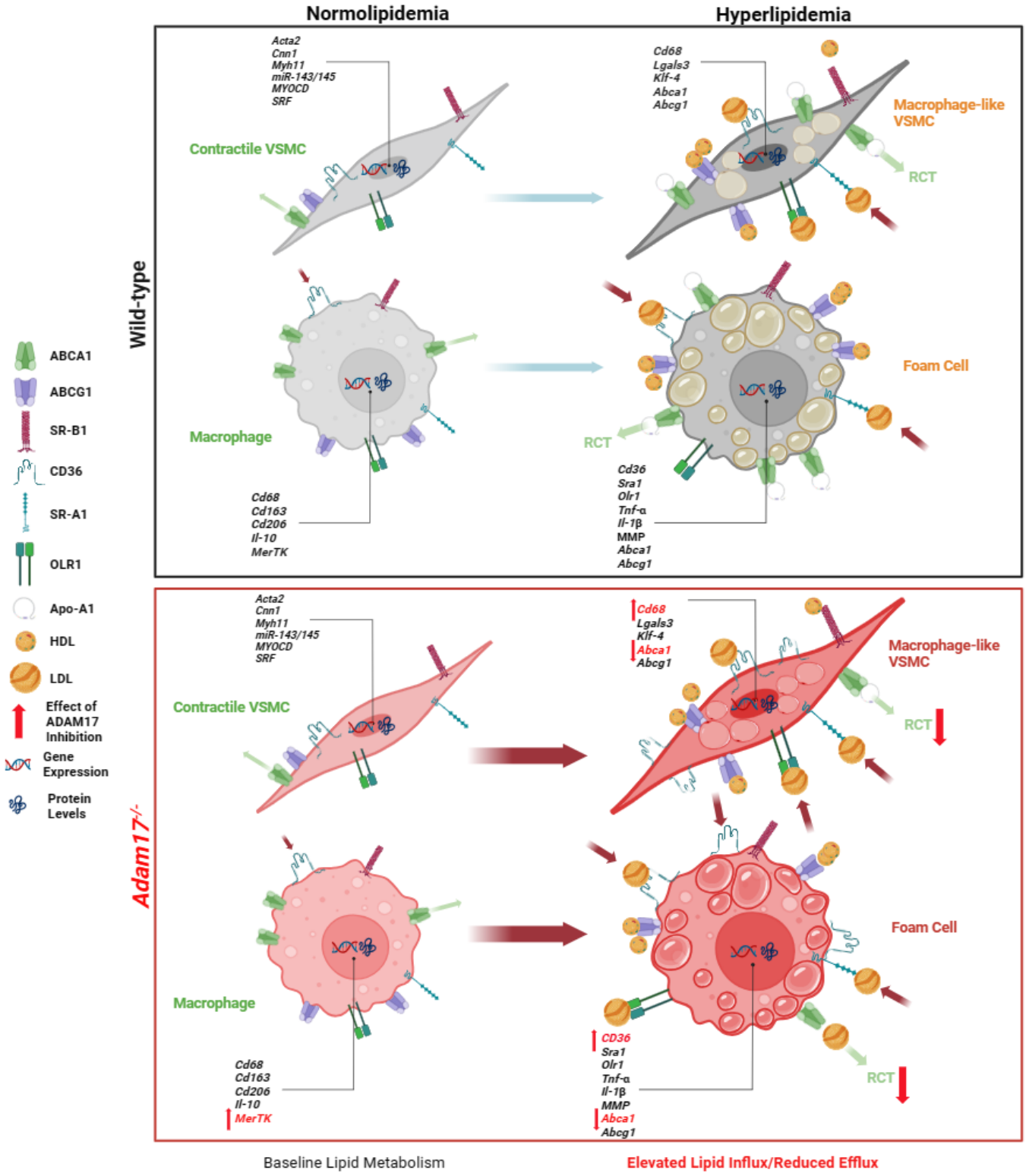

Figure 4.1 Proposed Effect of ADAM17 Knockdown in Lipid Loading in VSMC and Macrophages

Adam17^{KD} knockdown in VSMC and BMDM augments lipid loading, reduces *Abca1* expression, and accelerates the transition of VSMC to macrophage-like cells.

4.6 Macrophage Efferocytosis

The process of efferocytosis, the clearance of apoptotic cells, is a primary component of macrophage physiology and holds a pivotal significance in the context of atherosclerosis, a chronic inflammatory condition. Macrophage-mediated efferocytosis serves a critical mechanism in the resolution of inflammation by removing and processing apoptotic cells (AC) within the atherosclerotic milieu. *Adam17*^{KD} macrophages have increased capacity to recognize apoptotic stimuli and perform efferocytosis, highlighting an athero-protective role of ADAM17 in this context. ADAM17 has been shown to decrease efferocytotic capacity of macrophages through CD36 and MerTK cleavage.[20,21,156]

We found that expression of MerTK, a key cell surface receptor responsible for recognition of phosphatidylserine and activation of an anti-inflammatory response in the phagocyte, was augmented with the addition of IL-6 and TNF-α in both control and *Adam17* siRNA groups. *Adam17*^{KD} macrophages had increased MerTK expression compared to the control cells in both saline and inflammatory treatments. MerTK protein expression in *Adam17*^{KD} macrophages appear to be primarily on the membranes of the cells, which is expected for a receptor that binds to phosphatidylserine. Thus, this finding could explain the increased binding of *Adam17*^{KD} macrophages to apoptotic Jurkat cells.

Macrophages treated with oxLDL showed a significant increase in MerTK mRNA expression compared to saline treated cells, but this change was ameliorated in the *Adam17*^{KD} macrophages. It is possible that expression of MerTK mRNA is halted in this group due to the preservation of MerTK on the membrane, however this theory needs further investigation to make this claim. Western Blot analysis on whole cell lysates revealed that *Adam17*^{KD} macrophages may have slightly higher MerTK levels with oxLDL treatment, though these results

were not statistically significant. It may be necessary to determine MerTK protein levels in the membrane fractions of these cells to confirm its localization. One study has demonstrated that oxLDL increased soluble MerTK and decreased cell-surface MerTK, and this was ameliorated with an ADAM17 inhibitor.[190] This indicates that one response of ADAM17 to oxidized LDL in the atherogenic environment is cleaving MerTK, possibly exacerbating the disease in the context of atherosclerosis by reducing efferocytosis. Therefore, lack of ADAM17 may increase efferocytosis in an athero-protective manner via preservation of MerTK, but simultaneously, these cells are more prone to atherogenic lipid loading. Therefore, it would be important to look at plaque area in mice lacking ADAM17 in macrophages to determine if the improved efferocytosis could improve plaque area as compared to the *Ldlr*$^{-/-}$*/Adam17*^{SMC} mice.

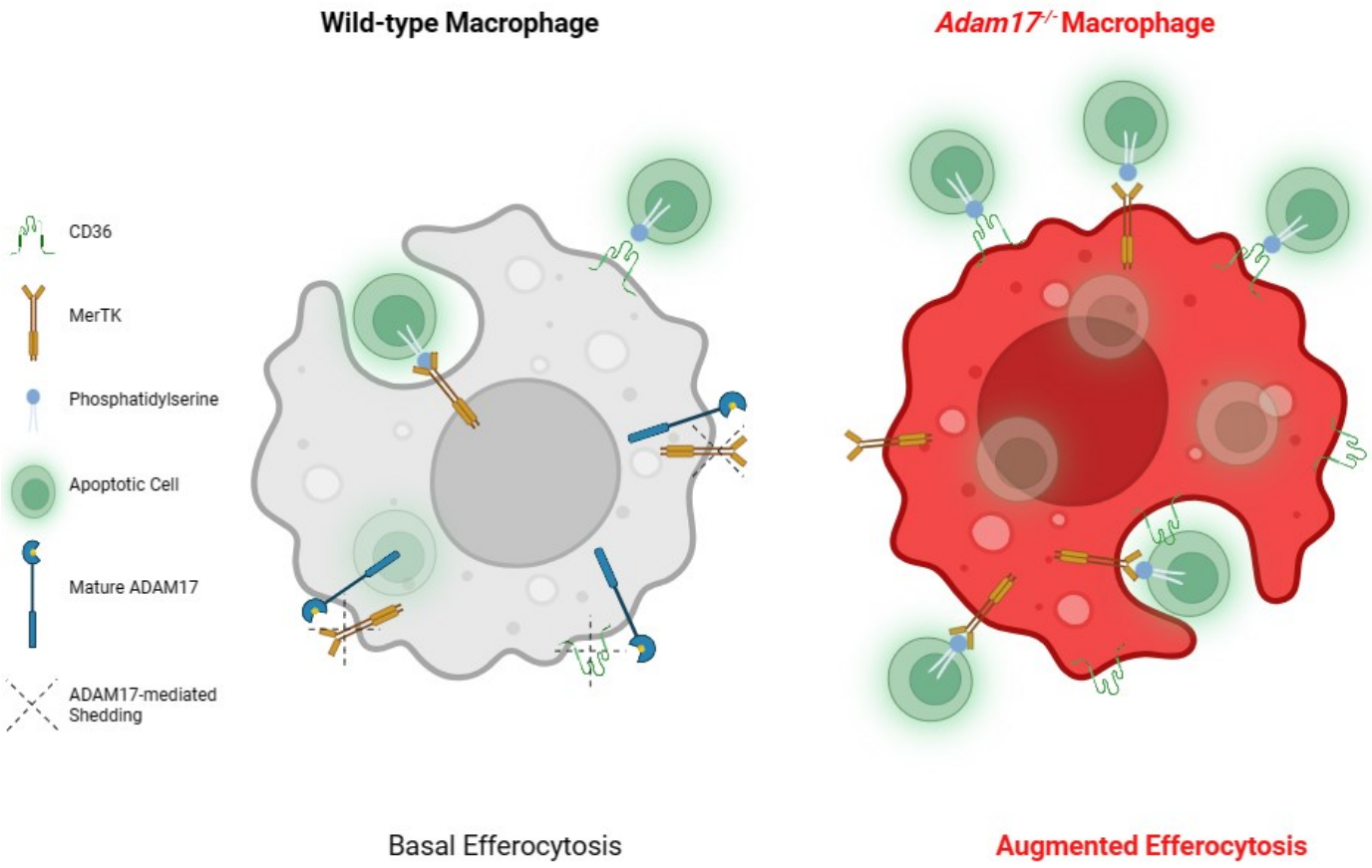

Figure 4.2 Effect of ADAM17 Knockdown on Macrophage Efferocytosis

ADAM17 knockdown in macrophages improves their ability to recognize and bind to apoptotic stimuli, and this is accompanied with increased levels of cell surface MerTK in the *Adam17KD* macrophages. The literature also states that CD36 is augmented in *Adam17KD* macrophages as well.

4.7 Smooth Muscle Cells Lack Efferocytotic Capabilities

In assessing the impact of *Adam17*^{KD} VSMC to conduct efferocytosis, we found that both apoptotic and non-apoptotic Jurkat cells remained bound to areas lacking VSMC, indicating non-efferocytotic interaction. It is known that in cell culture, VSMC can deposit extracellular matrix (ECM) proteins in response to certain stimuli, and it is well established that VSMC secretion of ECM proteins is common to normal vascular physiology.[191-193] Thus, these Jurkat cells were likely binding non-specifically to the ECM synthesized by the VSMCs. Macrophages are known to regulate ECM structure by release of MMPs or TGF-β, but they are not known to secrete or synthesize ECM proteins.[194-197] For this reason we do not see non-specifically bound Jurkat cells in the areas not occupied by BMDM, and the non-apoptotic Jurkat cells are easily removed

We have found that MerTK RNA is expressed to some level in VSMC, though there were no significant differences between the groups, however, we found minimal immunofluorescent staining for MerTK protein, which was primarily localized to the nuclei but not the membrane in the SMCs as is the case with macrophages. However, one study has shown that extracellular vesicles dose-dependently enhance VSMC migration and proliferation, and this was associated with increased MerTK phosphorylation in cell lysates, though they do not report cell surface MerTK expression. Thus, our data suggest that MerTK is not expressed on the surface of VSMC as it is in macrophages, thereby not contributing to efferocytosis.

4.8 Limitations & Future Directions

A major limitation in this study is linking the reduced *Abca1* expression in VSMC *in vitro* to the exacerbated phenotype seen in the *Ldlr*$^{-/-}$*/Adam17*^{SMC} mice. Another limitation is the lack of protein level data of lipid transporter levels in *Adam17*^{KD} VSMC and macrophages.

Specifically, levels of ABCA1 and CD36 in the VSMC (which could explain the reduced efflux and increased uptake) and the levels of ABCA1, CD36, SRA1, and SRB1 in the BMDM, as all of these showed significant changes in mRNA expression between control and *Adam17*^{KD} macrophages treated with oxLDL. Characterizing the levels of these proteins would provide a much more comprehensive understanding on the role of ADAM17 in lipid metabolism.

It is important to note that our *in vitro* studies specifically focused on oxLDL as the atherogenic stimulus. Atherosclerosis consists of a heterogenous combination of variously modified lipoproteins, and one must find the best model for their investigations. Oxidized LDL has certain advantages in our study as it is recognized by all scavenger receptors analyzed, and is relatively quickly loaded into cells via lysosomes, although, this consequently hinders cholesterol efflux. However, our efflux assays use fluorescently labelled cholesterol rather than oxLDL, therefore cholesterol efflux capacity is not impaired in this case. Other modified LDLs, for instance aggregated and acetylated LDL, would not be suitable for this study as they are mainly transported via LRP1 and SRA1, respectively.[115,118] These would fail to highlight any changes in CD36 levels with ADAM17 inhibition and possibly overlook important data. Overall, oxLDL is an efficient and suitable model to study the effect of ADAM17 modulation on the primary scavenger receptors involved in foam cell formation, though we acknowledge that many forms of LDL modifications exist *in vivo*.

Furthermore, characterizing the plaque area after 5-month HCD feeding in mice lacking ADAM17 specifically in macrophages would help determine if the improved efferocytosis seen in macrophages (and not VSMC) would improve the atherosclerotic area as compared to the *Ldlr*$^{-/-}$*/Adam17*^{SMC} mice. Also, it should be made certain that cholesterol efflux is not reduced in *Adam17*^{KD} BMDM, as it has been reported that efflux is in fact reduced.[23,183]

Another limitation is that the *Myh11* promoter is linked to the Y chromosome in mice, leaving no female mice with the triple transgenic *Ldlr*$^{-/-}$/*Adam17*$^{flox/flox}$/*Myh11*$^{cre/ERT2}$ genotype. Therefore, we utilized primary aortic smooth muscle cells from female mice to corroborate the major findings *in vitro*, including the lipid loading and phenotypic transformation data. The *Sm22α*-Cre driver is another widely used promoter for targeting smooth muscle cells, however our lab has found that this promoter is also expressed in keratinocytes.[198] ADAM17 deletion in these mice (*Ldlr*$^{-/-}$/*Adam17*^{Sm22Cre}) supplemented with a high fat diet show significant skin legions which make atherosclerosis studies unethical. This was attributed to a lack of TGF- α release and subsequent activation of epidermal growth factor receptor (EGFR) in keratinocytes. Fortunately, a new autosomal form of this model, termed the *Myh11-CreER*^{T2}*-RAD*, has been generated to study gene knockout studies in VSMC in both male and female mice.[199]

Future studies should look to stain for ABCA1 protein levels in the plaques between control and *Ldlr*$^{-/-}$/*Adam17*^{SMC} mice and analyze protein levels by Western blot in aortic lysates from these mice. More specifically, a colocalization experiment staining for ABCA1 and galectin-3 would determine the levels of ABCA1 between wild-type and *Adam17*$^{-/-}$ VSMC-derived macrophage-like cells. Also, the levels of lipid transporters (ABCA1, CD36, SR-A1, and SR-B1) should be analyzed by Western blot in lysates of VSMC and BMDM between control and *Adam17*^{KD} cells. However, these levels should be analyzed in membrane fractions of these lysates which would be a better indicator of functional lipid transporters rather than those that may be transported within the cytosol.

Future experiments should also investigate plaque area in mice lacking macrophage specific ADAM17, which would require generation of *Ldlr*$^{-/-}$/*Adam17*$^{f/f}$/*Lyz2*^{Cre} mice. Furthermore, in the macrophage cell cultures, cholesterol efflux can be analyzed again in the

absence of ADAM17 but with the use of an inducer of cholesterol efflux to see if this can clear up the discrepancy between the literature that *Adam17*^{KD} macrophages have reduced cholesterol efflux through reduced ABCA1. Moreover, as we did also detect a decrease in *Abca1* expression at the mRNA level, it should be made certain that ADAM17 does not elicit cholesterol efflux. Again, use of a cholesterol efflux agonist as opposed to baseline efflux may manifest the effect of reduced *Abca1* expression by helping to improve sensitivity of the assay. Macrophages are known to express high amount of ABCA1, which may not be affected with a reduction in *Abca1* expression. Therefore, with an agonist, a decrease in *Abca1* RNA expression may have a considerable effect on ABCA1-mediated efflux if the transporter is saturated. Finally, reproducing the *in vivo* data in female mice lacking VSMC ADAM17 is necessary to determine any effects of sex differences, possibly with the new mouse model *Myh11-CreER*^{T2}*-RAD*.

References

1. Gisterå A, Hansson GK. The immunology of atherosclerosis. *Nature reviews nephrology.* 2017;**13**(6):368-380.
2. Mahmoudi A, Atkin SL, Jamialahmadi T, Sahebkar A. Identification of key upregulated genes involved in foam cell formation and the modulatory role of statin therapy. *International Immunopharmacology.* 2023;**119**:110209.
3. Behbodikhah J, Ahmed S, Elyasi A, Kasselman LJ, De Leon J, Glass AD, et al. Apolipoprotein B and cardiovascular disease: biomarker and potential therapeutic target. *Metabolites.* 2021;**11**(10):690.
4. Orekhov AN, Sobenin IA, Revin VV, Bobryshev YV. Development of antiatherosclerotic drugs on the basis of natural products using cell model approach. *Oxidative Medicine and Cellular Longevity.* 2015;**2015**.
5. Williams KJ, Tabas I. The response-to-retention hypothesis of atherogenesis reinforced. *Current opinion in lipidology.* 1998;**9**(5):471-474.
6. Quispe R, Martin SS, Michos ED, Lamba I, Blumenthal RS, Saeed A, et al. Remnant cholesterol predicts cardiovascular disease beyond LDL and ApoB: a primary prevention study. *Eur Heart J.* 2021;**42**(42):4324-4332.
7. Alique M, Luna C, Carracedo J, Ramírez R. LDL biochemical modifications: a link between atherosclerosis and aging. *Food & nutrition research.* 2015;**59**(1):29240.
8. Libby P, Ridker PM, Maseri A. Inflammation and atherosclerosis. *Circulation.* 2002;**105**(9):1135-1143.
9. Harman JL, Jørgensen HF. The role of smooth muscle cells in plaque stability: Therapeutic targeting potential. *British journal of pharmacology.* 2019;**176**(19):3741-3753.
10. Bennett MR, Sinha S, Owens GK. Vascular smooth muscle cells in atherosclerosis. *Circulation research.* 2016;**118**(4):692-702.
11. Dreymueller D, Pruessmeyer J, Groth E, Ludwig A. The role of ADAM-mediated shedding in vascular biology. *European journal of cell biology.* 2012;**91**(6-7):472-485.
12. Hinkle CL, Sunnarborg SW, Loiselle D, Parker CE, Stevenson M, Russell WE, et al. Selective roles for tumor necrosis factor α-converting enzyme/ADAM17 in the shedding of the epidermal growth factor receptor ligand family: the juxtamembrane stalk

determines cleavage efficiency. *Journal of Biological Chemistry.* 2004;**279**(23):24179-24188.

13. Black RA, Rauch CT, Kozlosky CJ, Peschon JJ, Slack JL, Wolfson MF, et al. A metalloproteinase disintegrin that releases tumour-necrosis factor-α from cells. *Nature.* 1997;**385**(6618):729-733.
14. Takamune Y, Ikebe T, Nagano O, Shinohara M. Involvement of NF-κB-mediated maturation of ADAM-17 in the invasion of oral squamous cell carcinoma. *Biochemical and biophysical research communications.* 2008;**365**(2):393-398.
15. Rose-John S. ADAM17, shedding, TACE as therapeutic targets. *Pharmacological research.* 2013;**71**:19-22.
16. Zhao X, Kong J, Zhao Y, Wang X, Bu P, Zhang C, et al. Gene silencing of TACE enhances plaque stability and improves vascular remodeling in a rabbit model of atherosclerosis. *Scientific reports.* 2015;**5**(1):1-13.
17. Nicolaou A, Zhao Z, Northoff BH, Sass K, Herbst A, Kohlmaier A, et al. Adam17 deficiency promotes atherosclerosis by enhanced TNFR2 signaling in mice. *Arteriosclerosis, thrombosis, and vascular biology.* 2017;**37**(2):247-257.
18. Jia Y, Kong W. ADAM17: a molecular switch to control TNFR2 during atherogenesis in vivo. In. Vol 37. Am Heart Assoc2017, 176-178.
19. Tang J, Frey JM, Wilson CL, Moncada-Pazos A, Levet C, Freeman M, et al. Neutrophil and macrophage cell surface colony-stimulating factor 1 shed by ADAM17 drives mouse macrophage proliferation in acute and chronic inflammation. *Molecular and cellular biology.* 2018;**38**(17):e00103-00118.
20. Driscoll WS, Vaisar T, Tang J, Wilson CL, Raines EW. Macrophage ADAM17 deficiency augments CD36-dependent apoptotic cell uptake and the linked anti-inflammatory phenotype. *Circulation research.* 2013;**113**(1):52-61.
21. Zhang Y, Wang Y, Zhou D, Zhang L-S, Deng F-X, Shu S, et al. Angiotensin II deteriorates advanced atherosclerosis by promoting MerTK cleavage and impairing efferocytosis through the AT1R/ROS/p38 MAPK/ADAM17 pathway. *American Journal of Physiology-Cell Physiology.* 2019;**317**(4):C776-C787.

22. van der Vorst EP, Zhao Z, Rami M, Holdt LM, Teupser D, Steffens S, et al. Contrasting effects of myeloid and endothelial ADAM17 on atherosclerosis development. *Thromb Haemost.* 2017;**117**(3):644-646.
23. Kothari V, Tang J, He Y, Kramer F, Kanter JE, Bornfeldt KE. ADAM17 Boosts Cholesterol Efflux and Downstream Effects of High-Density Lipoprotein on Inflammatory Pathways in Macrophages. *Arteriosclerosis, Thrombosis, and Vascular Biology.* 2021;**41**(6):1854-1873.
24. Gasser TC. Chapter 8 - Aorta. In: Payan Y, Ohayon J (eds). *Biomechanics of Living Organs.* Vol 1. Academic Press: Oxford, 2017, 169-191.
25. Chen X-L, Varner SE, Rao AS, Grey JY, Thomas S, Cook CK, et al. Laminar flow induction of antioxidant response element-mediated genes in endothelial cells: a novel anti-inflammatory mechanism. *Journal of Biological Chemistry.* 2003;**278**(2):703-711.
26. Palmer RM, Ashton D, Moncada S. Vascular endothelial cells synthesize nitric oxide from L-arginine. *Nature.* 1988;**333**(6174):664-666.
27. Dimmeler S, Zeiher AM. Nitric oxide–an endothelial cell survival factor. *Cell Death & Differentiation.* 1999;**6**(10):964-968.
28. Bishop JE, Lindahl G. Regulation of cardiovascular collagen synthesis by mechanical load. *Cardiovascular research.* 1999;**42**(1):27-44.
29. Grote K, Flach I, Luchtefeld M, Akin E, Holland SM, Drexler H, et al. Mechanical stretch enhances mRNA expression and proenzyme release of matrix metalloproteinase-2 (MMP-2) via NAD (P) H oxidase–derived reactive oxygen species. *Circulation research.* 2003;**92**(11):e80-e86.
30. Steed E, Balda MS, Matter K. Dynamics and functions of tight junctions. *Trends in cell biology.* 2010;**20**(3):142-149.
31. Niessen CM. Tight junctions/adherens junctions: basic structure and function. *Journal of investigative dermatology.* 2007;**127**(11):2525-2532.
32. Tousoulis D, Kampoli A-M, Tentolouris Nikolaos Papageorgiou C, Stefanadis C. The role of nitric oxide on endothelial function. *Current vascular pharmacology.* 2012;**10**(1):4-18.
33. Yoshizumi M, Perrella MA, Burnett Jr J, Lee ME. Tumor necrosis factor downregulates an endothelial nitric oxide synthase mRNA by shortening its half-life. *Circulation research.* 1993;**73**(1):205-209.

34. John S, Schlaich M, Langenfeld M, Weihprecht H, Schmitz G, Weidinger G, et al. Increased bioavailability of nitric oxide after lipid-lowering therapy in hypercholesterolemic patients: a randomized, placebo-controlled, double-blind study. *Circulation.* 1998;**98**(3):211-216.
35. Schächinger V, Britten MB, Elsner M, Walter DH, Scharrer I, Zeiher AM. A positive family history of premature coronary artery disease is associated with impaired endothelium-dependent coronary blood flow regulation. *Circulation.* 1999;**100**(14):1502-1508.
36. Ogeng'o J, Ominde BS, Ongeti K, Olabu B, Obimbo M, Mwachaka P. Reappraisal of the structure of arterial tunica adventitia and its involvement in atherosclerosis. *Anatomy Journal of Africa.* 2017;**6**(1):824-833.
37. Ravikanth M, Soujanya P, Manjunath K, Saraswathi T, Ramachandran C. Heterogenecity of fibroblasts. *Journal of oral and maxillofacial pathology: JOMFP.* 2011;**15**(2):247.
38. Vaughan MB, Howard EW, Tomasek JJ. Transforming growth factor-β1 promotes the morphological and functional differentiation of the myofibroblast. *Experimental cell research.* 2000;**257**(1):180-189.
39. Walker M, Godin M, Pelling AE. Mechanical stretch sustains myofibroblast phenotype and function in microtissues through latent TGF-β1 activation. *Integrative Biology.* 2020;**12**(8):199-210.
40. Boström H, Willetts K, Pekny M, Levéen P, Lindahl P, Hedstrand H, et al. PDGF-A signaling is a critical event in lung alveolar myofibroblast development and alveogenesis. *Cell.* 1996;**85**(6):863-873.
41. Tonar Z, Tomášek P, Loskot P, Janáček J, Králíčková M, Witter K. Vasa vasorum in the tunica media and tunica adventitia of the porcine aorta. *Annals of Anatomy-Anatomischer Anzeiger.* 2016;**205**:22-36.
42. Xu F, Ji J, Li L, Chen R, Hu W-c. Adventitial fibroblasts are activated in the early stages of atherosclerosis in the apolipoprotein E knockout mouse. *Biochemical and Biophysical Research Communications.* 2007;**352**(3):681-688.
43. Owens GK. Regulation of differentiation of vascular smooth muscle cells. *Physiological Reviews.* 1995;**75**(3):487-517.

44. Van Der Loop FT, Gabbiani G, Kohnen G, Ramaekers FC, van Eys GJ. Differentiation of smooth muscle cells in human blood vessels as defined by smoothelin, a novel marker for the contractile phenotype. *Arteriosclerosis, thrombosis, and vascular biology.* 1997;**17**(4):665-671.
45. Skalli O, Pelte M, Peclet M, Gabbiani G, Gugliotta P, Bussolati G, et al. Alpha-smooth muscle actin, a differentiation marker of smooth muscle cells, is present in microfilamentous bundles of pericytes. *Journal of Histochemistry & Cytochemistry.* 1989;**37**(3):315-321.
46. Li T, Wang B, Ding H, Chen S, Cheng W, Li Y, et al. Effect of extracellular vesicles from multiple cells on vascular smooth muscle cells in atherosclerosis. *Frontiers in Pharmacology.* 2022;**13**:857331.
47. Alexander MR, Owens GK. Epigenetic control of smooth muscle cell differentiation and phenotypic switching in vascular development and disease. *Annual review of physiology.* 2012;**74**:13-40.
48. Gomez D, Owens GK. Smooth muscle cell phenotypic switching in atherosclerosis. *Cardiovascular research.* 2012;**95**(2):156-164.
49. Nakashima Y, Wight TN, Sueishi K. Early atherosclerosis in humans: role of diffuse intimal thickening and extracellular matrix proteoglycans. *Cardiovascular research.* 2008;**79**(1):14-23.
50. Lauper N, Unni K, Kottke B, Titus J. Anatomy and histology of aorta of White Carneau pigeon. *Laboratory Investigation; a Journal of Technical Methods and Pathology.* 1975;**32**(4):536-551.
51. Moss N, Benditt E. Spontaneous and experimentally induced arterial lesions. I. An ultrastructural survey of the normal chicken aorte. *Laboratory Investigation.* 1970;**22**:166-183.
52. Lu H, Cassis LA, Daugherty A. Atherosclerosis and arterial blood pressure in mice. *Current drug targets.* 2007;**8**(11):1181-1189.
53. Libby P. The changing landscape of atherosclerosis. *Nature.* 2021;**592**(7855):524-533.
54. Chistiakov DA, Melnichenko AA, Myasoedova VA, Grechko AV, Orekhov AN. Mechanisms of foam cell formation in atherosclerosis. *Journal of Molecular Medicine.* 2017;**95**(11):1153-1165.

55. Allahverdian S, Chehroudi AC, McManus BM, Abraham T, Francis GA. Contribution of intimal smooth muscle cells to cholesterol accumulation and macrophage-like cells in human atherosclerosis. *Circulation.* 2014;**129**(15):1551-1559.
56. Rafieian-Kopaei M, Setorki M, Doudi M, Baradaran A, Nasri H. Atherosclerosis: process, indicators, risk factors and new hopes. *International journal of preventive medicine.* 2014;**5**(8):927.
57. Tan YY, Gast G-CM, van der Schouw YT. Gender differences in risk factors for coronary heart disease. *Maturitas.* 2010;**65**(2):149-160.
58. Marsh MM, Walker VR, Curtiss LK, Banka CL. Protection against atherosclerosis by estrogen is independent of plasma cholesterol levels in LDL receptor-deficient mice. *Journal of lipid research.* 1999;**40**(5):893-900.
59. Rekhi UR, Omar M, Alexiou M, Delyea C, Immaraj L, Elahi S, et al. Endothelial cell CD36 reduces atherosclerosis and controls systemic metabolism. *Frontiers in Cardiovascular Medicine.* 2021;**8**:768481.
60. Geissmann F, Manz MG, Jung S, Sieweke MH, Merad M, Ley K. Development of monocytes, macrophages, and dendritic cells. *Science.* 2010;**327**(5966):656-661.
61. Fujiwara N, Kobayashi K. Macrophages in inflammation. *Current Drug Targets-Inflammation & Allergy.* 2005;**4**(3):281-286.
62. Chinetti-Gbaguidi G, Colin S, Staels B. Macrophage subsets in atherosclerosis. *Nature Reviews Cardiology.* 2015;**12**(1):10-17.
63. Jacobsen K, Lund MB, Shim J, Gunnersen S, Füchtbauer E-M, Kjolby M, et al. Diverse cellular architecture of atherosclerotic plaque derives from clonal expansion of a few medial SMCs. *JCI insight.* 2017;**2**(19).
64. Basatemur GL, Jørgensen HF, Clarke MC, Bennett MR, Mallat Z. Vascular smooth muscle cells in atherosclerosis. *Nature reviews cardiology.* 2019;**16**(12):727-744.
65. Clarke MC, Littlewood TD, Figg N, Maguire JJ, Davenport AP, Goddard M, et al. Chronic apoptosis of vascular smooth muscle cells accelerates atherosclerosis and promotes calcification and medial degeneration. *Circulation research.* 2008;**102**(12):1529-1538.

66. Wang Z, Wang D-Z, Hockemeyer D, McAnally J, Nordheim A, Olson EN. Myocardin and ternary complex factors compete for SRF to control smooth muscle gene expression. *Nature.* 2004;**428**(6979):185-189.

67. Shankman LS, Gomez D, Cherepanova OA, Salmon M, Alencar GF, Haskins RM, et al. KLF4-dependent phenotypic modulation of smooth muscle cells has a key role in atherosclerotic plaque pathogenesis. *Nature medicine.* 2015;**21**(6):628-637.

68. Clarke MC, Figg N, Maguire JJ, Davenport AP, Goddard M, Littlewood TD, et al. Apoptosis of vascular smooth muscle cells induces features of plaque vulnerability in atherosclerosis. *Nature medicine.* 2006;**12**(9):1075-1080.

69. Seals DF, Courtneidge SA. The ADAMs family of metalloproteases: multidomain proteins with multiple functions. *Genes & development.* 2003;**17**(1):7-30.

70. Hartl D, May P, Gu W, Mayhaus M, Pichler S, Spaniol C, et al. A rare loss-of-function variant of ADAM17 is associated with late-onset familial Alzheimer disease. *Molecular psychiatry.* 2020;**25**(3):629-639.

71. Duffy MJ, McKiernan E, O'Donovan N, McGowan PM. Role of ADAMs in cancer formation and progression. *Clinical Cancer Research.* 2009;**15**(4):1140-1144.

72. Arai J, Otoyama Y, Nozawa H, Kato N, Yoshida H. The immunological role of ADAMs in the field of gastroenterological chronic inflammatory diseases and cancers: a review. *Oncogene.* 2023;**42**(8):549-558.

73. Kawai T, Elliott KJ, Scalia R, Eguchi S. Contribution of ADAM17 and related ADAMs in cardiovascular diseases. *Cellular and Molecular Life Sciences.* 2021;**78**:4161-4187.

74. Huovila A-PJ, Turner AJ, Pelto-Huikko M, Kärkkäinen I, Ortiz RM. Shedding light on ADAM metalloproteinases. *Trends in biochemical sciences.* 2005;**30**(7):413-422.

75. Wolfsberg TG, Straight PD, Gerena RL, Huovila A-PJ, Primakoff P, Myles DG, et al. ADAM, a Widely Distributed and Developmentally Regulated Gene Family Encoding Membrane Proteins with A Disintegrin And Metalloprotease Domain. *Developmental biology.* 1995;**169**(1):378-383.

76. Zhong S, Khalil RA. A Disintegrin and Metalloproteinase (ADAM) and ADAM with thrombospondin motifs (ADAMTS) family in vascular biology and disease. *Biochemical Pharmacology.* 2019;**164**:188-204.

77. Zhang P, Shen M, Fernandez-Patron C, Kassiri Z. ADAMs family and relatives in cardiovascular physiology and pathology. *Journal of molecular and cellular cardiology.* 2016;**93**:186-199.
78. Blobel CP. Metalloprotease-disintegrins: links to cell adhesion and cleavage of TNFα and Notch. *Cell.* 1997;**90**(4):589-592.
79. Smith KM, Gaultier A, Cousin H, Alfandari D, White JM, DeSimone DW. The cysteine-rich domain regulates ADAM protease function in vivo. *The Journal of cell biology.* 2002;**159**(5):893-902.
80. Takeda S, Igarashi T, Mori H, Araki S. Crystal structures of VAP1 reveal ADAMs' MDC domain architecture and its unique C-shaped scaffold. *The EMBO journal.* 2006;**25**(11):2388-2396.
81. Stone AL, Kroeger M, Sang QXA. Structure–function analysis of the ADAM family of disintegrin-like and metalloproteinase-containing proteins. *Journal of protein chemistry.* 1999;**18**:447-465.
82. Endres K, Anders A, Kojro E, Gilbert S, Fahrenholz F, Postina R. Tumor necrosis factor-α converting enzyme is processed by proprotein-convertases to its mature form which is degraded upon phorbol ester stimulation. *European journal of biochemistry.* 2003;**270**(11):2386-2393.
83. Nyren-Erickson EK, Jones JM, Srivastava D, Mallik S. A disintegrin and metalloproteinase-12 (ADAM12): function, roles in disease progression, and clinical implications. *Biochimica et Biophysica Acta (BBA)-General Subjects.* 2013;**1830**(10):4445-4455.
84. Giebeler N, Zigrino P. A disintegrin and metalloprotease (ADAM): historical overview of their functions. *Toxins (Basel).* 2016;**8**(4):122.
85. Reiss K, Saftig P. The "a disintegrin and metalloprotease"(ADAM) family of sheddases: physiological and cellular functions. Paper presented at: Seminars in cell & developmental biology2009.
86. Kriegler M, Perez C, DeFay K, Albert I, Lu S. A novel form of TNF/cachectin is a cell surface cytotoxic transmembrane protein: ramifications for the complex physiology of TNF. *Cell.* 1988;**53**(1):45-53.

87. Mohler KM, Sleath PR, Fitzner JN, Cerretti DP, Alderson M, Kerwar SS, et al. Protection against a lethal dose of endotoxin by an inhibitor of tumour necrosis factor processing. *Nature.* 1994;**370**(6486):218-220.

88. Zunke F, Rose-John S. The shedding protease ADAM17: Physiology and pathophysiology. *Biochimica et Biophysica Acta (BBA) - Molecular Cell Research.* 2017;**1864**(11, Part B):2059-2070.

89. Peschon JJ, Slack JL, Reddy P, Stocking KL, Sunnarborg SW, Lee DC, et al. An essential role for ectodomain shedding in mammalian development. *Science.* 1998;**282**(5392):1281-1284.

90. Calvete JJ, Marcinkiewicz C, Sanz L. KTS and RTS-disintegrins: anti-angiogenic viper venom peptides specifically targeting the α1β 1 integrin. *Current pharmaceutical design.* 2007;**13**(28):2853-2859.

91. Düsterhöft S, Babendreyer A, Giese AA, Flasshove C, Ludwig A. Status update on iRhom and ADAM17: It's still complicated. *Biochimica et Biophysica Acta (BBA)-Molecular Cell Research.* 2019;**1866**(10):1567-1583.

92. Maretzky T, McIlwain DR, Issuree PDA, Li X, Malapeira J, Amin S, et al. iRhom2 controls the substrate selectivity of stimulated ADAM17-dependent ectodomain shedding. *Proceedings of the National Academy of Sciences.* 2013;**110**(28):11433-11438.

93. Adrain C, Zettl M, Christova Y, Taylor N, Freeman M. Tumor necrosis factor signaling requires iRhom2 to promote trafficking and activation of TACE. *Science.* 2012;**335**(6065):225-228.

94. Kwak H-i, Mendoza EA, Bayless KJ. ADAM17 co-purifies with TIMP-3 and modulates endothelial invasion responses in three-dimensional collagen matrices. *Matrix Biology.* 2009;**28**(8):470-479.

95. Cesaro A, Abakar-Mahamat A, Brest P, Lassalle S, Selva E, Filippi J, et al. Differential expression and regulation of ADAM17 and TIMP3 in acute inflamed intestinal epithelia. *American Journal of Physiology-Gastrointestinal and Liver Physiology.* 2009;**296**(6):G1332-G1343.

96. Müllberg J, Schooltink H, Stoyan T, Heinrich PC, Rose-John S. Protein kinase C activity is rate limiting for shedding of the interleukin-6 receptor. *Biochemical and biophysical research communications.* 1992;**189**(2):794-800.

97. Canault M, Peiretti F, Kopp F, Bonardo B, Bonzi M-F, Coudeyre J-C, et al. The TNF alpha converting enzyme (TACE/ADAM17) is expressed in the atherosclerotic lesions of apolipoprotein E-deficient mice: Possible contribution to elevated plasma levels of soluble TNF alpha receptors. *Atherosclerosis.* 2006;**187**(1):82-91.
98. Rizza S, Copetti M, Cardellini M, Menghini R, Pecchioli C, Luzi A, et al. A score including ADAM17 substrates correlates to recurring cardiovascular event in subjects with atherosclerosis. *Atherosclerosis.* 2015;**239**(2):459-464.
99. Oksala N, Levula M, Airla N, Pelto-Huikko M, Ortiz RM, Järvinen O, et al. ADAM-9, ADAM-15, and ADAM-17 are upregulated in macrophages in advanced human atherosclerotic plaques in aorta and carotid and femoral arteries—Tampere vascular study. *Annals of medicine.* 2009;**41**(4):279-290.
100. Canault M, Leroyer AS, Peiretti F, Lesèche G, Tedgui A, Bonardo B, et al. Microparticles of Human Atherosclerotic Plaques Enhance the Shedding of the Tumor Necrosis Factor-α Converting Enzyme/ADAM17 Substrates, Tumor Necrosis Factor and Tumor Necrosis Factor Receptor-1. *The American Journal of Pathology.* 2007;**171**(5):1713-1723.
101. Holdt LM, Thiery J, Breslow JL, Teupser D. Increased ADAM17 mRNA expression and activity is associated with atherosclerosis resistance in LDL-receptor deficient mice. *Arteriosclerosis, thrombosis, and vascular biology.* 2008;**28**(6):1097-1103.
102. van der Vorst EP, Zhao Z, Rami M, Holdt LM, Teupser D, Steffens S, et al. Contrasting effects of myeloid and endothelial ADAM17 on atherosclerosis development. *Thrombosis and Haemostasis.* 2017;**117**(03):644-646.
103. Zhao X, Kong J, Zhao Y, Wang X, Bu P, Zhang C, et al. Gene silencing of TACE enhances plaque stability and improves vascular remodeling in a rabbit model of atherosclerosis. *Scientific reports.* 2015;**5**(1):17939.
104. Ylä-Herttuala S, Palinski W, Rosenfeld ME, Parthasarathy S, Carew TE, Butler S, et al. Evidence for the presence of oxidatively modified low density lipoprotein in atherosclerotic lesions of rabbit and man. *The Journal of clinical investigation.* 1989;**84**(4):1086-1095.
105. Fan J, Kitajima S, Watanabe T, Xu J, Zhang J, Liu E, et al. Rabbit models for the study of human atherosclerosis: from pathophysiological mechanisms to translational medicine. *Pharmacology & therapeutics.* 2015;**146**:104-119.

106. Barter PJ, Brewer Jr HB, Chapman MJ, Hennekens CH, Rader DJ, Tall AR. Cholesteryl ester transfer protein: a novel target for raising HDL and inhibiting atherosclerosis. *Arteriosclerosis, thrombosis, and vascular biology.* 2003;**23**(2):160-167.

107. Okamoto H, Yonemori F, Wakitani K, Minowa T, Maeda K, Shinkai H. A cholesteryl ester transfer protein inhibitor attenuates atherosclerosis in rabbits. *Nature.* 2000;**406**(6792):203-207.

108. Tall AR. Plasma cholesteryl ester transfer protein. *Journal of lipid research.* 1993;**34**(8):1255-1274.

109. Abifadel M, Varret M, Rabès J-P, Allard D, Ouguerram K, Devillers M, et al. Mutations in PCSK9 cause autosomal dominant hypercholesterolemia. *Nature genetics.* 2003;**34**(2):154-156.

110. Steinberg D. The LDL modification hypothesis of atherogenesis: an update. *Journal of lipid research.* 2009;**50**:S376-S381.

111. Bowie A, Owens D, Collins P, Johnson A, Tomkin GH. Glycosylated low density lipoprotein is more sensitive to oxidation: implications for the diabetic patient? *Atherosclerosis.* 1993;**102**(1):63-67.

112. Bucala R, Makita Z, Koschinsky T, Cerami A, Vlassara H. Lipid advanced glycosylation: pathway for lipid oxidation in vivo. *Proceedings of the National Academy of Sciences.* 1993;**90**(14):6434-6438.

113. Sanda GM, Stancu CS, Deleanu M, Toma L, Niculescu LS, Sima AV. Aggregated LDL turn human macrophages into foam cells and induce mitochondrial dysfunction without triggering oxidative or endoplasmic reticulum stress. *PLoS One.* 2021;**16**(1):e0245797.

114. Llorente-Cortés V, Martínez-González J, Badimon L. LDL receptor–related protein mediates uptake of aggregated LDL in human vascular smooth muscle cells. *Arteriosclerosis, thrombosis, and vascular biology.* 2000;**20**(6):1572-1579.

115. Llorente-Cortés V, Otero-Vinas M, Camino-López S, Costales P, Badimon L. Cholesteryl esters of aggregated LDL are internalized by selective uptake in human vascular smooth muscle cells. *Arteriosclerosis, thrombosis, and vascular biology.* 2006;**26**(1):117-123.

116. Dhaliwal BS, Steinbrecher UP. Cholesterol delivered to macrophages by oxidized low density lipoprotein is sequestered in lysosomes and fails to efflux normally. *Journal of lipid research.* 2000;**41**(10):1658-1665.

117. Lougheed M, Lum CM, Ling W, Suzuki H, Kodama T, Steinbrecher U. High affinity saturable uptake of oxidized low density lipoprotein by macrophages from mice lacking the scavenger receptor class A type I/II. *Journal of Biological Chemistry.* 1997;**272**(20):12938-12944.

118. Sparrow CP, Parthasarathy S, Steinberg D. A macrophage receptor that recognizes oxidized low density lipoprotein but not acetylated low density lipoprotein. *Journal of Biological Chemistry.* 1989;**264**(5):2599-2604.

119. Nicholson AC, Frieda S, Pearce A, Silverstein RL. Oxidized LDL binds to CD36 on human monocyte-derived macrophages and transfected cell lines: evidence implicating the lipid moiety of the lipoprotein as the binding site. *Arteriosclerosis, thrombosis, and vascular biology.* 1995;**15**(2):269-275.

120. Adorni MP, Zimetti F, Billheimer JT, Wang N, Rader DJ, Phillips MC, et al. The roles of different pathways in the release of cholesterol from macrophages. *Journal of lipid research.* 2007;**48**(11):2453-2462.

121. Francis GA, Knopp RH, Oram JF. Defective removal of cellular cholesterol and phospholipids by apolipoprotein AI in Tangier Disease. *The Journal of clinical investigation.* 1995;**96**(1):78-87.

122. Mautner SL, Sanchez JA, Rader DJ, Mautner GC, Ferrans VJ, Fredrickson DS, et al. The heart in Tangier disease: severe coronary atherosclerosis with near absence of high-density lipoprotein cholesterol. *American journal of clinical pathology.* 1992;**98**(2):191-198.

123. Oram JF. Tangier disease and ABCA1. *Biochimica et Biophysica Acta (BBA)-Molecular and Cell Biology of Lipids.* 2000;**1529**(1-3):321-330.

124. Wang H, Liu Y, Zhu L, Wang W, Wan Z, Chen F, et al. 17β-estradiol promotes cholesterol efflux from vascular smooth muscle cells through a liver X receptor α-dependent pathway. *International Journal of Molecular Medicine.* 2014;**33**(3):550-558.

125. Delvecchio CJ, Bilan P, Radford K, Stephen J, Trigatti BL, Cox G, et al. Liver X receptor stimulates cholesterol efflux and inhibits expression of proinflammatory mediators in human airway smooth muscle cells. *Molecular Endocrinology.* 2007;**21**(6):1324-1334.

126. Rosenson RS, Brewer Jr HB, Chapman MJ, Fazio S, Hussain MM, Kontush A, et al. HDL measures, particle heterogeneity, proposed nomenclature, and relation to atherosclerotic cardiovascular events. *Clinical chemistry.* 2011;**57**(3):392-410.

127. Sacks FM, Rudel LL, Conner A, Akeefe H, Kostner G, Baki T, et al. Selective delipidation of plasma HDL enhances reverse cholesterol transport in vivo. *Journal of lipid research.* 2009;**50**(5):894-907.

128. Tardif J-C, Grégoire J, L'Allier PL, Ibrahim R, Lespérance J, Heinonen TM, et al. Effects of reconstituted high-density lipoprotein infusions on coronary atherosclerosis: a randomized controlled trial. *Jama.* 2007;**297**(15):1675-1682.

129. Ji Y, Jian B, Wang N, Sun Y, de la Llera Moya M, Phillips MC, et al. Scavenger receptor BI promotes high density lipoprotein-mediated cellular cholesterol efflux. *Journal of Biological Chemistry.* 1997;**272**(34):20982-20985.

130. Jian B, de la Llera-Moya M, Ji Y, Wang N, Phillips MC, Swaney JB, et al. Scavenger receptor class B type I as a mediator of cellular cholesterol efflux to lipoproteins and phospholipid acceptors. *Journal of Biological Chemistry.* 1998;**273**(10):5599-5606.

131. Zhang Y, Da Silva JR, Reilly M, Billheimer JT, Rothblat GH, Rader DJ. Hepatic expression of scavenger receptor class B type I (SR-BI) is a positive regulator of macrophage reverse cholesterol transport in vivo. *The Journal of clinical investigation.* 2005;**115**(10):2870-2874.

132. Zhang W, Yancey PG, Su YR, Babaev VR, Zhang Y, Fazio S, et al. Inactivation of macrophage scavenger receptor class B type I promotes atherosclerotic lesion development in apolipoprotein E–deficient mice. *Circulation.* 2003;**108**(18):2258-2263.

133. Tellier E, Canault M, Rebsomen L, Bonardo B, Juhan-Vague I, Nalbone G, et al. The shedding activity of ADAM17 is sequestered in lipid rafts. *Experimental Cell Research.* 2006;**312**(20):3969-3980.

134. Tellier E, Canault M, Poggi M, Bonardo B, Nicolay A, Alessi MC, et al. HDLs activate ADAM17-dependent shedding. *Journal of cellular physiology.* 2008;**214**(3):687-693.

135. Bianconi E, Piovesan A, Facchin F, Beraudi A, Casadei R, Frabetti F, et al. An estimation of the number of cells in the human body. *Annals of human biology.* 2013;**40**(6):463-471.

136. Doran AC, Yurdagul A, Tabas I. Efferocytosis in health and disease. *Nature Reviews Immunology.* 2020;**20**(4):254-267.

137. Kasikara C, Doran AC, Cai B, Tabas I. The role of non-resolving inflammation in atherosclerosis. *The Journal of clinical investigation.* 2018;**128**(7):2713-2723.
138. Truman LA, Ford CA, Pasikowska M, Pound JD, Wilkinson SJ, Dumitriu IE, et al. CX3CL1/fractalkine is released from apoptotic lymphocytes to stimulate macrophage chemotaxis. *Blood, The Journal of the American Society of Hematology.* 2008;**112**(13):5026-5036.
139. Gude DR, Alvarez SE, Paugh SW, Mitra P, Yu J, Griffiths R, et al. Apoptosis induces expression of sphingosine kinase 1 to release sphingosine-1-phosphate as a "come-and-get-me" signal. *The FASEB Journal.* 2008;**22**(8):2629.
140. Mueller RB, Sheriff A, Gaipl US, Wesselborg S, Lauber K. Attraction of phagocytes by apoptotic cells is mediated by lysophosphatidylcholine. *Autoimmunity.* 2007;**40**(4):342-344.
141. Elliott MR, Chekeni FB, Trampont PC, Lazarowski ER, Kadl A, Walk SF, et al. Nucleotides released by apoptotic cells act as a find-me signal to promote phagocytic clearance. *Nature.* 2009;**461**(7261):282-286.
142. Fadok VA, Voelker DR, Campbell PA, Cohen JJ, Bratton DL, Henson PM. Exposure of phosphatidylserine on the surface of apoptotic lymphocytes triggers specific recognition and removal by macrophages. *Journal of immunology (Baltimore, Md: 1950).* 1992;**148**(7):2207-2216.
143. Elliott MR, Ravichandran KS. The dynamics of apoptotic cell clearance. *Developmental cell.* 2016;**38**(2):147-160.
144. Zhou L, Matsushima GK. Tyro3, Axl, Mertk receptor-mediated efferocytosis and immune regulation in the tumor environment. *Int Rev Cell Mol Biol.* 2021;**361**:165-210.
145. Ait-Oufella H, Pouresmail V, Simon T, Blanc-Brude O, Kinugawa K, Merval R, et al. Defective mer receptor tyrosine kinase signaling in bone marrow cells promotes apoptotic cell accumulation and accelerates atherosclerosis. *Arteriosclerosis, thrombosis, and vascular biology.* 2008;**28**(8):1429-1431.
146. Thorp E, Cui D, Schrijvers DM, Kuriakose G, Tabas I. Mertk receptor mutation reduces efferocytosis efficiency and promotes apoptotic cell accumulation and plaque necrosis in atherosclerotic lesions of apoe−/− mice. *Arteriosclerosis, thrombosis, and vascular biology.* 2008;**28**(8):1421-1428.

147. Kiss RS, Elliott MR, Ma Z, Marcel YL, Ravichandran KS. Apoptotic cells induce a phosphatidylserine-dependent homeostatic response from phagocytes. *Current Biology.* 2006;**16**(22):2252-2258.

148. A-Gonzalez N, Bensinger S, Hong C, Beceiro S, Bradley M, Zelcer N, et al. edwards P, Parks J, Andujar M, Tontonoz P, Castrillo A (2009) Apoptotic cells promote their own clearance and immune tolerance through activation of the nuclear receptor LXR. *Immunity.***31**(2):245-258.

149. Noelia A, Castrillo A. Liver X receptors as regulators of macrophage inflammatory and metabolic pathways. *Biochimica et Biophysica Acta (BBA)-Molecular Basis of Disease.* 2011;**1812**(8):982-994.

150. Oldenborg P-A, Zheleznyak A, Fang Y-F, Lagenaur CF, Gresham HD, Lindberg FP. Role of CD47 as a marker of self on red blood cells. *Science.* 2000;**288**(5473):2051-2054.

151. Ye Z-m, Yang S, Xia Y-p, Hu R-t, Chen S, Li B-w, et al. LncRNA MIAT sponges miR-149-5p to inhibit efferocytosis in advanced atherosclerosis through CD47 upregulation. *Cell death & disease.* 2019;**10**(2):138.

152. Kojima Y, Volkmer J-P, McKenna K, Civelek M, Lusis AJ, Miller CL, et al. CD47-blocking antibodies restore phagocytosis and prevent atherosclerosis. *Nature.* 2016;**536**(7614):86-90.

153. Brophy ML, Dong Y, Tao H, Yancey PG, Song K, Zhang K, et al. Myeloid-specific deletion of epsins 1 and 2 reduces atherosclerosis by preventing LRP-1 downregulation. *Circulation research.* 2019;**124**(4):e6-e19.

154. Sather S, Kenyon KD, Lefkowitz JB, Liang X, Varnum BC, Henson PM, et al. A soluble form of the Mer receptor tyrosine kinase inhibits macrophage clearance of apoptotic cells and platelet aggregation. *Blood.* 2007;**109**(3):1026-1033.

155. Fredman G, Hellmann J, Proto JD, Kuriakose G, Colas RA, Dorweiler B, et al. An imbalance between specialized pro-resolving lipid mediators and pro-inflammatory leukotrienes promotes instability of atherosclerotic plaques. *Nature communications.* 2016;**7**(1):12859.

156. Thorp E, Vaisar T, Subramanian M, Mautner L, Blobel C, Tabas I. Shedding of the Mer tyrosine kinase receptor is mediated by ADAM17 protein through a pathway involving

reactive oxygen species, protein kinase Cδ, and p38 mitogen-activated protein kinase (MAPK). *Journal of Biological Chemistry.* 2011;**286**(38):33335-33344.

157. Du X, Jiang C, Lv Y, Dull RO, Zhao Y-Y, Schwartz DE, et al. Isoflurane promotes phagocytosis of apoptotic neutrophils through AMPK-mediated ADAM17/Mer signaling. *PLoS One.* 2017;**12**(7):e0180213.

158. Hu H, Cheng X, Li F, Guan Z, Xu J, Wu D, et al. Defective efferocytosis by aged macrophages promotes STING signaling mediated inflammatory liver injury. *Cell Death Discovery.* 2023;**9**(1):236.

159. Hu M, Jana S, Kilic T, Wang F, Shen M, Winkelaar G, et al. Loss of TIMP4 (tissue inhibitor of metalloproteinase 4) promotes atherosclerotic plaque deposition in the abdominal aorta despite suppressed plasma cholesterol levels. *Arteriosclerosis, thrombosis, and vascular biology.* 2021;**41**(6):1874-1889.

160. Gage MC. Measuring apoptotic cell engulfment (efferocytosis) efficiency. *Lipid-Activated Nuclear Receptors: Methods and Protocols.* 2019.):143-152.

161. Fok P-W. Growth of necrotic cores in atherosclerotic plaque. *Mathematical Medicine and Biology: A Journal of the IMA.* 2011;**29**(4):301-327.

162. Man JJ, Beckman JA, Jaffe IZ. Sex as a biological variable in atherosclerosis. *Circulation research.* 2020;**126**(9):1297-1319.

163. Mansukhani NA, Wang Z, Shively VP, Kelly ME, Vercammen JM, Kibbe MR. Sex differences in the LDL receptor knockout mouse model of atherosclerosis. *Artery research.* 2017;**20**:8.

164. Teupser D, Persky AD, Breslow JL. Induction of Atherosclerosis by Low-Fat, Semisynthetic Diets in LDL Receptor–Deficient C57BL/6J and FVB/NJ Mice: comparison of lesions of the aortic root, brachiocephalic artery, and whole aorta (en face measurement). *Arteriosclerosis, thrombosis, and vascular biology.* 2003;**23**(10):1907-1913.

165. McCracken JM, Allen L-AH. Regulation of human neutrophil apoptosis and lifespan in health and disease. *Journal of cell death.* 2014;**7**:JCD. S11038.

166. Bekkering S, Torensma R. Another look at the life of a neutrophil. *World Journal of Hematology.* 2013;**2**(2):44-58.

167. Rotzius P, Thams S, Soehnlein O, Kenne E, Tseng C-N, Björkström NK, et al. Distinct Infiltration of Neutrophils in Lesion Shoulders in ApoE−/− Mice. *The American Journal of Pathology.* 2010;**177**(1):493-500.

168. Soehnlein O, Lindbom L. Phagocyte partnership during the onset and resolution of inflammation. *Nature Reviews Immunology.* 2010;**10**(6):427-439.

169. Soehnlein O. Multiple roles for neutrophils in atherosclerosis. *Circulation research.* 2012;**110**(6):875-888.

170. Scheller J, Chalaris A, Garbers C, Rose-John S. ADAM17: a molecular switch to control inflammation and tissue regeneration. *Trends in immunology.* 2011;**32**(8):380-387.

171. Menghini R, Fiorentino L, Casagrande V, Lauro R, Federici M. The role of ADAM17 in metabolic inflammation. *Atherosclerosis.* 2013;**228**(1):12-17.

172. Lisi S, D'Amore M, Sisto M. ADAM17 at the interface between inflammation and autoimmunity. *Immunology letters.* 2014;**162**(1):159-169.

173. Vengrenyuk Y, Nishi H, Long X, Ouimet M, Savji N, Martinez FO, et al. Cholesterol loading reprograms the microRNA-143/145–myocardin axis to convert aortic smooth muscle cells to a dysfunctional macrophage-like phenotype. *Arteriosclerosis, thrombosis, and vascular biology.* 2015;**35**(3):535-546.

174. Dougherty U, Mustafi R, Zhu H, Zhu X, Deb D, Meredith SC, et al. Upregulation of polycistronic microRNA-143 and microRNA-145 in colonocytes suppresses colitis and inflammation-associated colon cancer. *Epigenetics.* 2021;**16**(12):1317-1334.

175. Doberstein K, Steinmeyer N, Hartmetz A-K, Eberhardt W, Mittelbronn M, Harter PN, et al. MicroRNA-145 targets the metalloprotease ADAM17 and is suppressed in renal cell carcinoma patients. *Neoplasia.* 2013;**15**(2):218-IN231.

176. Kzhyshkowska J, Neyen C, Gordon S. Role of macrophage scavenger receptors in atherosclerosis. *Immunobiology.* 2012;**217**(5):492-502.

177. Gerbod-Giannone M-C, Li Y, Holleboom A, Han S, Hsu L-C, Tabas I, et al. TNFα induces ABCA1 through NF-κB in macrophages and in phagocytes ingesting apoptotic cells. *Proceedings of the National Academy of Sciences.* 2006;**103**(9):3112-3117.

178. Edgel KA, LeBoeuf RC, Oram JF. Tumor necrosis factor-α and lymphotoxin-α increase macrophage ABCA1 by gene expression and protein stabilization via different receptors. *Atherosclerosis.* 2010;**209**(2):387-392.

179. Sato S, Imachi H, Lyu J, Miyai Y, Fukunaga K, Dong T, et al. Effect of TNF-α on the expression of ABCA1 in pancreatic β-cells. *Journal of Molecular Endocrinology.* 2018;**61**(4):185-193.

180. Field FJ, Watt K, Mathur SN. TNF-α decreases ABCA1 expression and attenuates HDL cholesterol efflux in the human intestinal cell line Caco-2. *Journal of lipid research.* 2010;**51**(6):1407-1415.

181. Dubland JA, Allahverdian S, Besler KJ, Ortega C, Wang Y, Pryma CS, et al. Low LAL (lysosomal acid lipase) expression by smooth muscle cells relative to macrophages as a mechanism for arterial foam cell formation. *Arteriosclerosis, thrombosis, and vascular biology.* 2021;**41**(6):e354-e368.

182. Xiang P, Blanchard V, Francis GA. Smooth Muscle Cell—Macrophage Interactions Leading to Foam Cell Formation in Atherosclerosis: Location, Location, Location. *Frontiers in Physiology.* 2022;**13**:921597.

183. Robichaud S, Rasheed A, Pietrangelo A, Doyoung Kim A, Boucher DM, Emerton C, et al. Autophagy is differentially regulated in leukocyte and nonleukocyte foam cells during atherosclerosis. *Circulation Research.* 2022;**130**(6):831-847.

184. Wang X, Collins HL, Ranalletta M, Fuki IV, Billheimer JT, Rothblat GH, et al. Macrophage ABCA1 and ABCG1, but not SR-BI, promote macrophage reverse cholesterol transport in vivo. *The Journal of clinical investigation.* 2007;**117**(8):2216-2224.

185. Huby T, Le Goff W. Macrophage SR-B1 in atherosclerotic cardiovascular disease. *Current Opinion in Lipidology.* 2022;**33**(3):167-174.

186. Ravi H, Baskaran V. Chitosan-glycolipid nanocarriers improve the bioavailability of fucoxanthin via up-regulation of PPARγ and SRB1 and antioxidant activity in rat model. *Journal of functional foods.* 2017;**28**:215-226.

187. Ma X, Li S-F, Qin Z-S, Ye J, Zhao Z-L, Fang H-H, et al. Propofol up-regulates expression of ABCA1, ABCG1, and SR-B1 through the PPARγ/LXRα signaling pathway in THP-1 macrophage-derived foam cells. *Cardiovascular Pathology.* 2015;**24**(4):230-235.

188. Kawahara R, Lima RN, Domingues RR, Pauletti BA, Meirelles GV, Assis M, et al. Deciphering the role of the ADAM17-dependent secretome in cell signaling. *Journal of proteome research.* 2014;**13**(4):2080-2093.

189. Van Eck M, De Winther MP, Herijgers N, Havekes LM, Hofker MH, Groot PH, et al. Effect of human scavenger receptor class A overexpression in bone marrow–derived cells on cholesterol levels and atherosclerosis in ApoE-deficient mice. *Arteriosclerosis, thrombosis, and vascular biology.* 2000;**20**(12):2600-2606.

190. Cai B, Thorp EB, Doran AC, Sansbury BE, Daemen MJ, Dorweiler B, et al. MerTK receptor cleavage promotes plaque necrosis and defective resolution in atherosclerosis. *The Journal of clinical investigation.* 2017;**127**(2):564-568.

191. Pustlauk W, Westhoff TH, Claeys L, Roch T, Geißler S, Babel N. Induced osteogenic differentiation of human smooth muscle cells as a model of vascular calcification. *Scientific reports.* 2020;**10**(1):5951.

192. O'Callaghan CJ, Williams B. mechanical strain–induced extracellular matrix production by human vascular smooth muscle cells: Role of TGF-β1. *Hypertension.* 2000;**36**(3):319-324.

193. Yu H, Clarke MC, Figg N, Littlewood TD, Bennett MR. Smooth muscle cell apoptosis promotes vessel remodeling and repair via activation of cell migration, proliferation, and collagen synthesis. *Arteriosclerosis, thrombosis, and vascular biology.* 2011;**31**(11):2402-2409.

194. Vignola A, Chanez P, Chiappara G, Merendino A, Zinnanti E, Bousquet J, et al. Release of transforming growth factor-beta (TGF-β) and fibronectin by alveolar macrophages in airway diseases. *Clinical & Experimental Immunology.* 1996;**106**(1):114-119.

195. O'Rourke SA, Dunne A, Monaghan MG. The role of macrophages in the infarcted myocardium: orchestrators of ECM remodeling. *Frontiers in cardiovascular medicine.* 2019;**6**:101.

196. Elkington PT, Green JA, Friedland JS. Analysis of matrix metalloproteinase secretion by macrophages. *Macrophages and Dendritic Cells: Methods and Protocols.* 2009.):253-265.

197. Winberg J-O, Kolset SO, Berg E, Uhlin-Hansen L. Macrophages secrete matrix metalloproteinase 9 covalently linked to the core protein of chondroitin sulphate proteoglycans. *Journal of molecular biology.* 2000;**304**(4):669-680.

198. Hu M, Hiroyasu S, Granville DJ, Kassiri Z. Implications of Sm22α-Cre expression in keratinocytes and unanticipated inflammatory skin lesion in a model of atherosclerosis. *American Journal of Physiology-Heart and Circulatory Physiology.* 2022;**323**(3):H528-H534.

199. Deaton RA, Bulut G, Serbulea V, Salamon A, Shankman LS, Nguyen AT, et al. A New Autosomal Myh11-CreERT2 Smooth Muscle Cell Lineage Tracing and Gene Knockout Mouse Model—Brief Report. *Arteriosclerosis, Thrombosis, and Vascular Biology.* 2023;**43**(2):203-211.